

# **The tube furnace as a new bench scale experiment for pyrolysis**

Karen De Lannoye

IAS Series

Band / Volume 72

ISBN 978-3-95806-839-1





Forschungszentrum Jülich GmbH  
Institute for Advanced Simulation (IAS)  
Zivile Sicherheitsforschung (IAS-7)

# **The tube furnace as a new bench scale experiment for pyrolysis**

Karen De Lannoye

Schriften des Forschungszentrums Jülich  
IAS Series

Band / Volume 72

ISSN 1868-8489

ISBN 978-3-95806-839-1



Bibliografische Information der Deutschen Nationalbibliothek.  
Die Deutsche Nationalbibliothek verzeichnet diese Publikation in der  
Deutschen Nationalbibliografie; detaillierte Bibliografische Daten  
sind im Internet über <http://dnb.d-nb.de> abrufbar.

Herausgeber  
und Vertrieb:      Forschungszentrum Jülich GmbH  
                         Zentralbibliothek, Verlag  
                         52425 Jülich  
                         Tel.: +49 2461 61-5368  
                         Fax: +49 2461 61-6103  
                         [zb-publikation@fz-juelich.de](mailto:zb-publikation@fz-juelich.de)  
                         [www.fz-juelich.de/zb](http://www.fz-juelich.de/zb)

Umschlaggestaltung:      Grafische Medien, Forschungszentrum Jülich GmbH

Druck:                      Grafische Medien, Forschungszentrum Jülich GmbH

Copyright:                Forschungszentrum Jülich 2025

Schriften des Forschungszentrums Jülich  
IAS Series, Band / Volume 72

D 468 (Diss. Wuppertal, Univ., 2024)

ISSN 1868-8489  
ISBN 978-3-95806-839-1

Vollständig frei verfügbar über das Publikationsportal des Forschungszentrums Jülich (JuSER)  
unter [www.fz-juelich.de/zb/openaccess](http://www.fz-juelich.de/zb/openaccess).



This is an Open Access publication distributed under the terms of the [Creative Commons Attribution License 4.0](https://creativecommons.org/licenses/by/4.0/),  
which permits unrestricted use, distribution, and reproduction in any medium, provided the original work is properly cited.

---

## Abstract

---

Electrical cables are a potential source of fire in many different application areas, ranging from residential buildings to spacecrafts. The current state of the art models for fire spread on a cable or cable tray are using a prescribed spread rate. Many efforts have been made within the research community, to enhance the understanding of cable fires. Nevertheless, many challenges still remain [1]. In order to better understand the influence of certain boundary conditions (e.g. composition and flow conditions of the surrounding atmosphere), a new designed set-up for gram scale pyrolysis experiments is proposed.

In fire safety science, the thermogravimetric analyser (TGA) and the cone calorimeter are both often used for pyrolysis and combustion experiments. The TGA allows examining milligram-scale samples under well-defined boundary conditions, while the cone calorimeter allows for larger (gram-scale) samples but with less well known boundary conditions. Within this thesis, experiments with polymethyl methacrylate (PMMA) are conducted in the TGA and the cone calorimeter. In the TGA, the effect of several different experiment and material parameters on the pyrolysis behaviour is investigated. Including, the effect of different sample colour and different atmospheres is included in this study. In the cone calorimeter, the effect of different sample colour is studied. PMMA was chosen as a material since its fire behaviour is often studied in the literature.

The newly designed experiment is based on the ISO-19700 standard for the steady state tube furnace. The set-up consists of a tube furnace which is combined with an online mass loss measurement. The advantage of the new set-up is that it provides well-defined boundary conditions, as well as radially symmetric heating. The mass loss measurement is enabled using a cantilever mechanism. This cantilever connects the specimen in the oven with a load cell outside the high temperature region of the oven. Additionally, the set-up is connected to a gas analyser with CO, CO<sub>2</sub> and O<sub>2</sub> measurements. Temperatures at the in- and outside of the set-up are recorded using K-type thermocouples. The functionality of the balance is demonstrated by comparing the mass loss rate of the balance with the rate obtained from the measurements by the gas analyser. A very good agreement was found between the results from the gas analyser and the balance, showing the excellent functionality of the new balance.

A comparison between the new device; the TGA and the cone calorimeter is done using PMMA. A difference in mass loss rate and heat release rate was found between black and transparent PMMA in the cone calorimeter. This difference becomes larger for higher external heat fluxes. It is believed that this might be due to a difference in absorption coefficient for both materials, however additional ex-

---

periments would have to be conducted to confirm this hypothesis. When comparing black and transparent PMMA in the tube furnace no difference in mass loss rate was found. This could indicate that the involved heat transfer process in the tube furnace is less dominated by radiation or this might be due to the lower temperatures in the tube furnace. When comparing the mass loss rate results of the tube furnace and the TGA, it was found that changing the atmosphere from nitrogen to air has a similar effect in both devices, namely the mass loss rate starts earlier under air atmosphere.

Additional experiments should be considered to further compare the three devices. The scale of the tube furnace does not allow to ignore heat and mass transfer. Additionally, a temperature gradient is present throughout the length of the furnace. This makes the tube furnace a more complicated experiments than e.g. the TGA, more experiments should be conducted to further characterize the boundary conditions in the tube furnace. In future, it should be considered to make a computational model of the tube furnace which can be used to determine kinetic parameters by inverse modelling. This would allow to further evaluate the added value of the tube furnace to predicting parameters needed for fire spread modelling.

---

## Zusammenfassung

---

Elektrische Kabel sind eine potenzielle Brandquelle in vielen verschiedenen Anwendungsbereichen, von Wohngebäuden bis zu Raumschiffen. Die aktuellen Modelle für die Brandausbreitung auf einem Kabel oder einer Kabeltrasse basieren auf einer vorgegebenen Ausbreitungsrate. In der Forschung wurden viele Anstrengungen unternommen, um das Verständnis von Kabelbränden zu verbessern. Dennoch bleiben noch viele Herausforderungen bestehen [1]. Um den Einfluss bestimmter Randbedingungen (z. B. Zusammensetzung und Strömungsbedingungen der umgebenden Atmosphäre) besser zu verstehen, wird ein neu konzipierter Aufbau für Pyrolyseversuche im Gramm-Maßstab vorgeschlagen.

In der Brandsicherheitswissenschaft werden für Pyrolyse- und Verbrennungsexperimente häufig der thermogravimetrische Analysator (TGA) und das Kegelkalorimeter verwendet. Mit der TGA können Proben im Milligramm-Maßstab unter genau definierten Randbedingungen untersucht werden, während mit dem Kegelkalorimeter größere (Gram-Maßstab) Proben untersucht werden können, bei denen die Randbedingungen weniger gut bekannt sind. Im Rahmen dieser Arbeit werden Experimente mit Polymethylmethacrylate (PMMA) in der TGA und im Kegelkalorimeter durchgeführt. In der TGA wird der Einfluss verschiedener Experiment- und Materialparameter auf das Pyrolyseverhalten untersucht. Unter anderem wird die Auswirkung verschiedener Probenfarben und verschiedener Atmosphären in diese Studie einbezogen. Im Kegelkalorimeter wird die Auswirkung der unterschiedlichen Probenfarbe untersucht. PMMA wurde als Material ausgewählt, da sein Brandverhalten in der Literatur häufig untersucht wird.

Das neu konzipierte Experiment basiert auf der ISO-19700-Norm für den Rohrofen. Der Versuchsaufbau besteht aus einem Rohrofen, der mit einer online Massenverlustmessung kombiniert ist. Der Vorteil des neuen Aufbaus ist, dass er gut definierte Randbedingungen sowie eine radialsymmetrische Beheizung bietet. Die Messung des Massenverlustes wird durch einen Ausleger-Mechanismus ermöglicht. Dieser Kragarm verbindet die Probe im Ofen mit einer Kraftmesszelle außerhalb des Hochtemperaturbereichs des Ofens. Zusätzlich ist der Aufbau an einen Gasanalysator mit CO-, CO<sub>2</sub>- und O<sub>2</sub>-Messungen angeschlossen. Die Temperaturen an der Innen- und Außenseite des Versuchsaufbaus werden mit Thermoelementen vom Typ K aufgezeichnet. Die Funktionalität der Waage wird durch den Vergleich der Massenverlustrate der Waage mit der aus den Messungen des Gasanalysators gewonnenen Rate demonstriert.

Ein Vergleich zwischen dem neuen Gerät, der TGA und dem Kegelkalorimeter wird mit PMMA durchgeführt. Es wurde ein Unterschied in der Massenverlustrate

---

und der Wärmefreisetzungsrate zwischen schwarzem und transparentem PMMA im Kegelkalorimeter festgestellt. Dieser Unterschied wird bei höheren externen Wärmeströmen größer. Es wird vermutet, dass dies auf einen unterschiedlichen Absorptionskoeffizienten der beiden Materialien zurückzuführen sein könnte, doch müssten weitere Versuche durchgeführt werden, um diese Hypothese zu bestätigen. Beim Vergleich von schwarzem und transparentem PMMA im Rohrofen wurde kein Unterschied in der Massenverlustrate festgestellt. Dies könnte darauf hindeuten, dass der Wärmeübertragungsprozess im Rohrofen weniger von der Strahlung dominiert wird, oder dies könnte auf die niedrigeren Temperaturen im Rohrofen zurückzuführen sein. Beim Vergleich der Ergebnisse der Massenverlustrate des Rohrofens und der TGA wurde festgestellt, dass der Wechsel der Atmosphäre von Stickstoff zu Luft in beiden Geräten eine ähnliche Wirkung hat, nämlich dass die Massenverlustrate unter Luftatmosphäre früher beginnt.

Zusätzliche Versuche sollten in Betracht gezogen werden, um die drei Geräte weiter zu vergleichen. Die Größe des Rohrofens erlaubt es nicht, den Wärme- und Stofftransport zu ignorieren. Außerdem ist über die gesamte Länge des Ofens ein Temperaturgradient vorhanden. Dies macht den Rohrofen zu einem komplizierteren Experiment als z.B. die TGA. Es sollten mehr Experimente durchgeführt werden, um die Randbedingungen im Rohrofen weiter zu charakterisieren. In Zukunft sollte die Erstellung eines Berechnungsmodells des Rohrofens in Betracht gezogen werden, das zur Bestimmung der kinetischen Parameter durch inverse Modellierung verwendet werden kann. Dies würde es ermöglichen, den Mehrwert des Rohrofens für die Vorhersage von Parametern, die für die Modellierung der Brandausbreitung benötigt werden, weiter zu bewerten.

---

# Table of Contents

---

<b>Abstract</b>	<b>i</b>
<b>Zusammenfassung</b>	<b>iii</b>
<b>Acknowledgements</b>	<b>vii</b>
<b>List of Publications</b>	<b>ix</b>
<b>1. Introduction</b>	<b>1</b>
1.1. Motivation	1
1.2. Objectives	2
<b>2. Results</b>	<b>5</b>
2.1. Publication 1	5
2.2. Publication 2	6
2.3. Publication 3	8
2.4. Comparison between the TGA, cone calorimeter and the tube furnace	10
<b>3. Conclusion and outlook</b>	<b>15</b>
<b>Publication I. Comparison of black and transparent PMMA in the cone calorimeter</b>	<b>19</b>
<b>Publication II. The Influence of Experimental Conditions on the Mass Loss for TGA in Fire Safety Science</b>	<b>27</b>
<b>Publication III. The tube furnace with online mass loss measurement as a new bench scale experiment</b>	<b>47</b>
<b>Appendix I: Technical drawings tube furnace</b>	<b>62</b>
<b>Curriculum Vitae</b>	<b>70</b>



---

## Acknowledgements

---

First and foremost, I would like to express my deepest gratitude to my three supervisors — Dr. Alexander Belt, Dr. Ernst-Arndt Reinecke, and Prof. Dr. Lukas Arnold — for their continuous guidance, valuable feedback, and unwavering support throughout my PhD journey. Their guidance has not only shaped this research but also significantly contributed to my growth as a scientist.

I would also like to extend my sincere thanks to the members of my examination committee: Prof. Dr. Simo Hostikka, Prof. Dr. Lukas Arnold, Prof. Dr. Armin Seyfried, Prof. Dr. Fabian Brannström, Dr. Ernst-Arndt Reinecke and Prof. Dr. Jaan-Willem Simon. Thank you for the time you have invested in evaluating my work and for your insightful questions and suggestions.

This thesis would not have been possible without the support of the two institutes where I carried out my research: IAS-7 and IEK-6. I am truly grateful for all the technical support, collaborative exchange, and valuable contributions I received from my colleagues. Equally, I deeply appreciate the friendly and welcoming atmosphere—the tea breaks, lunch conversation, and, of course, all the cakes! These moments made the work environment not only productive but also genuinely enjoyable. I would also like to thank all other institutes and colleagues within the research centre that have contributed to this work. In particular, the central institute ZEA-1 for their technical expertise and practical assistance, in particular the team in the glass workshop, whose skill and dedication made many of the experimental setups possible.

During the course of my PhD, I had the opportunity to collaborate with several international research groups, which significantly enriched my research experience. I would like to thank Frank Markert at DTU for giving me the opportunity to run my first cone calorimeter experiments. Many thanks also to Lucie Hasalova and Václav Vystrčil from TUPO for generously sharing Mike with me! A special thanks to Isaac Leventon and his colleagues at NIST for teaching me the importance of research ducks. All of you have been incredibly welcoming and supportive, and each of these experiences has helped shape me into a better scientist.

Finally, I would like to thank all the colleagues, technicians, family and friends who have supported me — directly or indirectly — over the past years. Your encouragement and assistance have meant more than words can say.





---

## List of Publications

---

### Publication I

De Lannoye, K.; Belt, A.; Reinecke, E.-A.; Markert, F.; Arnold, L. "Comparison of Black and Transparent PMMA in the Cone Calorimeter". in Obtaining Data for Fire Growth Models, ed. M. C. Bruns and M. L. Janssens (West Conshohocken, PA: ASTM International, 2023), 150–160. <http://doi.org/10.1520/STP164220210105>

### Publication II

De Lannoye, K.; Trettin, C.; Belt, A.; Reinecke, E.A.; Goertz, R.; Arnold, L. "The Influence of Experimental Conditions on the Mass Loss for TGA in Fire Safety Science". Fire safety journal, December 2023. <https://doi.org/10.1016/j.firesaf.2023.104079>

### Publication III

De Lannoye, K.; Belt, A.; Reinecke, E.A.; Arnold, L. "The tube furnace with on-line mass loss measurement as a new bench scale test", Fire Technol 60, 3689–3707 (2024). <https://doi.org/10.1007/s10694-024-01590-0>



# CHAPTER 1

---

## Introduction

---

### 1.1 Motivation

Electrical cables are a potential ignition source or fuel load in many different areas; like residential and industrial buildings, aero- and spacecrafts and (nuclear) power plants. Some of these fires result in civilian as well as fire fighter deaths and larger amounts of property damage. Around 12% of residential fires in the USA involve electrical malfunctioning [2]. Similar statistics are expected in Europe, for example Switzerland reports 26,7% of fires between 2002 and 2021 to be caused by 'electricity' [3], while in Germany 28% of structural fires in 2022 were estimated to be caused by 'electricity' [4]. A well-known example, are the Grenfell Towers in London (U.K.), where the fire was started due to a malfunctioning fridge-freezer [5]. In about 5 % of home structure fires in the USA the ignition source is an electrical cable or its insulating material [6].

An average passenger aeroplane contains a length of around 500 km of electrical cables, which is up to 3% of the total weight of the aeroplane [7]. In addition to the risk of a cable igniting, many safety and controlling systems in planes need electrical cables to function. Damage due to fire to these cables can be fatal, as several accidents in history have demonstrated. During the Königs Wusterhausen air disaster (1972) a fire destroyed electrical cables, disabling the aircraft flight control system [8]. This resulted in a crash, which none of the 156 passengers survived. In 1998 Swissair flight 111 crashed due to a fire caused by a short circuit in the entertainment system, none of the 269 persons on board survived the disaster [9]. In 2011, a fire started in an electrical panel on the Kolavia flight 348 [10]. Three people did not survive the crash.

Nuclear power plants contain kilometres of cables. A large part of the flammable material in a power plant comes from the insulation of electrical cables. According to the OECD nuclear energy agency [11], 5% of fires in nuclear power plants are directly caused by electrical cables. Additionally, areas with many cables are seen as a risk area for fire. Since a fire could not only cause damage to the cables, but many electrical wires also control vital safety systems within the plant, endangering the operation of the plant when cables get involved in a fire as secondary fuel. The

most famous example, is the fire at Browns Ferry nuclear power plant in 1975. Here, a cable penetration seal ignited after coming in contact with a candle flame. The fire spread and caused significant damage to several cables of the control units (e.g. controlling the cooling system) [12].

Additionally, cable fire products can cause other essential safety mechanism of the power plant to malfunction. For example, [13] showed that the presence of these products may affect the performance of the passive auto-catalytic recombiners, used to recombine hydrogen during an emergency in the nuclear power plant containment. Consequently, this hydrogen will accumulate, which can result in an explosion in the power plant.

An electrical cable is a complex, combined system in a fire scenario. The conducting metal core has a heat conduction coefficient orders of magnitude higher than the surrounding insulation material. Consequently, the core can act both as a heat sink as well as a heat source, depending on the location of the fire. Additionally, most cables consist of several insulating materials: jacket material, insulator and filling material, from which some might have a melt dripping flow. On top of that, the cylindrical shape of the cable makes the flame spread more complex. Usually the flame surrounds the entire surface of the cable, contrary to a flat sample where the flame spreads only over the top surface of the material. In many cases, several cables are stacked together on cable trays. In case of a fire, the heat transfer between several different cables should be taken into account.

Tremendous effort has been made to study cables fires, both on laboratory cables and on real-world cables. For example, the CHRISTIFIRE project [14, 15] (Cable Heat Release, Ignition, and Spread in Tray Installations During Fire) studied the fire behaviour of several electrical cables. Both mg-scale experiments and full horizontal or vertical cable tray experiments were conducted. Also intermediate scale experiments, like the cone calorimeter, were conducted within the project. The model, developed within the CHRISTIFIRE project, uses a prescribed flame spread.

As stated by [1], more studies are needed to better understand cable fires and to enhance the predictive modelling of flame spread on electrical cables. Several aspects of cable fires are not yet sufficiently understood, like the scale effect between the metallic core and the insulation material or the interaction between several layers of insulation.

To bridge the gap between modelling and experimental results for cable fires, a new bench scale experimental set-up is proposed. The aim and main advantage of the set-up is to have well controlled boundary conditions and time-resolved data. The goal of this thesis is to conceptualize, implement and demonstrate the functionality and accuracy of such an experimental set-up.

## 1.2 Objectives

Two devices often used in fire safety science are the thermogravimetric analyser (TGA) [16, 17] and the cone calorimeter [18, 19]. In the TGA, a sample is heated, typically at a constant heating rate, while the mass loss is measured. The device has well controlled boundary conditions and allows running tests both under inert and non-inert atmosphere. This permits to study the influence of the surrounding

atmosphere on the pyrolysis behaviour of the material. It is assumed that heat and mass transport effects can be neglected, therefore only milligram scale samples can be tested in this set-up. For cables, it is very difficult to obtain a representative portion of a cable if only a few milligrams can be taken. The cone calorimeter on the other hand allows for samples with a surface area of 10 cm by 10 cm and a maximum thickness of 7 cm. The sample is packed into a sample holder together with isolation material. This holder is placed under a conical heater, which will heat up the sample predominantly by radiation. During an experiment, the mass loss and the heat release rate (HRR) of the sample is measured. For the latter, the set-up is placed under a hood, connected to a gas analyser measuring  $O_2$  and often also  $CO$  and  $CO_2$ . Oxygen consumption calorimetry is used to determine the HRR of the sample. The boundary conditions in this set-up are less well-defined and controlled than in the TGA. For example, the boundary conditions of the convective heat transfer, e.g. the flow field around the sample, is not well known.

The new experiment that is proposed tries to combine the advantages of the TGA and the cone calorimeter. The aim is to be able to study larger samples under well controlled boundary conditions. The new set-up is based on the ISO-19700 [20] tube furnace. In the standard, a sample is introduced into the oven at a constant rate to achieve steady state burning. The tube furnace is connected to a mixing chamber where the effluents are mixed with oxygen. The main goal of the set-up is to determine the yields of combustion and pyrolysis products.

For model development, the mass loss rate is an important variable, since it prescribes the HRR in a simulation. Both the TGA and the cone calorimeter are equipped with a balance system to measure the sample mass online. Therefore, in order to make the tube furnace a valuable pyrolysis experiment, an online mass loss measurement needs to be installed. Within this work, a balance concept will be designed, installed and tested in the tube furnace. Additionally, to the balance other diagnostics have been added to the tube furnace, like thermocouples, to allow for a thorough characterisation of the temperature profile of the set-up. The tube furnace is connected to a gas analyser allowing to measure  $CO$ ,  $CO_2$  and  $O_2$  concentrations.

In order to demonstrate the functionality and accuracy of the balance, commissioning experiments have been conducted. This is done by comparing the results of the mass loss rate with the results of the gas composition measurements. For this purpose,  $CaCO_3$  powder is used, since upon heating it releases  $CO_2$ , while the  $CaO$  remains solid. The third paper will introduce the tube furnace and present the results of the commissioning experiments.

Additionally, it is aimed to compare the tube furnace with the TGA and the cone calorimeter. In order to avoid the complex nature of electrical cables, polymethyl methacrylate (PMMA) was chosen as a material to conduct a first comparison. A lot of literature data is available on PMMA, e.g. [21]. However, there is a large scatter in the available data, depending on the exact conditions of the experiments. Therefore, new experiments were performed in the different devices. When conducting PMMA experiments in the cone calorimeter, both transparent and black material was tested. The aim of this is to estimate the influence of different sample colour on its fire performance, as electrical cables also come in many different colours. The first paper presents the results of the cone calorimeter experiments and the influence

of the sample colour on its results. In the second paper, the influence of several different experimental and material conditions on the mass loss rate are tested, e.g. the influence of sample colour. The aim of this is to understand the deviation in mass loss curves within one device before comparing these results to another experiment set-up.

# CHAPTER 2

---

## Results

---

The main part of this thesis consists of three articles. The following section briefly summarizes the results of the articles.

### 2.1 Publication 1

The first paper investigates differences in the burning behaviour between transparent and black PMMA in the cone calorimeter [18, 19, 22]. The experiments were conducted at four different external heat fluxes ( $25 \text{ kW/m}^2$ ,  $35 \text{ kW/m}^2$ ,  $50 \text{ kW/m}^2$  and  $75 \text{ kW/m}^2$ ) to compare their autoignition time, HRR, mass loss rate and  $\text{CO}$ ,  $\text{CO}_2$  and  $\text{O}_2$  concentrations.

The experiments were performed using cast, 6 mm, transparent PMMA (0F00) and black PMMA (9H01) by Evonik Germany. A C, H, O analysis was conducted to confirm that the atomic composition of both types of PMMA are identical, within the measurement uncertainty. The study used a standardised cone heater, placed under a 2.6 m by 2.6 m hood, and a gas analysis system to measure the concentration of  $\text{O}_2$ ,  $\text{CO}_2$ , and  $\text{CO}$ , with a drift correction applied to the measured values. Methanol calibrations were conducted to validate the (HRR) measurements. The experiments were performed with the samples placed in a specimen holder with retainer frame [18] but without a grid. Stone wool insulation (TF plate from Rockwool) was used underneath the sample. All experiments were conducted in triplicate.

During the experiments it was observed, for both sample colours and all four heat fluxes, that ignition occurred at the cone heater rather than at the sample surface. Additionally, for all test conditions, it was seen that the sample deforms towards the conical heater and bubbles form on the surface of the sample during heating. For samples with a long ignition time, swelling or bending of the sample was observed before ignition. As is expected for cast PMMA, no dripping of the sample was noticed. However, ghost flames at the side of the sample holder were sometimes seen during the experiments.

Within the measurement uncertainty, there is no noticeable difference between the ignition time of cast black and cast transparent PMMA samples. After ignition all samples show a fast rising HRR, until a more stable plateau is reached. In this



plateau, the HRR is still slowly rising until the maximum HRR. Afterwards a fast drop in HRR occurs, which ends in a slowly fading tail at which only some leftover material below the edge of the retainer frame is still burning. The tests performed at low external heat flux ( $25 \text{ kW/m}^2$ ) show a very large uncertainty, due to large fluctuations in ignition time between different repetitions. For some samples, up to 50% of the mass was lost before ignition. All differences between black and transparent PMMA are within uncertainty for this low heat flux. For the higher external heat fluxes ( $35 \text{ kW/m}^2$ ,  $50 \text{ kW/m}^2$  and  $75 \text{ kW/m}^2$ ), black PMMA shows a more stable plateau phase, and the transparent PMMA had a higher peak HRR. The differences between the two types of PMMA become more pronounced at higher external heat fluxes. Based on the difference in measured  $\text{O}_2$  and  $\text{CO}_2$  concentration, other small molecules like for example water are also formed in the burning process.

The difference in behaviour between black and transparent PMMA can be due to the difference in absorption coefficient. While black PMMA has a constant absorption coefficient of 0.94, the absorption coefficient for transparent PMMA decreases with increasing temperature of the radiator [23]. For example, for a heater temperature of 1000 K (at  $50 \text{ kW/m}^2$ , the cone heater has a temperature of 1010 K), this absorption coefficient becomes 0.85. Dedicated experiments to confirm the cause of the difference in behaviour between black and transparent PMMA are out of the scope of this paper.

## 2.2 Publication 2

For detailed flame spread modelling, reaction kinetics of the specific material considered in the flame spread are needed. It is common practise to derive these reaction kinetics from TGA data. A TGA measures the mass loss of a sample undergoing a pre-defined heating program, often a constant heating rate. Based on the obtained mass loss rate curves, kinetic parameters are derived. The obtained mass loss rates depend on the experimental conditions and on the material parameters of the tested samples. In this second publication, several experimental conditions and material parameters are studied to determine their influence on the mass loss rate. Additionally, three different TGA devices (referred to as TGA M, TGA L and TGA S) were used to determine the influence of a specific device. Figure 2.1 gives an overview of all the different conditions tested. The number of reactions, maximum mass loss rate, onset temperature and peak temperature are compared between the different experiments.

For this paper three different types of PMMA are used, referred to as 'PMMA 2016', 'PMMA 2020' and 'Transparent PMMA'. All three materials are cast plexiglass by Evonik. PMMA 2016 and PMMA 2020 are both black PMMA, PMMA 2016 was order in 20 mm thick samples in 2016, while PMMA 2020 was ordered in 2020 in 3 mm thick samples. Both samples have product code 9H01. The transparent PMMA was ordered in 2020, as 3 mm thick samples with product code 0F00. A C, H, O analysis was performed on all three samples. Within the measurement uncertainty, the atomic composition of all three materials is identical. Small discs with a diameter of 5 mm or 6 mm, and a thickness below 0.5 mm, have been cut out of the purchased material. For most of the experiments, 8.5 mg samples are used.

Apparatus	Sample colour	Material	Atmosphere	Heating rate	Sample mass	Purge gas
TGA M	Black	PMMA 2016	Air	2; 10; 60; 80 K/min	8.5 mg	
				5 K/min	8.5; 17; 35; 75 mg	
				20; 40 K/min	8.5 mg	
			Inert	2; 20; 40; 80 K/min	8.5 mg	
				5 K/min	8.5; 17 mg	
				10; 60 K/min	8.5; 15 mg	
TGA L	Black	PMMA 2016	Inert	5; 10; 20 K/min	8.5 mg	
				40 K/min	8.5 mg	20 ml/min 40 ml/min
	Transparent	PMMA 2020	Inert	5; 10; 20 ; 40 K/min	8.5 mg	
TGA S	Black	PMMA 2020	Inert	5 K/min	8.5 mg	20 ml/min 40 ml/min
				10; 20 K/min	8.5 mg	
	Transparent		Inert	5 K/min	8.5 mg	20 ml/min 40 ml/min
				10; 20 K/min	8.5 mg	

**Figure 2.1.:** Overview of the different conditions tested in the TGA.

To study the effect of varying mass, larger samples were examined as well.

Under inert atmosphere, PMMA decomposes in three to four reactions: two smaller reactions, caused by impurities and end-chain scission; one main reaction driven by random chain scission and sometimes a small shoulder behind the main reaction is present. The tested PMMA shows a similar behaviour, where the smaller peaks before the main reaction are not always clearly distinguishable. Under air atmosphere PMMA starts reacting later, the reactions caused by end chain-scission and impurities are not present, while the main reaction starts earlier compared to the inert atmosphere. Under air atmosphere it has been observed that the TGA samples form bubbles while reacting. It is expected that this also happens under nitrogen atmosphere, although this was not visually confirmed.

Under inert atmosphere, large differences were found between two of the TGAs, 30 °C difference in onset temperature and 14 °C in peak temperature. This is assumed to be caused by the not well regulated heating rate of one of the two TGAs. Different flow rates were tested under inert atmosphere, under these conditions the flow rate does not have any significant effect on the mass loss rate. Under both inert and air atmosphere, the maximum mass loss rate shifts to higher temperature and is larger for higher heating rates, as has also been previously shown in literature. Under air atmosphere, low heating rates (e.g. 2 K/min and 5 K/min) have poorer reproducibility than higher heating rates and a different number of reactions is needed to model the mass loss rates depending on the heating rate. The poor reproducibility is assumed to be caused by the formation of large bubbles at low heating rates. Under inert atmosphere, two different masses were tested for 5 K/min, 10 K/min and 60 K/min. For low heating rates no difference in mass loss rate was found, for 60 K/min the relative importance of the different reactions changes. Under air atmo-

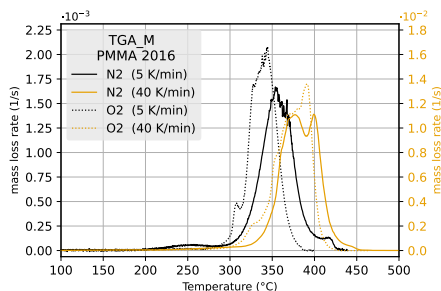


**Figure 2.2.:** Mass loss rate of PMMA 2016 for 5 K/min and 40 K/min under air and under nitrogen atmosphere.

sphere, both the amount of distinguishable reactions and the relative importance of the reactions, changes with sample mass. Changing from a sample mass of 8.5 mg to 75 mg results in a shift of 33 °C in peak temperature. The biggest difference in mass loss rates is between different atmospheres. Depending on the surrounding atmosphere different reactions take place resulting in completely different mass loss rates. As an example, the comparison between nitrogen and air atmosphere is shown in figure 2.2 for 5 K/min and 40 K/min. For 5 K/min, the main reaction starts earlier under air atmosphere, while the smaller peaks (around 250 °C for 5 K/min) before the main reaction are not present under nitrogen atmosphere.

When modelling fire spread, different experimental conditions should be taken into account, depending on the phase that is being modelled. Depending on the accuracy needed for prediction of the kinetic parameters based on mass loss rates measured in the TGA, effects like the lay-out of the device might have to be taken into account in the model used to determine the kinetic parameters.

## 2.3 Publication 3

The third publication introduces a tube furnace as a new gram-scale pyrolysis experiment. The paper first introduces the new experimental set-up. A thorough characterisation of the boundary conditions of the oven is presented and the functionality of the newly designed balance is proven.

A schematic view of the experiment set-up is shown in figure 2.3, more detailed technical drawings can be found in appendix I. A sample can be introduced into the oven with a step-motor, allowing both experiments at a constant temperature or at a constant heating rate. The set-up is based on the ISO 19700, in this norm the sample is moved into the oven at a continuous rate; this is not possible in the adjusted set-up. The flow gas composition and flow rates through the tube are controlled with mass flow controllers. Gas is introduced at the upstream end of the quartz glass tube. At the downstream end of the oven, a mixing piece is installed. This gas mixer is needed to ensure that the pyrolysis gases are full mixed with the carrier gas before being introduced into the gas analyser. This analyser is connected with the glass tube after a conical reduction. The analyser can measure

CO, CO<sub>2</sub> and O<sub>2</sub>. At the sample region of the oven, thermocouples are installed at the outside. Additionally, thermocouples can be installed on the inside of the glass tube to do temperature measurements in the sample region. However, temperature measurement at the inside of the glass tube can not be performed simultaneously with the mass loss measurement.

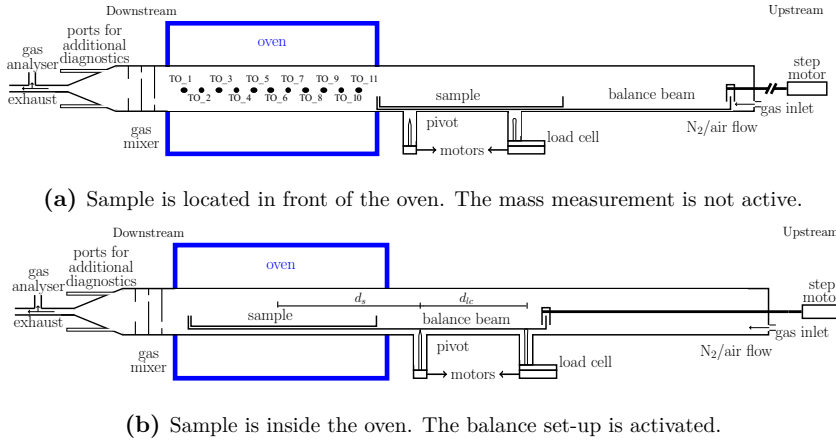


**Figure 2.3.:** Schematic picture of the set-up.

An online mass loss measurement is enabled using a cantilever mechanism. The sample is connected with the load cell via a balance beam. The center of the balance beam rests on a pivot, while the downstream side of the balance beam is free and the upstream side is lying on the load cell. When the pyrolysis process starts, the sample will lose mass resulting in a force on the load cell. This force can be converted to a mass loss of the sample, assuming the mass was lost symmetrically around the center of mass of the sample.

In order to characterize the thermal boundary conditions, thermocouple measurements were made both at the in- and outside of the tube, for heating rates of 5 K/min and 3 K/min. In the sample region, a maximum temperature difference of 142 K was measured at 1173 K. The temperature distribution is mostly symmetric around the sample, although the upstream side is slightly colder due to the inflow of fresh air or nitrogen.

The previous two publications have demonstrated that the burning and pyrolysis behaviour of PMMA is more complex than originally thought. Therefore, an easier material was chosen to conduct the commissioning experiments in the tube furnace. Preferably, this material would have only one single reaction peak. Additionally, it is preferred that this reaction would release CO or CO<sub>2</sub>, since this would allow correlating the mass loss data measured by the balance with the CO<sub>2</sub> measured by the gas analyser. Thus, calcium carbonate (CaCO<sub>3</sub>) was chosen for the commissioning experiments. It releases CO<sub>2</sub> upon heating, while calcium oxide (CaO) remains in solid form:



The  $\text{CaCO}_3$  experiments were conducted at constant heating rates (3 K/min and 5 K/min) and at two different masses (8.5 g and 25 g). An excellent agreement was found between the mass loss rate and the  $\text{CO}_2$  production rate for both heating rates and both masses. It can be concluded that the newly installed balance is working.

The mass loss rate of  $\text{CaCO}_3$  in the tube furnace was compared for 3 K/min and 5 K/min with mass loss rates from TGA experiments. The shape of the mass loss rate is similar in the tube furnace and the TGA, although the tube furnace has a wider peak. It is expected that the onset temperature between the TGA and the tube furnace is the same. In order to measure the onset temperature in the tube furnace, a thermocouple would have to be installed at the hottest point of the sample. This would be the sample surface in the centre of the oven. Unfortunately, with a pulverised sample it is not possible to precisely install a thermocouple at the surface of the sample. Further experiments with a solid sample are advised.

In conclusion, the third paper has introduced the new experimental set-up, has demonstrated its functionality and a first comparison with the TGA was done, using  $\text{CaCO}_3$ .

## 2.4 Comparison between the TGA, cone calorimeter and the tube furnace

In order to further compare the tube furnace with the TGA and the cone calorimeter, experiments with cast transparent PMMA from Evonik (0F00) and cast black PMMA (9H01) with 6 mm thickness in the tube furnace were conducted. The samples had a length of 50 cm and a width of 2 cm, resulting in a sample mass of around 67 g. Samples were installed in the sample region between measurement positions TO1 and TO11. The inside of the specimen boat was covered with a thin layer of Boron nitride spray, to avoid that the PMMA would react with the quartz glass, destroying the specimen boat. Experiments were conducted both under air as well as under nitrogen atmosphere. Both atmospheres had a flow rate of 10 l/min. The heating rate was 5 K/min. The data was processed as explained in publication 3.

Figure 2.4 shows the normalised mass loss rate for both atmospheres and both colours. The results are the average of three experiments. A Savitsky Golay filter was used to smoothen the data (first order, 33 data points). An uncertainty band is plotted, taking into account the standard deviation determined from averaging.

Both the inert and the air experiments show a drop in mass loss rate shortly before 300 °C. This is the point where the sample starts reacting. The first part of the curve shows a lot of noise which is filtered out by the smoothing algorithm. At this point, the sample makes popping sounds. Therefore, it is assumed that this apparent increase in mass comes from volatile bursts of bubbles on the sample surface resulting in a strong and unstable force on the load cell. After this initial phase, the mass loss rate under air atmosphere increases linearly until the maximum mass loss rate is reached. The mass loss rate of the inert sample increases initially more slowly, but reaches a higher maximum mass loss rate than under air atmosphere. After the main peak, both mass loss rates show a linear decrease, until around 450 °C, where the decrease in mass loss rate is slowed down. It should be noted that

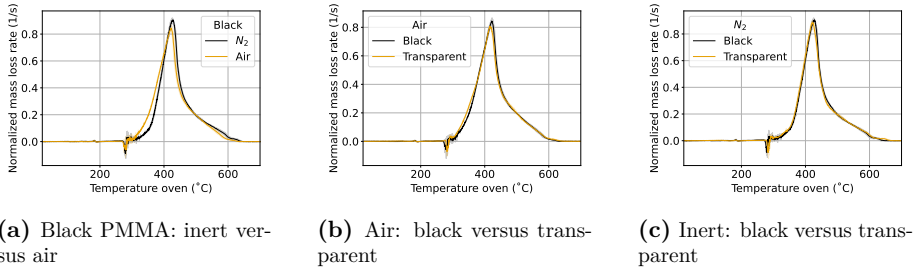


**Figure 2.4.:** Normalised mass loss rate of PMMA in the tube furnace

the samples did not ignite. In the tube furnace, there is no significant difference between the behaviour of transparent and black PMMA, both under nitrogen and air atmosphere.

A first comparison between the TGA and the tube furnace was presented in publication 3. As is indicated there, it is expected that the offset temperature of the reaction is the same between the TGA and the tube furnace. In order to compare these, the temperature needs to be measured at the hottest point of the sample, when a mass loss starts occurring. For this comparison, additional temperature measurements were conducted in the tube furnace. A thermocouple was installed at the middle of the sample to measure the surface temperature. In figure 2.5 the results of these measurements versus the measurement at position TO\_6 are shown. The result is the average of two repetition experiments, one standard deviation is shown as uncertainty. In solid gray, the average mass loss for PMMA under nitrogen atmosphere as function of TO\_6 is shown. The surface temperature has a linear increase until a sudden drop in temperature is reached. It should be noted that at this point the sample starts reacting, therefore it is no longer guaranteed that the thermocouple is in contact with the sample. The negative peak in temperature might be an apparent effect from the sample reacting away, rather than the actual sample temperature. A linear fit has been made through the surface temperature data. The mass loss rate data is plotted against this fitted temperature, the result is shown in the figure as a dashed gray line. It is this temperature that is used in the comparison with the TGA data, which is shown in figure 2.6. For both devices, the normalised mass loss rate is plotted.

From figure 2.6 it can be seen that the onset temperature of the main reaction peak is similar for the tube furnace as for the TGA, i.e. both onset temperatures are found to be 327°C. Here, the onset temperature is defined as the temperature at which 5% of the initial mass is lost. This is to be expected since the tube furnace data is plotted against the surface temperature at the hottest part of the sample, implying that the temperature measured here is the very first part of the sample starting to react. The small reactions before the main peak present in the TGA are less distinct for the tube furnace data. The normalised mass loss rate for the tube furnace extends over a longer temperature range as for the TGA, which is to be expected due to the larger amount of sample material and the temperature gradient in the oven. As demonstrated in the first publication, a difference in HRR after ignition and peak HRR was found between black and transparent PMMA in

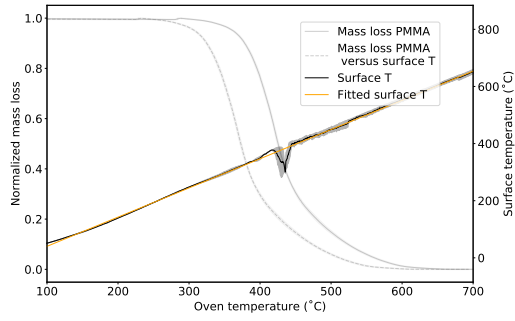


**Figure 2.5.:** Surface temperature of PMMA as function of TO\_6.

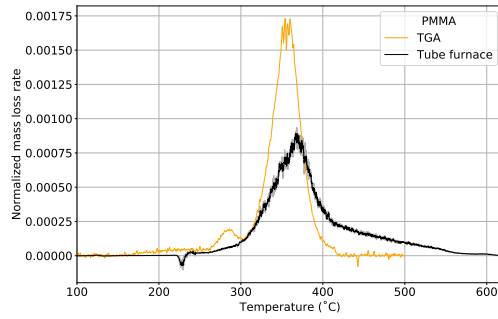


**Figure 2.6.:** Normalised mass loss rate in the tube furnace versus mass loss rate in the TGA for PMMA

the cone calorimeter. Nevertheless, in the tube furnace no difference was found between both samples. This could indicate that the heat transfer from the oven to the sample is less dominated by radiation. It should however also be considered that the temperature of the oven is significantly lower than the temperature of the heating element in the cone calorimeter. As is shown in [23, 24], the absorption coefficient of transparent versus black PMMA is more similar for low temperature radiators.

To conclude, a new experimental set-up for pyrolysis has been designed and implemented. Its functionality has been demonstrated. The first comparison between the tube furnace and the TGA has been made using  $\text{CaCO}_3$ . The next step is to construct a model that can be used to predict kinetic parameters based on tube furnace data. This would allow comparing flame spread predictions based on tube furnace data with predictions based on TGA data.





## CHAPTER 3

---

### Conclusion and outlook

---

In this thesis, a new experimental set-up to study the pyrolysis behaviour of gram scale samples has been introduced. The aim of this experiment was to combine the advantages of the TGA and the cone calorimeter. The newly introduced set-up is a tube furnace, in which an online mass loss measurement was enabled, using a cantilever mechanism. The functionality of the experiment was demonstrated with commissioning experiments using  $\text{CaCO}_3$ , in which very good agreement was found between the gas analyser and the balance. Further work should be performed to examine the influence of several experimental conditions on the mass loss rate of the samples. For example, different flow rates, different sample dimensions or masses as well as experiments at constant temperature should be examined.

Experiments with PMMA were conducted in the TGA and the cone calorimeter. The aim of these experiments was to compare the tube furnace with both devices. In the cone calorimeter, the difference in behaviour between black and transparent cast PMMA was examined. This was done for four different external heat fluxes ( $25 \text{ kW/m}^2$ ,  $35 \text{ kW/m}^2$ ,  $50 \text{ kW/m}^2$  and  $75 \text{ kW/m}^2$ ) under auto-ignition conditions. Three repetitions were done for each experiment. Within the measurement uncertainty, the ignition times for black and transparent PMMA are the same. The results for  $25 \text{ kW/m}^2$ , contain a large uncertainty due to the difference in ignition time between the different repetitions. Therefore, no conclusion can be made concerning the difference between black and transparent PMMA. For the higher heat fluxes, transparent PMMA shows a larger maximum HRR, while, black PMMA has a higher HRR right after ignition. The differences become larger for a higher external heat flux. It is assumed that these differences are caused by a difference in absorption coefficient between both materials. Dedicated experiments would have to be conducted to confirm this hypothesis. In the tube furnace, no difference in mass loss rate was found between black and transparent PMMA. This could be because the heat transfer is less dominated by radiation in the tube furnace, or because the temperature of the radiator is significantly lower in the tube furnace. It could be considered to conduct experiments at a constant high temperature with PMMA in the tube furnace to investigate whether there are differences between black and transparent PMMA.

In the TGA the influence of several experiment and material parameters on the mass loss rate of PMMA was studied. The biggest influence is the atmosphere. Since different reactions take place depending on the atmosphere, the mass loss rate curves for nitrogen or air atmosphere are not comparable. Both atmospheres have also been tested in the tube furnace. Similar as in the TGA the main reaction peak of the samples tested under air atmosphere starts earlier than the samples tested under an inert atmosphere.

It should be considered to conduct a more rigorous comparison between the three different devices. For example, it would be of interest to predict kinetic parameters with the tube furnace and compare those to the parameters found based on the TGA mass loss curves. In order to do this, a model considering the heat and mass transfer in the tube furnace should be built, so that this can be used for inverse modelling to estimate the parameters. Additionally, an appropriate method to measure the external heat flux that is received by the sample could be investigated. This would be beneficial for a better understanding and an easier comparison with the cone calorimeter. Additionally, it would make it easier to build a model for the tube furnace.

---

## Bibliography

---

- [1] Xinyan Huang and Yuji Nakamura. “A Review of Fundamental Combustion Phenomena in Wire Fires”. en. In: *Fire Technology* 56.1 (Jan. 2020). Company: Springer Distributor: Springer Institution: Springer Label: Springer Number: 1 Publisher: Springer US, pp. 315–360. ISSN: 1572-8099. DOI: [10.1007/s10694-019-00918-5](https://doi.org/10.1007/s10694-019-00918-5). URL: <https://link.springer.com/article/10.1007/s10694-019-00918-5> (visited on 12/28/2022).
- [2] Shelby Hall. *Fire in the United States 2005-2014*. Tech. rep. U.S. Fire Administration, Jan. 2017.
- [3] *Centre d’information pour la prévention des incendies: Statistiques sur les incendies et sur leurs conséquences*. Accessed: 2023-12-20.
- [4] *Institute fuer Schadenverhuetung und Schadenforschung: Ursachenstatistik*. Accessed: 2023-12-20.
- [5] *BBC Grenfell Tower What happend?* Accessed: 2022-03-11.
- [6] Shelby Hall. *Home structure fires*. Tech. rep. National Fire protection Association, 2023.
- [7] *Aerospace America War on wiring*. Accessed: 2023-11-19.
- [8] *Aviation safety network Monday 14 August 1972*. Accessed: 2023-12-23.
- [9] *Swissinfo Swiss aviation’s worst air disaster remembered 25 years on*. Accessed: 2023-12-23.
- [10] *Air Transport Intelligence Tu-154 fire sparked by electrical short-circuit: ministry*. Accessed: 2023-12-23.
- [11] NEA (2015). “Collection and Analysis of Fire Events (2010-2013) – Extensions in the Database and Applications: Fire Project Report”. In: *OECD Publishing* ().
- [12] R L Scott. “Browns Ferry nuclear power-plant fire on March 22, 1975”. In: *Nucl. Saf.; (United States)* 17.5 (Jan. 1976). URL: <https://www.osti.gov/biblio/7143173>.
- [13] M. Klauck et al. “Experimental investigation on the impact of cable fire products from flame-retardant cables on catalysts used in passive auto-catalytic recombiners”. In: *Progress in Nuclear Energy* 152 (2022), p. 104365. ISSN: 0149-1970. DOI: <https://doi.org/10.1016/j.pnucene.2022.104365>. URL: <https://www.sciencedirect.com/science/article/pii/S0149197022002402>.

- [14] Kevin McGrattan et al. *Cable Heat Release, Ignition, and Spread in Tray Installations During Fire (CHRISTIFIRE) Phase 1: Horizontal Trays*. Tech. rep. National Institute of Standards and Technology Engineering Laboratory; Fire Research Division Gaithersburg, Maryland 20899, July 2012.
- [15] Kevin McGrattan, Scott Bareham, and David Stroup. *Cable Heat Release, Ignition, and Spread in Tray Installations During Fire (CHRISTIFIRE) Phase 2: Vertical Shafts and Corridors*. Tech. rep. National Institute of Standards and Technology Engineering Laboratory; Fire Research Division Gaithersburg, Maryland 20899, Dec. 2013.
- [16] *Thermische Analyse (TA)-Thermogravimetrie (TG)- Grundlagen*. Standard. Berlin, Germany: DIN Deutsches Institut für Normung e.V, 2005.
- [17] A. W. Coats and J. P. Redfern. “Thermogravimetric analysis. A review”. en. In: *The Analyst* 88.1053 (1963), p. 906. ISSN: 0003-2654, 1364-5528. DOI: 10.1039/an9638800906. URL: <http://xlink.rsc.org/?DOI=an9638800906> (visited on 06/05/2022).
- [18] *Reaction-to-fire tests — Heat release, smoke production and mass loss rate — Part 1: Heat release rate (cone calorimeter method) and smoke production rate (dynamic measurement)*. Standard. Geneva, CH: International Organization for Standardization, Mar. 2015.
- [19] Vytenis Babrauskas. *Development of the Cone Calorimeter - A Bench-Scale Heat Release Rate Apparatus Based on Oxygen Consumption*. English. Tech. rep. Washington, DC 20234: U.S. DEPARTMENT OF COMMERCE National Bureau of Standards Center for Fire Research, Nov. 1982. URL: <https://nvlpubs.nist.gov/nistpubs/Legacy/IR/nbsir82-2611.pdf>.
- [20] *Controlled equivalence ratio method for the determination of hazardous components of fire effluents — Steady-state tube furnace*. Standard. Geneva, CH: International Organization for Standardization, 2016.
- [21] Benjamin Batiot et al. *The MaCFP Condensed Phase Working Group - Modeling*. 13th International Symposium on Fire Safety Science. Apr. 2021.
- [22] B. Scharrel and T. R. Hull. “Development of fire-retarded materials—Interpretation of cone calorimeter data”. In: *Fire and Materials* 31.5 (2007), pp. 327–354. ISSN: 1099-1018. DOI: 10.1002/fam.949.
- [23] Morgan J. Hurley et al., eds. *SFPE Handbook of Fire Protection Engineering - 5th ed.* en. 5th ed. New York, NY: Springer New York, 2016. ISBN: 978-1-4939-2564-3 978-1-4939-2565-0. DOI: 10.1007/978-1-4939-2565-0. URL: <http://link.springer.com/10.1007/978-1-4939-2565-0> (visited on 03/02/2023).
- [24] Farid Alinejad et al. “Spectroscopic determination of the optical constants and radiative properties of black PMMA for pyrolysis modeling”. In: *International Journal of Thermal Sciences* 176 (2022), p. 107501. ISSN: 1290-0729. DOI: <https://doi.org/10.1016/j.ijthermalsci.2022.107501>. URL: <https://www.sciencedirect.com/science/article/pii/S1290072922000412>.

---

## Comparison of black and transparent PMMA in the cone calorimeter

---

**Note:** This article was published as K. De Lannoye, A. Belt, E.-A. Reinecke, F. Markert, and L. Arnold, “Comparison of Black and Transparent PMMA in the Cone Calorimeter,” in Obtaining Data for Fire Growth Models, ed. M. C. Bruns and M. L. Janssens (West Conshohocken, PA: ASTM International, 2023), 150–160. <http://doi.org/10.1520/STP164220210105>

### Author Contributions

CONCEPTUALIZATION: Karen De Lannoye and Alexander Belt

DATA CURATION: Karen De Lannoye

FORMAL ANALYSIS: Karen De Lannoye

FUNDING ACQUISITION: Ernst-Arndt Reinecke and Lukas Arnold

INVESTIGATION: Karen De Lannoye

METHODOLOGY: Karen De Lannoye

SUPERVISION: Alexander Belt, Ernst-Arndt Reinecke, Lukas Arnold

VISUALIZATION: Karen De Lannoye

WRITING—ORIGINAL DRAFT PREPARATION: Karen De Lannoye

WRITING—REVIEW AND EDITING: Karen De Lannoye, Alexander Belt, Ernst-Arndt Reinecke, Frank Markert and Lukas Arnold

---

# COMPARISON OF BLACK AND TRANSPARENT PMMA IN THE CONE CALORIMETER

---

**K. De Lannoye<sup>a,b</sup>, A. Belt<sup>a</sup>, E.-A. Reinecke<sup>b</sup>, F. Markert<sup>c</sup>, and L. Arnold<sup>a,d</sup>**

<sup>a</sup>Institute for Advanced Simulation (IAS-7), Forschungszentrum Jülich, Wilhelm-Johnen-Straße, 52428 Jülich, Germany

<sup>b</sup>Institute for Energy and Climate (IEK-14), Forschungszentrum Jülich, Wilhelm-Johnen-Straße, 52428 Jülich, Germany

<sup>c</sup>Technical University of Denmark, Dept. of Civil and Mechanical Engineering, Brovej 118, 2800 Kgs. Lyngby, Denmark

<sup>d</sup>University of Wuppertal, Computational Civil Engineering, Gaußstraße 20 42119 Wuppertal, Germany

First Author: [k.de.lannoye@fz-juelich.de](mailto:k.de.lannoye@fz-juelich.de); ORCID: 0000-0003-2617-5557

Second Author: [a.belt@fz-juelich.de](mailto:a.belt@fz-juelich.de); ORCID: 0000-0002-6091-9321

Third Author: [e.-a.reinecke@fz-juelich.de](mailto:e.-a.reinecke@fz-juelich.de); ORCID: 0000-0003-1414-9183

Fourth Author: [fram@dtu.dk](mailto:fram@dtu.dk); ORCID: 0000-0002-1396-2810

Fifth Author: [l.arnold@fz-juelich.de](mailto:l.arnold@fz-juelich.de); ORCID: 0000-0002-5939-8995

## ABSTRACT

The cone calorimeter is one of the standard devices used to assess the flammability of polymers. Several publications have been made studying different types of polymers and different set-ups in this apparatus. Polymers come in different forms and colors. It is unknown, however, whether the color of a polymer influences its burning behavior in the cone calorimeter. The color of a sample influences the amount of absorbed and reemitted thermal radiation, emitted by the cone calorimeter. This contribution presents the effect of different sample colors by performing cone calorimeter experiments with both transparent and black polymethyl methacrylate (PMMA) plates. Experiments were performed for four different heat fluxes: 25 kW/m<sup>2</sup>, 35 kW/m<sup>2</sup>, 50 kW/m<sup>2</sup>, and 75 kW/m<sup>2</sup>. All tests were autoignition experiments and 6-mm-thick PMMA plates were used. The effect of sample color on autoignition time, heat release rate, and mass loss data as well as oxygen (O<sub>2</sub>), carbon monoxide (CO), and carbon dioxide (CO<sub>2</sub>) production was assessed. Black PMMA showed a higher heat release rate (HRR) in the beginning of the tests, whereas transparent PMMA has a higher peak HRR. The color of the samples does not seem to influence the ignition time.

**Keywords** cone calorimeter · color effect · polymethyl methacrylate · transparent PMMA · black PMMA

## 1 Introduction

Polymethyl methacrylate (PMMA) is a frequently studied polymer in fire research because of its simple burning behavior: it degenerates almost completely to monomer MMA. Several studies on the behavior of black PMMA plates in the cone calorimeter have been published [1–5]. However, few publications have studied nonblack (transparent or colored) PMMA, despite PMMA being used in many different colors and forms (e.g., as decoration material or shielding in buildings). Transparent PMMA often is used to replace glass constructions.

Some publications have indirectly studied the effect of color. For example, Schartel et al.[6] studied the effect of, among other things, black composites on the absorption coefficient of the material. Few previous studies have focused on the differences in burning behavior between transparent and black PMMA specimens in the cone calorimeter. A comparison between the pyrolysis of black cast and transparent extruded PMMA was made by Fiola, Chaudhari, and Stoliarov [7]. They concluded that the pyrolysis properties of these materials were adequately comparable to be represented with a generic model. An article comparing transparent and black PMMA [8] was published, but the black PMMA

Table 1: The mass composition (C, H, O) of the sample materials

Element	Transparent	Black
C (wt%)	$59.7 \pm 0.1$	$59.8 \pm 0.5$
H (wt%)	$7.83 \pm 0.01$	$7.75 \pm 0.09$
O (wt%)	$32.4 \pm 0.01$	$32.4 \pm 0.01$

samples were thicker than the transparent slabs in this study. The authors concluded that the black PMMA samples had a prolonged steady burning period compared with transparent specimens, which they suggested might have been due to a larger thermal capacity of black PMMA. In the same paper, however, they concluded that the thicker slabs had longer steady burning periods, based on a study with different thickness of transparent slabs.

This paper focuses on comparing black and transparent PMMA without varying other parameters of the samples. Transparent and black PMMA slabs were investigated in the cone calorimeter. Experiments with four different heat fluxes were performed, while the heat release rate (HRR) and mass loss of the samples were recorded. All experiments were repeated in triplicate.

## 2 Sample Material

PMMA is a thermoplastic material. When PMMA is heated to sufficiently high temperatures, monomer methyl methacrylate (MMA) is released due to end-chain scission and random chain scission [9]. The mechanisms initiating the scission processes are different under inert and oxidative environments. Nevertheless, in both cases, monomer MMA is formed. The MMA is released from the solid material. Almost no dripping is observed when PMMA is heated. MMA further decomposes to lighter gaseous products, like carbon monoxide (CO) and carbon dioxide (CO<sub>2</sub>). The PMMA used for the experiments is Plexiglass by Evonik.[\*] Both transparent and black PMMA were cast, with the respective color codes of CLEAR 0F00 and Black 9H01. The samples were 6mm thick and had a surface of 100 mm by 100 mm. An analysis of the atomic composition, regarding carbon (C), hydrogen (H), and oxygen (O) content, was conducted for both samples. The results are shown in table 1. For this analysis, a 2-mg piece of the material was placed in an elemental analyzer (i.e., vario EL cube by Elementar). This process was repeated three times for every mode (C, H, N mode and O mode). As shown in the table, the amounts of C, H, and O atoms present in both sample types are nearly identical.

## 3 Method

A standardized cone heater by Fire Testing Technology Ltd. [10] was used to conduct the experiments. The cone heater used in the set-up was placed under a hood with dimensions of 2.6m x 2.6 m.

The pyrolysis and combustion products coming from the tested sample are collected in the extraction hood. An exhaust fan directs the collected flue gases to the duct. In the exhaust duct, a sampling ring draws the combustion gases into the Servomex (ServoPro 4100) gas analysis system of the cone calorimeter. The gas analysis system is equipped with O<sub>2</sub>, CO<sub>2</sub>, and CO analyzers which measure the volume fractions of O<sub>2</sub>, CO<sub>2</sub>, and CO in the sampled gas, respectively. These fractions were then used to calculate the heat release rate determined on the principle of oxygen consumption as outlined by Janssens [11].

The gas analyser was calibrated at the beginning of every experiment day. Pure nitrogen (99.999 %) was used for the null calibration. For CO and CO<sub>2</sub>, the following concentrations were used for calibration: (5,000 ± 100) ppm and (5.00 ± 0.10) mol% respectively. For O<sub>2</sub>, there was no dedicated calibration gas. Calibration was conducted using air, assuming 20.95 mol% oxygen.

Methanol calibrations (99.8%) were done to check the correctness of the calculated HRR. To do so, methanol was burned under the nonheated cone heater, while the mass loss and HRR were determined. The theoretical value for the HRR, which is determined by multiplying the measured mass loss rate by the theoretical heat of combustion per unit mass (22.68 kJ/g) [11], is compared with the measured value. Figure 1 presents the results of one of these comparisons. It was concluded that the time-variant traces of experimentally obtained and theoretical HRR were comparable.

The delay time for the gas analysis was determined, using methanol as described in ISO5660 [10]. The quantification of the delay time was repeated three times on different days during the experimental period. The average delay time was estimated to be (28 ± 3) s.

The measured O<sub>2</sub>, CO<sub>2</sub>, and CO concentrations from the gas analyzer were used to determine the HRR. The gas analyzer showed a small drift over the time of the experiment. Therefore, a drift correction was done on the measured values before the results were used to calculate the HRR. This was done by fitting a linear function through the starting points of the experiment, before the shutter was opened, and the end points of the experiments, after the sample was



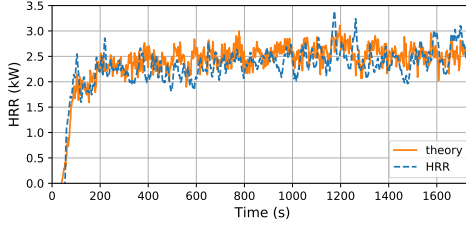


Figure 1: Experimentally obtained and theoretical HRR for methanol as a function of time.

burned away. This fit was then subtracted from the measured data. A Savitzky-Golay filter [12] was applied to the HRR and mass loss data. Here, a filter with second-order polynomial and 91 data points was applied to all captured time series.

The samples were placed into a specimen holder, a description of the holder can be found in ISO5660 [10]. All experiments were conducted with retainer frame but without wire grid. According to Schartel, Bartholmai, and Knoll [13] the external heat flux as function of the distance to the cone heater is considered homogeneously enough to test samples that deform less than 2.5 cm without grid. Below the sample, the frame was filled up with approximately 4.5 cm of insulation material. Stone wool, specifically TF plate from Rockwool, with a thermal conductivity of 0.039 W/(m K) was used as insulation. No aluminum foil was placed between the sample and the insulation, which is often done to avoid dripping of the sample. Dripping of the samples was not observed in the experiments. Nevertheless, ghost flames on the side of the sample holder were sometimes observed. Additionally, no residue of the sample was found on the insulation material after the experiment.

Experiments were carried out with heat fluxes of 25 kW/m<sup>2</sup>, 35 kW/m<sup>2</sup>, 50 kW/m<sup>2</sup>, and 75 kW/m<sup>2</sup>. Every experiment was repeated three times. Before every experiment, the heat flux was checked with a water-cooled heat flux sensor. The deviation in measured heat flux was never larger than 0.2 kW/m<sup>2</sup> from the aimed value. The heat flux sensor was centrally positioned 25 mm below the base of the cone heater, which was consistent with the separation distance between the exposed sample surface and the bottom of the heater. All experiments were run under autoignition conditions.

## 4 Results

The datasets resulting from the experiments conducted in the scope of this article are publicly available in a repository [14]. In table 2, the average ignition times for the different experiments are shown. These times were determined by the appearance of flames in the recordings of the experiments. As shown in figure 2, the pyrolysis gas ignites at the cone heater, rather than close to the sample surface. This was observed for both colors at all four heat fluxes. The pictures displayed in figure 2 are from an experiment with a transparent sample at an external heating flux of 35 kW/m<sup>2</sup>.

During the experiments, we observed that the sample surfaces deformed. An example is shown in figure 3. The

Table 2: Ignition times

Heating power, kW/m <sup>2</sup>	Ignition time of transparent sample, s	Ignitions time of black sample, s
25	350 ± 29	461 ± 154
35	90 ± 6	90 ± 6
50	25 ± 4	31 ± 2
75	14 ± 1	13 ± 3

swelling of the surface was observed for both transparent and black samples. For samples with a longer ignition time, swelling could be observed before ignition. In addition, bubble formation on top of the sample surface was perceived for both colors at all four heat fluxes.

In this work, the HRR and specimen mass is reported as the average of the time-indexed HRR and sample mass for the three replicate tests conducted at a prescribed incident heat flux level. Average HRR and specimen mass traces are shown in figure 4. The average HRR is expressed per unit area of sample surface, and 0.0088 m<sup>2</sup> is used as area because this is the window size in the retainer frame. The results for the transparent plates are plotted in orange, and the results for the black plates are plotted in black, with solid and dashed lines corresponding to HRR and specimen mass, respectively. An uncertainty band of one standard deviation is added to all plots in the corresponding transparent color. The only uncertainty that has been taken into account is the standard deviation when averaging.

Figure 2: Close-up from sample ignition.

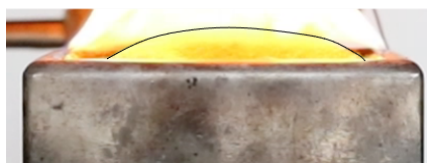
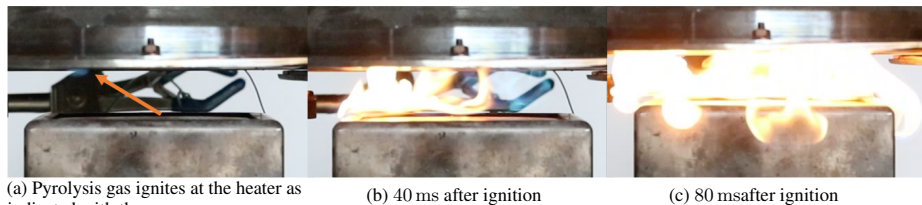
Figure 3: Swelling of a sample during an experiment, for a transparent sample at a heat flux of  $35 \text{ kW/m}^2$ .

Figure 5 is an overview of the averaged  $\text{O}_2$ ,  $\text{CO}_2$ , and  $\text{CO}$  concentrations for both materials at four different levels of incident heat flux. The results for the black samples are plotted in black, and the results for the transparent samples are plotted in orange. As stated in the “Method” section a drift correction was performed on the  $\text{O}_2$ ,  $\text{CO}_2$ , and  $\text{CO}$  traces. In the plots, the concentration at the start of the experiments is putted to 0 % or 0 ppm; thus, only the relative increase or decrease in concentration during the experiment is shown. An uncertainty band of one standard deviation is plotted in the shaded corresponding color.

## 5 Discussion

Taking into account the uncertainties on the ignition time, there does not seem to be a difference in ignition time for black versus transparent PMMA. For experiments conducted at a lower heat flux ( $25 \text{ kW/m}^2$ ), the uncertainty is larger. This is because for lower heat fluxes there is a bigger dependency on environmental variabilities, as has been reported by Tsai et al [4].

The averaged HRR and specimen mass traces were presented in the previous section. The HRR at  $25 \text{ kW/m}^2$  has a large uncertainty. This is partially caused by the big deviations in ignition time for this heat flux. For this low heat flux experiments, up to 50 % of the mass is lost before ignition. There seems to be large differences in the HRR of black and transparent PMMA subjected to an external heat flux of  $25 \text{ kW/m}^2$ . The uncertainties on these measurements are so large, however, that it is not possible to draw a conclusion on the difference between transparent and black PMMA. The effect of external factors might be bigger than the difference between transparent and black PMMA. The experiments conducted for the higher external heat fluxes have very good reproducibility.

The HRR increases fast from zero to a plateau, once the sample ignites. During the plateau, the whole sample is burning. After reaching the peak HRR, there is a sharp decrease in HRR. This decrease ends in a tail, at which point, most of the material is already burned away. A small amount of material still burns in the edges, until all material is burned away. It is expected that this tail would not exist if the tests were performed without a sample frame. This behavior is exactly what is to be expected for a thick to intermediate thick noncharring sample [15].

For  $35 \text{ kW/m}^2$ ,  $50 \text{ kW/m}^2$ , and  $75 \text{ kW/m}^2$ , the mass loss shows similar behavior: starting with a small plateau, followed by a steep decline and a slow burning out phase, where the starting plateau lasts longer for lower external heat fluxes. The steep decline in the mass loss trace starts at the moment the sample ignites. Toward the end of the experiment, the flame becomes smaller, as more and more of the fuel material is used up. In this final stage, eventually only some material will be left on the sides or in the corners of the sample holder, which will slowly burn up.

From the average gas concentrations, it can be seen that the largest part of the oxygen consumed by the samples is transformed into  $\text{CO}_2$ . The  $\text{O}_2$  consumption has the same form as the  $\text{CO}_2$  production. The oxygen consumption, however, is slightly higher than the amount of  $\text{CO}_2$  produced. The rest of the oxygen will be consumed in the creation of other small gaseous species, such as water. During the experiments, there is a small rise in  $\text{CO}$  concentration. The  $\text{CO}$  concentration follows a similar trend as the  $\text{CO}_2$  concentration, but the amounts are much smaller. This result is

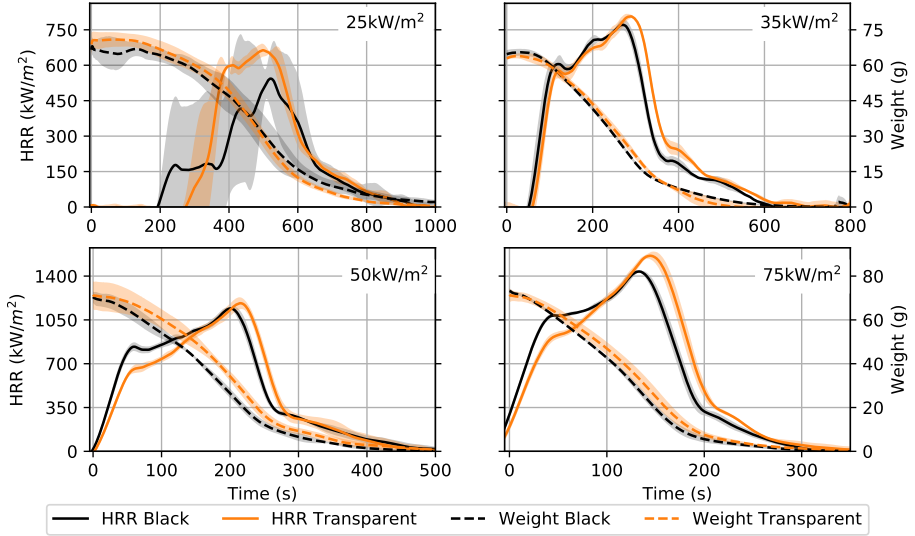


Figure 4: Average HRR per unit area and specimen mass as function of time for black and transparent PMMA. Exposure to four different external heat flux levels: 25 kW/m<sup>2</sup>, 35 kW/m<sup>2</sup>, 50 kW/m<sup>2</sup>, and 75 kW/m<sup>2</sup>.

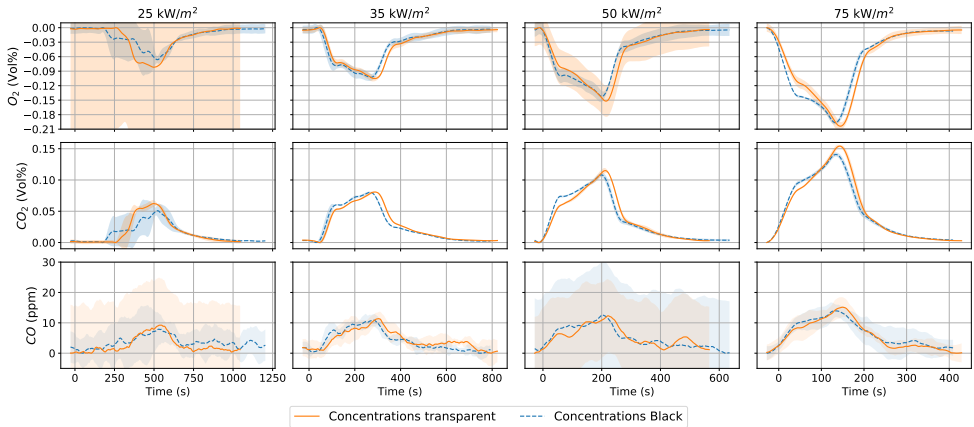


Figure 5: The average O<sub>2</sub>, CO<sub>2</sub>, and CO concentration for black (plotted in dashed) and transparent (plotted in solid) samples. From left to right: 25 kW/m<sup>2</sup>, 35 kW/m<sup>2</sup>, 50 kW/m<sup>2</sup>, and 75 kW/m<sup>2</sup>.

expected for experiments conducted in well-ventilated environments [8]. As with the previous results, the  $25 \text{ kW/m}^2$  tests have a rather large uncertainty.

For tests conducted at  $35 \text{ kW/m}^2$ , there are only small differences between black and transparent samples regarding average and peak HRR and mass loss. For  $50 \text{ kW/m}^2$  and  $75 \text{ kW/m}^2$ , the mass loss for the black samples is slightly faster until the peak HRR. For  $50 \text{ kW/m}^2$  and  $75 \text{ kW/m}^2$ , the initial increase in HRR takes longer for the black samples. The black samples show a more stable plateau than the transparent samples. Yet, the transparent samples have a higher peak HRR, which is reached a bit later than the peak HRR from the black samples. After the peak HRR value, both types of samples behave similar. The differences regarding average HRR, peak HRR, and mass loss between black and transparent samples become larger for higher external heat fluxes.

The different behavior for black and transparent PMMA might be caused by a difference in absorption factor. According to Lautenberger et al. [16], the total hemispherical absorptivity is about 0.94 for black PMMA and 0.85 for transparent PMMA when irradiated by a black body emitter with a temperature of 1000 K. Although the integrated surface absorptivity remains constant for black samples when the temperature of the black body rises, it decreases for transparent PMMA. Note that the temperature of the heater is around 1010 K for an external heat flux of  $50 \text{ kW/m}^2$  and 1135 K for  $75 \text{ kW/m}^2$ . This difference in absorptivity might be the reason for the different behavior; however, no dedicated measurements of, for example, the absorption coefficients of these specific samples, have been conducted to confirm this hypothesis.

## 6 Conclusions

A comparison of the burning behavior of black versus transparent PMMA in the cone calorimeter was made with respect to autoignition times, average and peak HRR, and mass loss, as well as  $\text{O}_2$ ,  $\text{CO}_2$ , and CO production. Experiments were performed for four different heat fluxes ( $25 \text{ kW/m}^2$ ,  $35 \text{ kW/m}^2$ ,  $50 \text{ kW/m}^2$ , and  $75 \text{ kW/m}^2$ ), and three repetitions were done for each experiment. Based on the results, it can be concluded that there is no significant difference in ignition time for the two types of samples. The uncertainties on the  $25 \text{ kW/m}^2$  experiments are too large to draw any conclusion about the different behavior for black and transparent PMMA. For the other experiments, the black samples show a higher increase in HRR right after ignition. The black samples have a more slowly rising plateau phase, and the transparent samples have a higher peak HRR. The differences between black and transparent samples increase with external heat flux.

The differences in behavior between the black and transparent samples might be caused by a difference in absorption coefficient. More dedicated studies would have to be performed to confirm this. The experiment could be performed with different colors of PMMA that would have a different absorption coefficient. PMMA in a cone calorimeter could be studied numerically, while varying the absorption coefficient for different runs.

Additionally, it would be of importance to test whether differences in burning behavior of black and transparent PMMA also manifest themselves in full-scale fires. Similarly, it would be of interest to study whether models, such as the Fire Dynamics Simulator, would predict different outcomes for large-scale experiments based on the difference in cone calorimeter data.

## 7 References

1. J. Luche, T. Rogaume, F. Richard, and E. Guilleme, "Characterization of Thermal Properties and Analysis of Combustion Behavior of PMMA in a Cone Calorimeter," *Fire Safety Journal* 46 (2011): 451–461.
2. L. Shi and M. Chew, "Fire Behaviors of Polymers under Autoignition Conditions in a Cone Calorimeter," *Fire Safety Journal* 61 (2013): 243–253.
3. B. Rhodes and J. Quintiere, "Burning Rate and Flame Heat Flux for PMMA in a Cone Calorimeter," *Fire Safety Journal* 26 (1996): 221–240.
4. T. Tsai, M. Li, I. Shih, R. Jih, and S. Wong, "Experimental and Numerical Study of Autoignition and Pilot Ignition of PMMA Plates in a Cone Calorimeter," *Combustion and Flame* 124, no. 3 (2001): 466–480.
5. D. Huang, C. Wang, Y. Shen, P. Lin, and L. Shi, "Fire Behaviors of Vertical and Horizontal Polymethyl Methacrylate Slabs under Autoignition Conditions," *Process Safety Progress* 39, no. 3 (2020): 1–12.
6. B. Scharrel, U. Beck, H. Bahr, A. Hertwig, U. Knoll, and M. Weise, "Sub-Micrometre Coatings as an Infrared Mirror: A New Route to Flame Retardancy," *Fire and Materials* 36, no. 8 (2012): 671–677.
7. G. Fiola, D. Chaudhari, and S. Stoliarov, "Comparison of Pyrolysis Properties of Extruded and Cast Poly(Methyl Methacrylate)," *Fire Safety Journal* 120 (2021): 103083.

8. W. Zeng, S. Li, and W. Chow, "Preliminary Studies on Burning Behavior of Polymethyl- Methacrylate (PMMA)," *Journal of Fire Sciences* 20, no. 4 (2002): 297–317.
9. W. Zeng, S. Li, and W. Chow, "Review on Chemical Reactions of Burning Poly(Methyl Methacrylate) PMMA," *Journal of Fire Sciences* 20, no. 5 (2002): 401–433.
10. Reaction-to-Fire Tests—Heat Release, Smoke Production and Mass Loss Rate—Part 1: Heat Release Rate (Cone Calorimeter Method) and Smoke Production Rate (Dynamic Measurement), ISO5660-1.2015(E) (Geneva, Switzerland: International Organization for Standardization, March 2015).
11. M. Janssens, "Calorimetry," in *SFPE Handbook of Fire Protection Engineering*, 5th ed., ed. M. Hurley (New York, NY: Springer, 2016), 905–951.
12. A. Savitzky and M. Golay, "Smoothing and Differentiation of Data by Simplified Least Squares Procedure," *Analytical Chemistry* 64 (1964): 1627–1639.
13. B. Schartel, M. Bartholmai, and U. Knoll, "Some Comments on the Use of Cone Calorimeter Data," *Polymer Degradation and Stability* 88 (2005): 540–547.
14. K. De Lannoye, A. Belt, E. Reinecke, F. Markert, and L. Arnold, "Data Repository: Comparison of Black and Transparent PMMA in the Cone Calorimeter," *Zenodo* (2022), <https://doi.org/10.5281/zenodo.6301397>
15. B. Schartel and T. Hull, "Development of Fire-Retarded Materials—Interpretation of Cone Calorimeter Data," *Fire and Materials* 31, no. 5 (2007): 327–354.
16. C. Lautenberger, C. L. Tien, K. Y. Lee, and A. J. Stretton, "Radiation Heat Transfer," in *SFPE Handbook of Fire Protection Engineering*, 5th ed., ed. M. Hurley (New York, NY: Springer, 2016), 102–137.

---

### The Influence of Experimental Conditions on the Mass Loss for TGA in Fire Safety Science

---

**Note:** This article was published as K. De Lannoye, C. Trettin, A. Belt, E.A. Reinecke, R. Goertz and L. Arnold, "The Influence of Experimental Conditions on the Mass Loss for TGA in Fire Safety Science". Fire safety journal, December 2023. <https://doi.org/10.1016/j.firesaf.2023.104079>

### Author Contributions

CONCEPTUALIZATION: Karen De Lannoye and Corinna Trettin

DATA CURATION: Karen De Lannoye and Corinna Trettin

FORMAL ANALYSIS: Karen De Lannoye and Corinna Trettin

FUNDING ACQUISITION: Ernst-Arndt Reinecke, Roland Goerths and Lukas Arnold

INVESTIGATION: Karen De Lannoye and Corinna Trettin

METHODOLOGY: Karen De Lannoye and Corinna Trettin

SUPERVISION: Alexander Belt, Ernst-Arndt Reinecke, Roland Goerths and Lukas Arnold

VISUALIZATION: Karen De Lannoye

WRITING—ORIGINAL DRAFT PREPARATION: Karen De Lannoye and Corinna Trettin

WRITING—REVIEW AND EDITING: Karen De Lannoye, Alexander Belt, Ernst-Arndt Reinecke, Roland Goerths and Lukas Arnold

# The Influence of Experimental Conditions on the Mass Loss for TGA in Fire Safety Science

K. De Lannoye<sup>a,b</sup>, C. Trettin<sup>c</sup>, A. Belt<sup>a</sup>, E. A. Reinecke<sup>b</sup>, R. Goertz<sup>c</sup>, L. Arnold<sup>a,d,\*</sup>

<sup>a</sup>*Institute for Advanced Simulation, Forschungszentrum Jülich, Germany*

<sup>b</sup>*Institute of Energy and Climate Research, Forschungszentrum Jülich, Germany*

<sup>c</sup>*Chemical Safety and Fire Defence, University of Wuppertal, Germany*

<sup>d</sup>*Computational Civil Engineering, University of Wuppertal, Germany*

---

## Abstract

A thermogravimetric analyser (TGA) measures the mass loss of a sample as function of temperature, during a predefined heating program. The results are applied for developing reaction kinetics in fire safety science. It is assumed that the sample and the apparatus are in perfect thermal equilibrium. Therefore, the analysis ignores any apparatus or sample specific aspects. However, different experimental and material parameters, like the reacting atmosphere or sample mass, influence the observed mass loss. This research work illustrates the impact of experimental and material conditions on the measurement results. Polymethyl methacrylate (PMMA) is used for this study because of its important role in fire safety science. The influence of different atmospheres, sample mass, colour and flow rates was examined in three different TGA devices at heating rates between 2 K/min and 80 K/min. The major difference was observed for different atmospheres, inert versus synthetic air atmosphere. A difference up to 75°C in onset temperature was found. The flow rate does not have any influence under inert atmosphere. The colour of the samples has a small influence on the mass loss rates. When comparing different devices, it was found that the peak temperature differs less than 10°C under inert atmosphere. This contribution discusses and compares the observed influence of the different conditions.

---

## 1. Introduction

Thermogravimetric analysis (TGA) examines the chemical reactions and physical processes by analysing the time resolved mass loss of a sample under specific thermal conditions in an inert or oxidising atmosphere. The purpose of the TGA measurement is to characterise gasification reactions as function of sample temperature and time [1, 2, 3, 4]. The significant quantity to specify the reaction kinetics is the time resolved mass loss. The use of TGA data in fire safety science is based on the idea that decomposition reactions can be identified, while thermal inertia (i.e. a temperature gradient within the sample) can be neglected. For obtaining representative mass loss results, different aspects must be considered. On the one hand the experimental conditions, like heating rate, atmosphere,

inflow rate of gases, type of crucible (e.g. its material or diameter) must be defined. On the other hand the sample properties, like amount of material influence the mass loss. Several aspects have been studied in previous publications, e.g. molecular weight [5], heating rate [6], sample preparation [7].

In contrast to fire simulations, which are based on a prescribed design fire, the modelling of the flame spread involves chemical and physical processes in the solid, which emits the fuel. One of the main processes here is pyrolysis, which decomposes the solid material. It is common practice to describe the rate at which solid mass is converted into gas species with a set of Arrhenius equations. The involved parameters, i.e., the kinetic parameters for each reaction, are derived from the outcome of a TGA measurement. However, these parameters are not a direct output of a TGA measurement, but need to be derived from the data. For complex decompositions, an inverse modelling approach is

---

\*Corresponding author

needed, which uses the TGA data as target in an optimisation method. In the fire safety science community, this is a common method to find the kinetic parameters for flame spread simulations [8, 9, 10].

Independent of the used method to find the kinetic parameters, the characteristics of the mass loss rate curve have to be analysed. Before the inverse modelling [11] starts, the number of reaction steps is estimated, e.g., by the number of local maxima. In the common approaches, this needs to be done manually. Additionally, depending on the experimental conditions and the material, reactions can overlap, which makes this estimation more complex. In this process, it needs to be decided to what extent reaction steps with small peaks have to be taken into account – every considered reaction step increases the number of pyrolysis parameters. Consequently, the number of considered reactions influences directly the modelled flame spread, as small reactions, especially with low activation energies, may have a significant impact. By considering a higher number of endothermic reactions, the modelled flame spread in the fire simulation will be reduced or even limited. The quality of the TGA data and the above-mentioned decisions about the interpretation of mass loss can essentially influence the modelled fire scenario.

Furthermore, fire spread is a dynamical process, involving different atmospheres and heating rates [12]. For example, the material that is not yet burning will pre-heat and start to decompose under air atmosphere. While under the flame, the oxygen concentration is reduced. These different conditions should be taken into account when modelling fire spread. Therefore, the condition of the considered fire scenario must be transferred to the experimental configuration of TGA to determine the correct number of reaction steps as well as pyrolysis parameters.

In this research work, different experimental and material parameters influencing the mass loss results are examined. For this purpose, TGA experiments were conducted with polymethyl methacrylate (PMMA). The aim of this work is to show which parameters influence the results when conducting TGA experiments. In a next step it should than be considered what the influence of these changing results is on the parameters that are estimated based on TGA data, this is out of the scope of this contribution. PMMA was chosen due to its prominent role in fire safety engineering, e.g. [13]. Upon heating the PMMA surface melts, re-

leasing pyrolysis gases which ignite. The flame radiation heats the surface, which continues to melt. This process takes place, because upon heating the PMMA releases monomer methyl methacrylate (MMA). The MMA decomposes further in smaller combustible products, which react with oxygen creating smaller molecules like CO<sub>2</sub>, CO, H<sub>2</sub>O, etc [14].

## 2. Method

For this work, experiments with three different apparatuses were conducted: a METTLER TOLEDO AG: TGA/DSC 1 (TGA M), a LINSEIS STA PT1600 (TGA L) and a SETARAM Themys duo TGA (TGA S). All three measure the mass loss of a sample during a defined temperature program, e.g. a linear increase of the temperature with a constant heating rate. Both TGA M and L are a combination of thermogravimetry and differential scanning calorimetry (DSC). All three TGAs have a different sample loading system. In figures 1a, 1b and 1c a schematic overview of the different TGA devices can be found. A sample is indicated in grey. The gas flow through the devices is shown by the dashed lines. Thermocouples measuring the assumed sample temperature are shown. Other thermocouples present in the device are not shown in the schemes. TGA M is a side-loaded TGA. Since it is a combined DSC system, it has one empty crucible (on the left) as reference for the DSC signal. The crucible on the right is filled with the sample. Both crucibles stand on the balance arm, which allows to measure the mass loss. TGA S has an electromagnetic suspension balance. This TGA consists of two identical ovens on both sides of a balance. The sample is placed in one of the ovens, while the other identical oven has an empty crucible. Buoyancy effects are compensated by the crucible in the counteracting empty oven. TGA L has a top load balance. The sample (on the right) and an empty reference crucible (on the left) are loaded from the top onto the balance. The empty reference crucible is for the DSC function of the device. In TGA M and TGA L, the thermocouples, measuring the sample temperature, are in contact with the crucible containing the sample. This is not the case for TGA S. Specifications of the furnaces and balance of the TGA's can be found in table 1.

For the measurements, constant heating rates between 2 K/min and 80 K/min are chosen, since the heating rate influences the mass loss rates obtained



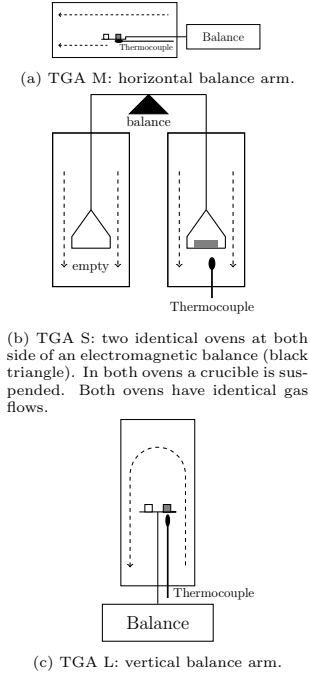


Figure 1: Schematic view of the different TGA devices. The gasflow is indicated with the dashed lines, in gray a sample is indicated. All three devices have a filled crucible on the right and an empty crucible on the left.

Table 1: Specifications of the TGA's.

	TGA L	TGA S	TGA M
Oven diameter (mm)	28	18	20
Volume furnace (ml)	200	67	N/S
Balance capacity (mg)	25	20	5000
Balance sensitivity ( $\mu\text{g}$ )	0.5	0.002	1.0

from the TGA. In real scale fires broad ranges of heating rates can be found [15]. The samples are tested in a gas atmosphere similar to the ambient air atmosphere (21 vol%  $\text{O}_2$  and 79 vol%  $\text{N}_2$ ) and in an inert atmosphere (100 Vol%  $\text{N}_2$  for TGA M and TGA L or Ar for TGA S). According to [6], under an inert atmosphere the composition of the inert gas does not influence the TGA results. Tests under air atmosphere were repeated at least three times, tests under inert atmosphere were repeated two or three times, unless explicitly mentioned otherwise. The recommended flow rates were used for the devices, this is 40 ml/min for TGA M and 20 ml/min for TGA S and TGA L. The reacting atmosphere represents the conditions before ignition and thermal processing without flame or ignition.

For the measurements, in TGA M, 70  $\mu\text{l}$  aluminium oxide ( $\text{Al}_2\text{O}_3$ ) crucibles with an inner diameter of 5 mm were used. In TGA L, aluminium oxide crucibles were used with a volume of 120  $\mu\text{l}$ . In TGA S, a 130  $\mu\text{l}$  platinum crucible was used. No lid was used in any of the experiments.

Buoyancy effects in a TGA apparatus will cause an apparent mass loss. These effects need to be compensated, in order to resolve the real mass loss of the sample. In TGA S this is done by the counteracting oven. Empty runs were performed to test the accuracy of this system. The mass for an empty run does not deviate more than  $7 \cdot 10^{-3}$  mg. TGA L and TGA M only have one single oven. Blank curves need to be recorded in order to compensate for the buoyancy effects. This is a TGA run without sample under exactly the same conditions as the experiment. TGA data was corrected with the average of three blank curves, both for TGA M and L. Table 2 shows the maximal difference between three different empty repetitions for TGA M and TGA L.

The data sampling frequency is 1 Hz. This implies that in a fixed temperature range, higher heating rates have less data points than lower heating rates. This causes a natural smoothing for higher heating rates. The data originating from the measurements is the sample temperature and sample mass versus time. The mass loss data is derived over time to show the mass loss rate versus temperature. All result shown in this paper are normalised mass loss rates, using the total mass of the sample, and are labelled 'mass loss rate (1/s)'. Neither smoothing algorithm, nor a filter is applied to the displayed mass loss results. All results shown are averages of three measurements, unless explicitly

Table 2: Reproducibility of the blank curves for TGA M and TGA L. Maximal difference between three repeated blank curves are shown (in mg). Only two repetitions are used for results marked with \*.

Heating rate	TGA L Inert	TGA M Inert	TGA M Syn. air
2 K/min	-	0.0086	0.0040*
5 K/min	0.037	0.0084	0.015
10 K/min	0.022	0.10	0.12*
20 K/min	0.026	0.052*	0.095*
40 K/min	0.027	0.23	0.13*
60 K/min	-	0.016*	0.0025*
80 K/min	-	0.0070	0.0084

Table 3: Reproducibility of the PMMA experiments. Maximal difference between the normalised mass of three repetition measurements under inert atmosphere are shown. Only two repetitions are used for results marked with \*.

Heating rate	TGA L	TGA S	TGA M
2 K/min	-	-	0.0079*
5 K/min	0.0077	0.0152	0.0085*
10 K/min	0.0099	0.0333	0.0233
20 K/min	0.0172	0.0131	0.0309
40 K/min	0.0105	-	0.0106*
60 K/min	-	-	0.0196*
80 K/min	-	-	0.0276

stated otherwise. No error margin is displayed in the results because of the good reproducibility. Table 3 shows the maximum difference between three repeated experiments under inert atmosphere for TGA L (with PMMA 2020), TGA M (with PMMA 2016) and TGA S (with PMMA 2020).

Table 4 gives an overview of the different conditions that were examined, as is explained in the next section three different PMMAs were used. The results will be discussed in section 4.

### 3. Sample material

All used PMMA is commercial, cast PMMA from Plexiglas<sup>®</sup>, by Evonik. Two types of black PMMA where used, both with product name 9H01, one was ordered in 2016 (with a plate thickness of 20 mm) and the second one was ordered in 2020 from 3 mm thick plates. The third type of PMMA is transparent, with product code 0F00, also ordered as 3 mm thick plates in 2020. Photographs of the different PMMA samples can be seen in figures 2a, 2b and 2c. The samples will be referred to as 'PMMA 2020' and 'PMMA 2016': for the black PMMA and

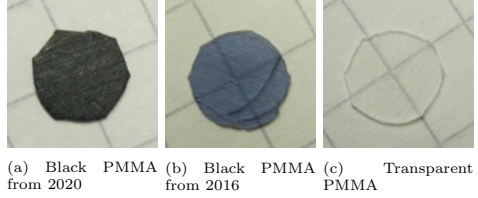


Figure 2: Different TGA samples used in the experiments.

'PMMA Transparent' for the transparent samples. Elemental analysis has been conducted on all three sample types to determine the C,H, O content. The analysis was performed with a VarioLcube from Elementar [16], both in C,H,N mode and in O(xygen)-mode. For these measurements 2 mg samples were burned. The measurements were repeated three times for every mode and every sample type. The results of this analysis confirm that the atomic content of all three samples is the same (table 5).

To produce sample thin slices were shaved of the PMMA block for the 20 mm thick material. For the 3mm thick material, the material was milled down to a thickness of 5mm. Samples were produced by pressing out thin slices of the PMMA with a hollow punch (diameter 4.5 mm for TGA M and 5 mm for TGA L and TGA S) and a hammer. Afterwards the circles were filed down to obtain the right mass. The thickness of the samples was altered by filing, the diameter did not change. A mass limit was based on the thermal characteristics such that mass and heat transfer can be neglected [17]. Samples with a mass of  $(8.50 \pm 0.10)$  mg were tested, unless explicitly stated otherwise. The thickness was between 0.45 mm and 0.6 mm for the 4.5 mm diameter and around 0.4 mm for the 5 mm diameter samples. Both PMMA 2020 and PMMA 2016, which is the same product that has been ordered in different years, were analysed in the Linseis TGA to examine the similarity of the material. From figure 3 it can be seen that both materials exhibit a similar mass loss rate, apart from a small shoulder after the main reaction peak, explained in subsection 4.2. The figure compares the materials for heating rates 5 K/min and 40 K/min. As stated in the previous section the displayed results are averages. The uncertainty on the averages is not shown because of the good reproducibility.

Table 4: Overview table of the experiments

Conditions	TGA	Heating rate (K/min)	Atmosphere	Sample
Colour	S,L	5, 10, 20, 40	inert	PMMA 2020, Transparent
Flow rate	S,L	5, 40	inert	PMMA 2020, Transparent, PMMA 2016
Device	S,M,L	5, 10, 20, 40	inert	PMMA 2016, PMMA 2020, Transparent
Heating rate	S,M,L	2,5,10,20,40,60,80	inert, air	PMMA 2016, PMMA 2020, Transparent
Mass	M	5, 10, 20, 40, 60	inert, air	PMMA 2016
Atmosphere	M	2, 5, 10, 20, 40, 60, 80	inert, air	PMMA 2016

Table 5: C,H,O composition of the different sample materials

Sample	C (wt%)	H (wt%)	O (wt%)
PMMA 2020	60.0 $\pm$ 0.2	7.86 $\pm$ 0.06	32.3 $\pm$ 0.1
PMMA 2016	59.8 $\pm$ 0.1	7.96 $\pm$ 0.03	32.5 $\pm$ 0.2
PMMA T	59.9 $\pm$ 0.1	7.98 $\pm$ 0.02	32.3 $\pm$ 0.1

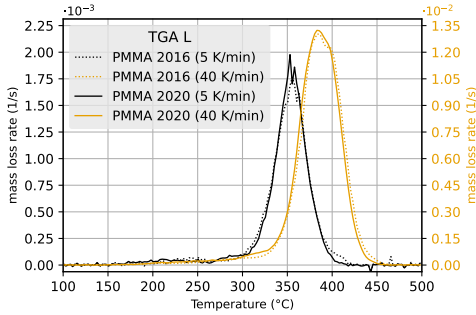


Figure 3: Comparison between PMMA 2020 and PMMA 2016

#### 4. Results

From literature, it is known that under inert atmosphere PMMA decomposes in 3 to 4 reaction steps [5, 18], of which two smaller reaction peaks occur before a main decomposition reaction. This is schematically shown in figure 4. The samples studied in this contribution show one or two, depending on the conditions, smaller reactions prior to the main mass loss rate. Under some conditions the samples exhibit a small shoulder behind the main peak. For example figure 7 shows the four distinct reactions described in the literature. The first smaller peak is caused by impurities in the sample [18, 19, 20]. The second smaller peak is caused by end chain scission of the PMMA bonds. The main decomposition peak of PMMA is due to random chain scission of the polymer chain. According to

[18, 21] the shoulder behind the main peak is due to volatilisation of char residues.

It has been shown that under air atmosphere, the decomposition starts later [18]. The reactions caused by the impurities and end chain scission can not be distinguished. The decomposition starts immediately with the main peak, caused by random chain scission. Below a temperature of 230 °C, oxygen increases the stability of the polymer. While, above this temperature it enhances the decomposition [18].

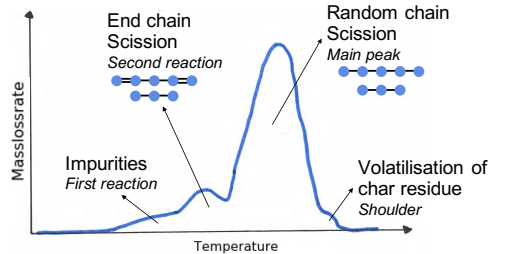


Figure 4: Schematic of reactions observed in PMMA decomposition under nitrogen atmosphere.

Under air atmosphere, it is observed that PMMA forms bubbles during decomposition in the TGA. In figure 6 pictures of PMMA samples are shown, where bubble formation can be seen. The pictures are taken at different temperatures and for different sample masses. The pictures were made by heating the samples in the TGA at a heating rate of 5K/min. At the temperature indicated below the picture, the TGA was opened and the sample was photographed. The sample was then removed from the TGA and photographed again under a magnifier glass. No difference was observed between the pictures in the TGA and the ones under the magnifier glass. Therefore the later are shown. None of the TGA devices allowed live visual monitoring of the

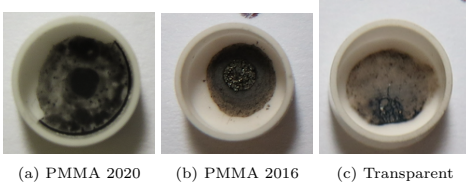


Figure 5: Sample crucible with residue after an experiment under inert atmosphere.

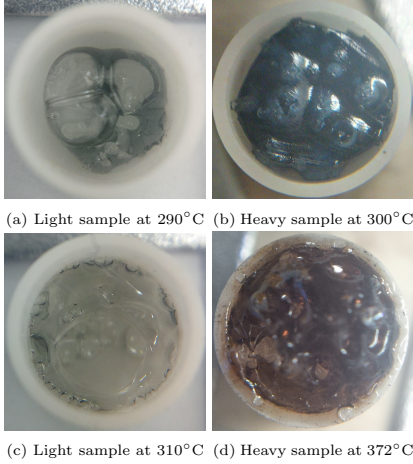


Figure 6: Bubble formation for small (approx. 8.5 mg) and large samples (approx. 75 mg) under air atmosphere.

sample. Under inert atmosphere the samples were not visually investigated. Therefore, no statement can be made on the presence of bubbles. Nevertheless, based on literature [22, 23] and the observation of bubbles in other inert experiments with PMMA, it is expected that under inert atmosphere bubbles are also formed.

At the end of the experiment a negligible amount of residue was found in the crucibles for experiments under inert atmosphere. This can be seen in figure 5 for the three different kinds of PMMA. Note that black residue is also found for transparent samples. This indicates that the residue is not purely consisting of the colouring agent added to the black samples. Under air atmosphere no residue was found.

#### 4.1. Different measurement devices

As outlined in section 2, three different TGA devices were used to characterise the effect of the mea-

surement devices. The biggest difference between the apparatuses is the orientation of the oven and the suspension of the balance.

Comparison between TGA M and TGA L was done with PMMA 2016 under nitrogen atmosphere and for four different heating rates: 5 K/min, 10 K/min, 20 K/min and 40 K/min.

Comparison between TGA L and TGA S was made with PMMA 2020 under inert atmosphere: nitrogen in TGA L and argon in TGA S. In TGA L, alumina crucibles were used, while in TGA S a platinum crucible was utilised. Three different heating rates were tested: 5 K/min, 10 K/min and 20 K/min. The comparison between TGA M and TGA L is shown in figure 7 for 5 K/min and 40 K/min. Figure 8 shows the differences between TGA L and TGA S both for transparent and PMMA 2020 samples.

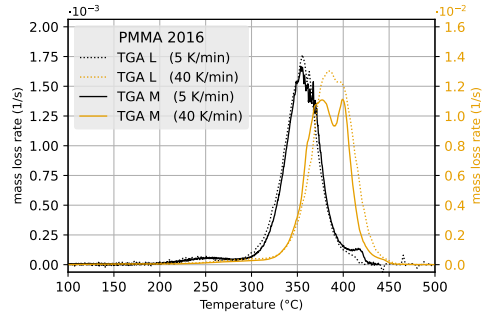


Figure 7: Comparison between TGA L and TGA M

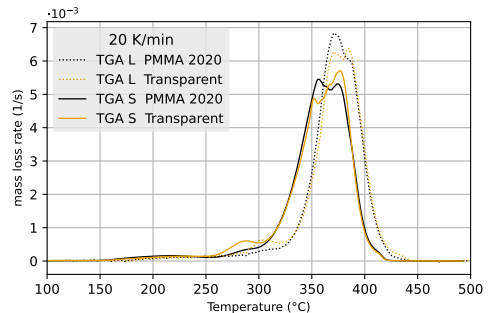


Figure 8: Comparison between TGA S and TGA L

For 5 K/min the behaviour of the samples in

TGA M and TGA L is almost identical, except for a small shoulder between 400 °C and 450 °C. For 40 K/min the mass loss rates in both devices show significant differences. The maximum mass loss is higher for TGA L, while the width of the peak mass loss rate is slightly larger for TGA M. Additionally, TGA M has two clearly distinguishable peaks in the main reaction, while for TGA L the peaks are merged together. This suggests that the main mass loss is caused by multiple reactions. Looking in detail to the top of the main peak of TGA L, shows that this peak might also consist out of two distinct reactions merged together. The difference in shoulder, between 400 °C and 450 °C, disappears for higher heating rates. In contrast, the difference in main peak becomes larger for higher heating rates.

For TGA S and TGA L, the qualitative behaviour of the samples remains the same up till 400 °C, i.e. form of the main peak, presence of the reactions before the main peak, etc. The mass loss rate measured by TGA S is shifted by 20 °C to 30 °C to lower temperature compared to TGA L. The maximum mass loss rate is higher for TGA L. The temperature shift between both devices becomes larger for higher heating rates.

Since the comparisons were carried out with the same sample material, it is excluded that differences in the mass loss rate are caused by a difference in reagent in the chemical reactions.

Due to the different layouts of the ovens, see figures 1a, 1b, 1c the radiation fraction received by the sample, originating from the oven walls might be different. The TGAs have a different gas inlet and different flow directions, which might also result in differences in convective cooling by the gas. The carrier gas in the oven transports heat from the oven wall to the sample. It might be that at higher heating rates the gas temperature becomes less homogeneous, causing temperature gradients between the TGA thermocouples and the samples.

Figure 9 shows the derivative of the measured temperature against time. As can be seen from the figure both TGA L and TGA M approximate well the ideal heating curve, while for TGA S there are stronger deviations from the desired heating rate. For 5 K/min and 10 K/min the heating rates of TGA S are relatively stable above 300 °C, where the main reaction is taking place. For 20 K/min however there are still deviations of around 5K/min at 300 °C. This in combination with the different location of the thermocouple might be the cause of the offset in temperature between TGA S and

TGA L. For TGA L and TGA M the thermocouple is located directly under sample, which is not the case for TGA S. Additional, crucibles made out of a different materials were used in the comparison between TGA S and TGA L. Platinum crucibles used in TGA S, have a heat capacity that is 7 times smaller than the aluminiumoxide crucibles in TGA L. This might also influence the heating rate received by the sample.

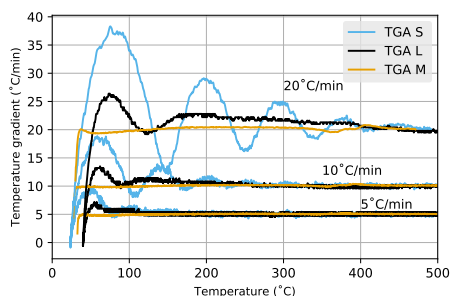


Figure 9: Temperature gradient for different heating rates and different devices

To summarise, the most relevant differences between the results of different devices are

- Difference in peak height and width of the mass loss rate
- Offset in reaction temperature
- Number of reactions (in main mass loss rate peak)

#### 4.2. Different sample colour

To determine the effect of sample colour on the mass loss rate, TGA experiments were performed both with transparent and black PMMA samples. Black PMMA is favoured in fire safety research due to its high absorption coefficient, while transparent PMMA is more often used in applications, e.g. as replacement for glass. By testing both materials in the TGA it can be examined whether the absorption and emission properties of the sample influence the mass loss rate in small scale experiments. In the near infrared region, black PMMA has a 0% transmission degree, while transparent has a 85% transmission in this region [24]. Four different heating rates were tested under inert atmosphere: 5 K/min,

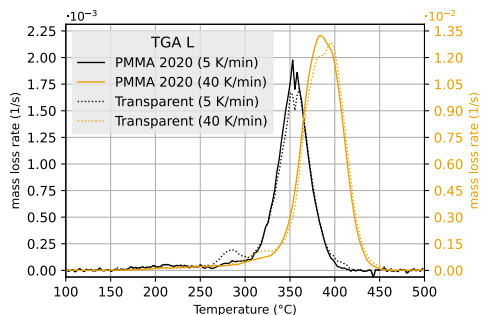


Figure 10: Comparison between black (PMMA 2020) and transparent PMMA

10 K/min, 20 K/min and 40 K/min. The mass loss results can be found in figure 10.

For 5 K/min, the slow increase in mass loss between 150 °C and 250 °C is the same for both transparent and black samples (first reaction). Between 250 °C and 300 °C the transparent samples have a significantly higher mass loss rate than the black samples (second reaction). Between 300 °C and 400 °C both samples show a high increase in mass loss rate. At 400 °C transparent samples depict a small shoulder, which is not present for PMMA 2020. For 40 K/min the samples behave similar to 5 K/min where all peaks are shifted towards higher temperatures. The difference between transparent and black samples becomes smaller for the second reaction, while the main peak of the transparent sample seems to be shifted to higher temperatures. The shoulder after the main reaction peak disappears for higher heating rates. The mass loss rate of PMMA 2016 has a similar shoulder as transparent PMMA. From the sample pictures in figure 2, it can be seen that PMMA 2016 is more transparent than PMMA 2020. Therefore, it is expected that the shoulder behind the main peak is related to the transparency of the sample. Based on the colour or transparency of the sample, the absorption properties of the sample change. This shoulder is caused by the reaction of the char residue at the end of the decomposition process. To the authors knowledge, it is unknown whether there is a difference in amount of char formation between black and transparent PMMA.

The first small reaction in mass loss rate caused by impurities is the same for black and transpar-

ent PMMA. Transparent PMMA has a higher mass loss at the moment when end chain scission is taking place (second reaction). Consequently, in the main peak black PMMA has a slightly higher mass loss rate. Transparent and black plates are made of the same PMMA, the only difference is the addition of the colour-agent. Therefore it is unlikely that the difference in this peak is caused by difference in molecule length. For higher heating rates, end chain scission is not yet finished, when the sample is already hot enough to additionally start random chain scission. Consequently, the difference in the second reaction peak between transparent and black becomes smaller. This small peak is less distinguishable as a separate reaction. The main peak on the other hand seems to be made out of two phases from which one might be slightly dependent on the other. It could be the case that a different mechanism triggers the random chain scission causing different reaction peaks. It might be that one mechanism needs an educt of the first mechanism to trigger the random chain scission.

Consequently, for the pyrolysis modelling of different colours of PMMA the following aspects need to be considered

- Different number of distinguishable reactions
- Difference in maximum peak height

#### 4.3. Different flow rate

The effect of the flow rate was examined for 5 K/min under argon atmosphere in TGA S and for 40 K/min in TGA L. In TGA S, this was done both for transparent PMMA and PMMA 2020. In TGA L, PMMA 2016 was used. The comparison is made between a flow rate of 20 ml/min and 40 ml/min.

The average results are shown in figures 11 and 12. As can be seen from the figure the flow rate does not have any significant influence on the behaviour of the mass loss rate within the same device under inert atmosphere. This is the case independent on the specific device, heating rate or type of PMMA sample. The flow rate was not varied under air atmosphere.

#### 4.4. Different heating rates in inert atmosphere

The effect of different heating rates has often been studied in literature, e.g. [4, 17, 25]. For higher heating rates the mass loss curve shifts to higher temperatures and the reactions take place

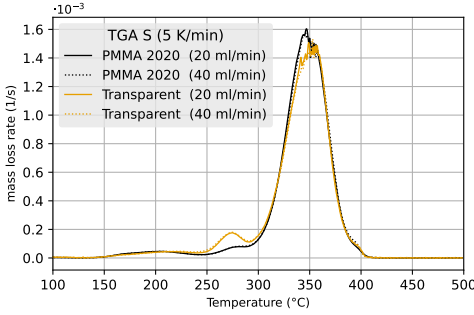


Figure 11: Different flow rates in TGA S for 5 K/min.

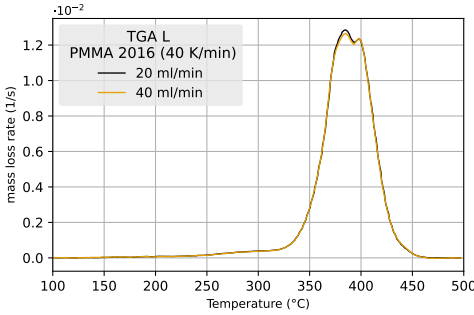


Figure 12: Different flow rates in TGA L for 40 K/min

over a wider temperature range. The heating rate also influences the amount of reactions that can be distinguished [26], since high heating rates might result in overlapping reactions. Figure 13 shows the effect of different heating rates on a theoretical Arrhenius equation:

$$\frac{d\alpha}{dt} = A \exp(-Ea/RT)(1 - \alpha)^n, \quad (1)$$

where  $\alpha$  is the unreacted mass fraction,  $A$  is the pre-exponential factor,  $Ea$  is the activation energy and  $n$  is the reaction order. For the plot literature values for PMMA have been used: 200.4 kJ/mol was used as activation energy;  $10^{16}$  as pre-exponential factor and  $n$  was put to 1.21 [5].

Experiments were conducted for different heating rates for all devices, as is recommended by [17]. With TGA M seven different heating rates were tested: 2 K/min, 5 K/min, 10 K/min, 20 K/min, 40 K/min, 60 K/min and 80 K/min. Every mea-

surement was repeated two times under nitrogen atmosphere.

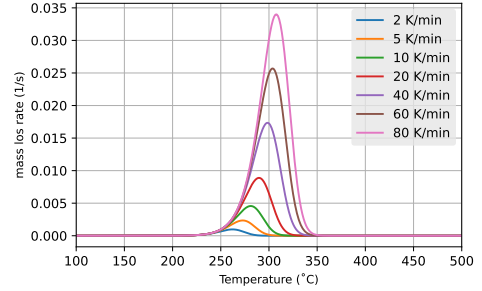


Figure 13: The solution of the Arrhenius equation for different heating rates.

Figure 14 displays the mass loss rates for different heating rates. A comparison is made between 2 K/min, 5 K/min, 10 K/min, 20 K/min, 40 K/min, 60 K/min and 80 K/min.

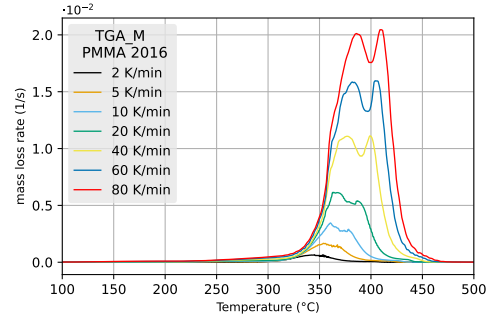


Figure 14: Different heating rates under nitrogen atmosphere

For higher heating rates the mass loss curve shifts to higher temperature. Note that, especially at lower heating rates, the complete mass loss rate curve shifts, not only the temperature of the main peak. The main difference in mass loss rate for the different heating rates is in the main reaction. For higher heating rates the main reaction is more and more manifested by two separate peaks, while for low heating rates only one peak is distinguishable. At lower heating rates the mass loss rate has a linear increase until the maximum value. For higher heating rates the increase of the mass loss rate be-



comes slower towards the maximum. The first reaction caused by the impurities becomes less present for higher heating rates. The same is valid for the shoulder, between 400 °C and 500 °C, behind the main peak: the higher the heating rate, the less present the shoulder is.

At this points we need to stress that at higher heating rates differences between TGA devices are more present, see section 4.1. In the appendix, a comparison for different heating rates for TGA L can be found. For TGA L the division of the main peak into two reactions is less distinguishable. The shift towards higher temperatures for higher heating rates, the disappearing shoulder after the main peak and the less present peak caused by impurities can also be observed in TGA L.

Since the division in multiple reactions in the main peak is only present for one of the TGAs, this will not be discussed further. The reaction before the main peak gets less present for higher heating rates. Either, due to the high heating rate, the sample is not in thermal equilibrium, or the reaction could be time dependent (i.e. for slow reaction rates, the reaction just needs time to progress). This would imply that the reaction occurs too slowly and therefore interferes with the main peak. The main shift is most likely also caused by the sample not being in thermal equilibrium due to the high heating rate. According to figure 13, only a temperature shift in the main peak temperature and not in the onset temperature is expected in theory. As pointed out before, the shift in main peak is a known phenomena for TGA experiments. The shoulder behind the main peak gradually disappears for higher heating rates. The amount of char formed by the sample is small. Therefore the char is in thermal equilibrium, and starts reacting at the same temperature for every heating rate. Since the main peak is shifting towards higher temperatures, the char related shoulder becomes part of this main reaction for higher heating rates.

The effect of different heating rates can be summarised as follows. For higher heating rates

- the mass loss rate curve shifts towards higher temperatures
- the number of distinguishable reactions changes (e.g. main reaction, impurities)

#### 4.5. Different heating rates in synthetic air

Experiments were performed for different heating rates under synthetic air atmosphere. All ex-

periments were done with TGA M for 2 K/min, 5 K/min, 10 K/min, 20 K/min, 40 K/min, 60 K/min and 80 K/min. Every experiment was repeated at least three times.

The results are shown in figures 15, 16 and 17. The individual experiments are plotted, because contrary to nitrogen atmospheres there is more variation between individual experiments.

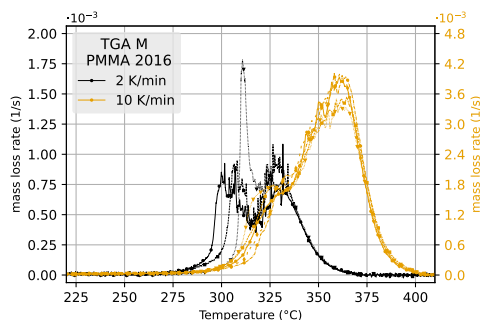


Figure 15: 2 K/min and 10 K/min under synthetic air atmosphere.

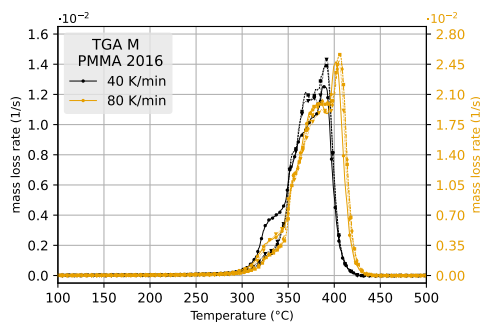


Figure 16: 40 K/min and 80 K/min under synthetic air atmosphere.

The mass loss rate for low heating rates is less reproducible than for high heating rates. For low heating rates, e.g. 2 K/min and 5 K/min, two reaction peaks can be distinguished. There is a spread on the onset temperature of the first reaction phase between the different samples for one heating rate. When looking only at the mean values this would present itself wrongly as three reaction peaks. For 2 K/min, there is one measurement with a very high



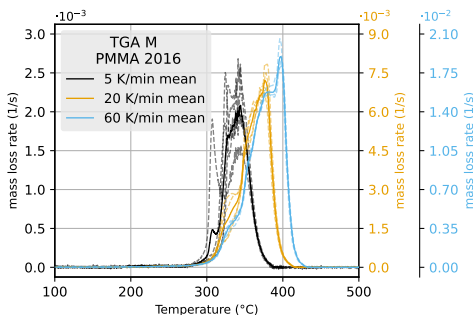


Figure 17: 5 K/min, 20 K/min and 60 K/min under synthetic air atmosphere.

and steep first reaction peak. The end of the second reaction phase is at the same temperature for all samples.

For higher heating rates, the onset temperature of the first reaction phase is more alike between the different repetition experiments. The endset temperature is the same for all repetition experiments in one heating rate, even for low heating rates. For higher heating rates, the first main peak becomes less distinguishable. The increase towards the main mass loss rate is less steep and takes place more step-wise. It can be seen that for intermediate heating rates, like e.g. 20 K/min, the first reaction phase is not present for every sample. While for higher heating rates, this first stage disappears completely. The second reaction phase becomes more a plateau. Starting from 10 K/min, more than two distinguishable reaction peaks can be observed. Additionally, the maximum mass loss rate shifts to higher temperatures for higher heating rates. The temperature range, in which the mass loss takes place, increases for higher heating rates. While, the last reaction stage becomes more separated.

Under thermal decomposition, PMMA forms bubbles in a random process. When a bubble pops this results in a sudden release of gas. Because of the small size of the PMMA samples and the momentum of a sudden release, this can have a strong effect on the mass loss.

Upon heating the surface of the PMMA samples melts. Around the melting temperature PMMA has a high viscosity [27]. It is known, that for liquids the viscosity decreases with temperature [28]. This effect is larger for more viscous liquids and has also

been observed for dilute solutions of PMMA [29]. In other fields of research it has been shown, that in more viscous fluids smaller sized bubbles are formed than in less viscous fluids [30].

As the temperature becomes higher the PMMA becomes more viscous, allowing bubbles to form. The high heating rate causes inhomogeneities in the surface tension, which results in the bubbles releasing gas sooner due to shears compared to samples that heat up slower. The bubbles contain MMA gas. As the sample continues to be heated in the TGA, the gas inside the bubbles also gets heated. The higher the heating rate, the faster the gas in the bubble heats. This results in a higher pressure inside the bubble which also contributes to bubbles popping sooner for higher heating rates. Due to the oxygen in the surrounding atmosphere, the random chain scission process starts earlier [14, 23]. Burstured bubbles leave holes, allowing a larger surface area of the sample to interact with oxygen. As a consequence, the reproducibility under oxygen atmosphere strongly depends on the bubble size and form. Therefore, these experiments show a worse reproducibility. The sudden mass loss for the outlier at 2 K/min could be caused by a bubble that suddenly pops. As explained these bubbles can become quite large (compared to the sample size) for low heating rates, while the higher heating rates produce smaller bubbles. As the sample continues to heat it reaches the point where the viscosity becomes small enough to form bigger bubbles and the sharp increase to the main reaction peak starts.

Under air atmosphere, two competing processes take place. Bubbles containing monomer MMA that is formed in the sample diffuse towards the surface, while oxygen diffuses into the sample. This competing interaction of the inward and outward diffusion, is time and temperature dependent. This could explain the more step-wise curves for higher heating rates.

As with inert atmosphere, the mass loss curves shift to higher temperature for higher heating rate. A shift in main peak, as can be observed when comparing 40 K/min and 80 K/min, is expected (see figure 13). However, when comparing 2 K/min and 10 K/min it can be seen that not only the temperature of the main peak shifts but e.g. also the onset temperature of the reactions. This is most likely also caused by the sample not being in thermal equilibrium due to the high heating rate.

Under synthetic air atmosphere the following observations should be considered when modelling or

using TGA data

- The amount of reaction stages depends on heating rate
- On- and endset temperatures shift to higher values for higher heating rates.
- The temperature range of the reactions extends for higher heating rates
- Low heating rates have poor reproducibility

#### 4.6. Different masses under inert atmosphere

There is no consensus on which sample mass to use for TGA analysis. Even the standard norms [1, 2] do not provide a clear specification. The effect of sample mass has been examined in a dedicated study. For 5 K/min 8.5 mg and 17 mg were compared; for 10 K/min and 60 K/min, 8.5 mg and 15 mg. The 15 mg experiments were only conducted once. Experiments were conducted under nitrogen atmosphere in TGA M.

In figures 18 and 19 the results for 5 K/min and 60 K/min, respectively 10 K/min are shown.

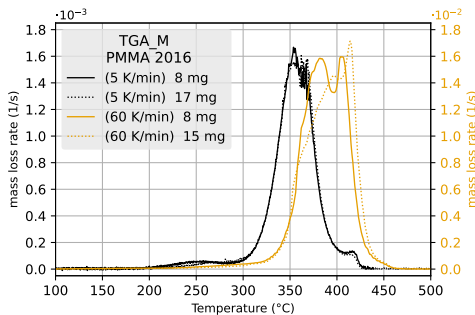


Figure 18: Different sample masses for 5 K/min and 60 K/min under nitrogen atmosphere.

Independent of the mass, the reactions start at the same temperature. As can be seen from the figure, there is very little difference between 8.5 mg and 17 mg for low heating rates. There might be a difference in the first reaction, but this is difficult to distinguish. For 10 K/min, the main peaks of heavier samples have a small shift towards higher temperatures. Otherwise the mass loss rate of both heavier and light samples are identical. For higher heating rates the difference in mass loss rate increases. Initially, the mass loss rate for higher

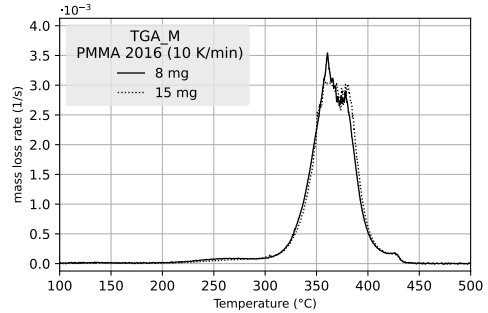


Figure 19: Comparison between different masses for 10 K/min under nitrogen atmosphere.

masses increases strongly afterwards the increase becomes slower. The first part of the main peak merges more to the second part for heavier samples. Causing the first peak to be lower and the maximal mass loss rate to be higher. For lower masses, these two parts are separated. The peak width of both reactions widens for higher masses.

For higher heating rates and higher masses, the sample does not reach thermal equilibrium. This causes a part of the main peak to move to higher temperatures since the reaction temperature is not reached through out the full sample. Nevertheless, the onset temperature for the main peak is the same since the surface of the sample is sufficiently heated to start reacting. The main reaction peak is higher for heavier samples. The sample reaches the limiting temperature for random chain scission through out the whole sample, causing a faster mass loss and a higher main peak.

The effect of sample mass under inert atmosphere can be summarised by the following points:

- The sample mass has no influence for low heating rates;
- For high heating rates, the sample mass impacts the maximum mass loss rate as well as the amount of reactions needed to model the mass loss rate.

#### 4.7. Different masses in synthetic air

Experiments were conducted with different masses under a synthetic air atmosphere with TGA M. For 5 K/min, the following masses were tested: 8.5 mg, 17 mg, 35 mg and 75 mg. For

20 K/min and 40 K/min, 8.5 mg and 17 mg were tested. The results of the experiments are shown in figures 20 and 21.

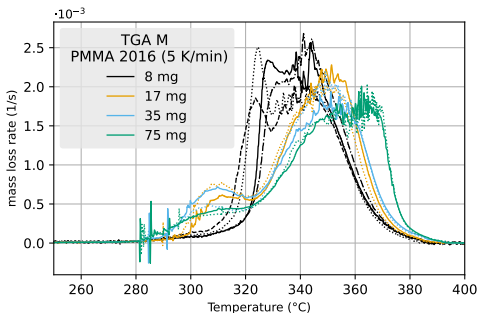


Figure 20: Different sample masses for 5 K/min under synthetic air atmosphere. Individual experiments are plotted, using different line-styles. The colour of the lines correspond to the sample mass.

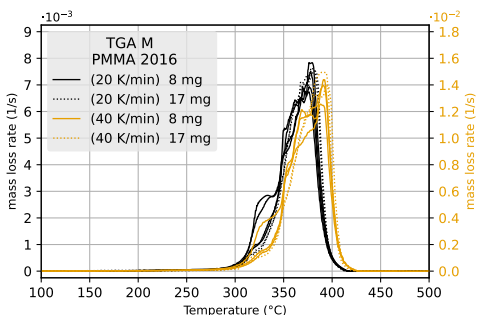


Figure 21: Different sample masses for 20 and 40 K/min under synthetic air atmosphere. Individual experiments are shown, not the average.

For the low heating rate (5 K/min), the first reaction phase starts earlier for higher masses. The first reaction phase for 8.5 mg starts at 320 °C, while for the other masses it starts already around 300 °C. For higher masses, the first reaction stage shows a slower increase while for lower masses the first reaction merges with the main peak. Both 35 mg and 75 mg have some noise in the start of the first reaction peak, as well as in the main peak.

The second reaction phase shows a slower increase for higher masses. Additionally, the maximum mass loss rate decreases with sample mass.

For the highest mass, 75 mg, the second reaction phase reaches a plateau between 340 °C and 380 °C. At least two reactions would be needed to model this plateau form. The endset temperature is similar for all sample masses. The final decrease in mass loss rate is steeper for higher masses. The trend that is seen for higher masses with 5 K/min is similar to the trend seen for higher heating rates with 8.5 mg. However, the temperature shift present for the different heating rates is not present for the different masses. The reproducibility increases with higher masses.

For the high heating rates, 20 K/min and 40 K/min, the influence of the mass is smaller. It can be seen that the on- and endset temperature for the reactions is the same for all masses. Between the different masses, there is no temperature shift observed. The first reaction phase is not present for the higher masses, while for the lower mass for some samples it is present. The last reaction phase is less separated for higher masses. A nearly linear increase towards the main peak is observed for higher mass. At least two reactions would be needed to model this increase. The decrease after the maximum mass loss rate is steeper for higher masses.

As stated in section 4.5, under air atmosphere MMA is released by the formation of bubbles. In figure 6, photographs are shown for different sample masses. Samples with a low mass get heated more uniform than samples with a high mass. This results in lower sample and surface, as heat is transported to the bulk of the sample, temperatures for heavier samples. Hence, the viscosity (at the surface) will be larger for lighter samples. The MMA bubbles that are formed inside the sample mitigate to the surface, where they can accumulate in larger bubbles. Due to the low viscosity, big bubbles can be formed. While heavier samples with a higher viscosity can only form smaller bubbles, since they will burst before reaching a big volume. Consequently, thicker samples start reacting earlier (see figure 20, at 290 °C). Additionally, for thinner (and therefore lighter) samples, the large surface to volume ratio allows a big part of the sample to interact with oxygen, which enhances the random chain scission. For low masses, the burst of one bubble, leads to a significant loss in mass. Additionally, space is freed in the sample through which oxygen can diffuse. This implies, that the release of one big bubble can enhance the random chain scission process. For higher masses, the formed bubbles are smaller.

Since the amount of bubbles becomes larger, the reproducibility of the experiments becomes higher. During the heating of the sample, the viscosity becomes lower, resulting in larger bubbles for higher temperatures. The change in viscosity and bubble formation causes a small decrease in mass loss rate around 310 °C. Furthermore, the sample deforms due to the thermal stress, which influences its volume and consequently density. The noise within the main peak is attributed to the random process of larger bubbles bursting. The main peak gets wider, since for a heavier sample it takes longer before the oxygen can interact with the full sample. The cause of the signal noise for higher masses at the beginning of the first reaction is unclear.

When modelling TGA data under oxygen atmosphere, the following observations should be considered

- The number of distinguishable reaction phases changes with the sample mass
- The relative importance of the different reactions changes with the sample mass
- The maximum mass loss rate decreases for higher masses

#### 4.8. Different atmospheres

Mass loss rate curves under inert and under synthetic air are compared in figure 22 for 2 K/min, 20 K/min, and 60 K/min.

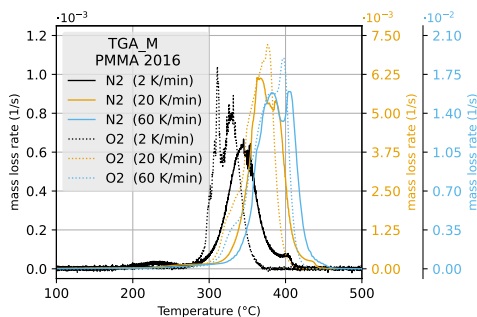


Figure 22: Comparison between synthetic air and N<sub>2</sub> atmosphere.

The on- and endset temperature of the main reaction is different between both atmospheres for all heating rates. While the temperature range of the

main reaction is similar under both atmospheres, the main mass loss rate of the sample starts earlier under oxygen atmosphere and has a steeper increase. The maximum mass loss rate is lower for samples heated under an inert atmosphere. In general, the mass loss curves from samples under inert atmosphere can be represented with fewer reactions than those under synthetic air atmosphere.

Table 6 summarises the differences between the samples behaviour under a synthetic air atmosphere and nitrogen atmosphere. A division is made between low (2 K/min and 5 K/min) and high heating rates (starting from 40 K/min). The mass loss rates for low heating rates under an air atmosphere are less reproducible as under an inert atmosphere. Therefore, the mean curves might show different characteristics and amounts of reaction phases due to the variation in individual mass loss curves. The behaviour for intermediate heating rates, like 10 K/min and 20 K/min, can be seen as a separator between the comparison for low and high heating rates. For example, for heating rates below 20 K/min, the samples under an inert atmosphere have a smooth increase towards the main peak. Whereby, reaction modelling for an air atmosphere would need multiple reaction phases to represent the increase towards the maximum.

The mechanisms triggering the scission process are different under air than under an inert atmosphere, therefore the mass loss curves are completely different. Under an inert atmosphere, the main process influencing the mass loss rate, is the diffusion of MMA towards the surface. Under an air atmosphere, the formation of MMA is influenced by the interaction of oxygen with the sample and therefore the diffusion of oxygen into the sample. Under an air atmosphere, the mass loss starts later, since no end chain scission is taking place due to the stabilising effect of oxygen at low temperatures. However, the main peak starts earlier due to the enhancing effect of oxygen at higher temperatures [23]. Under an air atmosphere, no shoulder originating from decomposition of char residues is present, since char is more reactive in the presence of oxygen.

When modelling TGA data, the following should be taken into account

- depending on the atmosphere, different processes take place
- Therefore, the mass loss rate for both atmospheres have significant deviations

Table 6: Main difference between samples tested under an inert atmosphere and samples tested under an air atmosphere.

Low heating rate
<ul style="list-style-type: none"> <li>• Shoulder before main peak: only present under nitrogen atmosphere.</li> <li>• Main peak: one reaction phase under nitrogen atmosphere, at least two under air atmosphere.</li> <li>• Shoulder behind main peak: only present under nitrogen atmosphere.</li> </ul>
High heating rate
<ul style="list-style-type: none"> <li>• First part of main reaction peak have similar temperature and mass loss rate in nitrogen and air.</li> <li>• Second main part of main reaction peak is earlier for air.</li> </ul>

#### 4.9. Comparison

The effects of different conditions are compared, in table 7, by calculating the root mean square error (RMSE) between the averaged normalised mass loss rates of both conditions, the difference in onset temperature, peak temperature and maximum mass loss rate. It is expected that for higher heating rates, the RMSE increases since the maximum mass loss rate increases. Within one column (i.e. one heating rate) one can compare which experimental or material parameters result in the largest difference in normalised mass loss rate.

Different atmospheres result in significantly different mass loss rates. Under air atmosphere, larger mass seem to result in larger differences in maximum mass loss rate as well as in peak temperature. However, due to the large uncertainty, especially on the 8.5 mg experiments at 5 K/min, all differences are within the uncertainty. Under nitrogen atmosphere large differences are found between TGA S and TGA L, as explained in 4.1 this is most likely due to the not well regulated heating rate of TGA S. When looking at the results of TGA M and TGA L, the biggest difference in maximum mass loss rate (up to  $0.213 \text{ s}^{-1}$ ) for low heating rates (5 K/min) is caused by different sample colours. While the biggest offset in onset and peak temperature is between different mass at low heating rate. For high heating rates (40 K/min and 60 K/min), different devices cause the biggest difference in onset temperature (up to  $29^\circ\text{C}$ ) and maximum mass loss rate (up to  $1.92 \text{ s}^{-1}$ ). While different masses cause the biggest difference in peak temperature (up to  $21.5^\circ\text{C}$ ). Note that in table 7, the effect of the heating rate on maximum mass loss rate, peak temperature and onset temperature was not shown. As is well known from literature, for higher heating rates, the maximum mass loss rate and the peak temperature increase. This is also the case for the experiments conducted for this study, as was discussed in sections 4.5 and 4.4.

#### 5. Conclusion

In this paper, the influence of experimental settings on TGA experiments was discussed. Black and transparent PMMA from Plexiglas®, by Evonik, was used. Furthermore, products of different manufacturing years were considered.

The research work shows, that the number of decomposition reactions and the amount of mass loss depends on specific experimental conditions. Under nitrogen atmosphere, the colour effect is small, while the flow rate of the purge gas has no effect. For TGAs with a similar set-up, little difference is found between the measurement devices, especially for low heating rates. For high heating rates, differences occur in the main decomposition peak. Between different set-ups, it was identified, that the accuracy of the heating rate as well as of the thermocouple positions are responsible for differences in the results.

Under nitrogen atmosphere, changing the heating rate, as well as changing the mass, affects the main decomposition process. This is caused by the sample not being in thermal equilibrium. For higher heating rates, the main peak will be shifted to higher temperatures. For higher masses, the mass loss is slower until a limiting temperature is achieved, at which the mass loss accelerates.

The decomposition mechanism under synthetic air differs significantly from a measurement under nitrogen atmosphere, due to the enhancing effect of oxygen. MMA is released under the form of bubbles, which creates holes for oxygen diffusing into the sample. For low heating rates and small masses, a poor reproducibility is found, caused by the formation of big bubbles. For higher heating rates and high masses, multiple smaller bubbles are formed, improving the reproducibility and the amount of measurement noise.

Decomposition conditions change during the spread of a fire. The parts of the material that

are not yet burning are heated up under air atmosphere. Under the flame, the oxygen concentration is reduced. Additionally, the heating rate increases under the flame. These different conditions were analysed in the TGA and influences illustrated. As results, it can be stated, that for fire spread modelling the different conditions should be considered depending on the modelled fire spread phase. Additionally, depending on the accuracy needed from the TGA data for estimating kinetic parameters for modelling, one needs to take into account parameters like the lay-out of the device. Most of the current models used for determining these parameters are over simplified and can not take these effects into account.

## References

- [1] Plastics — Thermogravimetry (TG) of polymers — Part 1: General principles. Standard, European standard, July 2022.
- [2] DIN 51006: Thermal analysis (TA) - Thermogravimetry (TG) - Principles. Standard, German National Standard, January 2005.
- [3] Thermal analysis (TA) - Vocabulary. Standard, German National Standard, January 2005.
- [4] A. W. Coats and J. P. Redfern. Thermogravimetric analysis. A review. *The Analyst*, 88(1053):906, 1963.
- [5] M. Ferriol, A. Gentilhomme, M. Cochez, N. Oget, and J. L. Mieloszynski. Thermal degradation of poly(methyl methacrylate) (PMMA): modelling of DTG and TG curves. *Polymer Degradation and Stability*, 79(2):271–281, January 2003.
- [6] O.P. Korobeinichev, A.A. Paletsky, M.B. Gonchikhzapov, R.K. Glaznev, I.E. Gerasimov, Y.K. Naganovsky, I.K. Shundrina, A.Yu. Snegirev, and R. Vinu. Kinetics of thermal decomposition of PMMA at different heating rates and in a wide temperature range. *Thermochimica Acta*, 671:17–25, 2019.
- [7] Matthew J. DiDomizio and Mark B. McKinnon. Impact of Specimen Preparation Method on Thermal Analysis Testing and Derived Parameters. In Morgan C. Bruns and Marc L. Janssens, editors, *Obtaining Data for Fire Growth Models*, pages 64–87. ASTM International, 100 Barr Harbor Drive, PO Box C700, West Conshohocken, PA 19428-2959, March 2023.
- [8] Anna Matala. Methods and applications of pyrolysis modelling for polymeric materials.pdf.
- [9] Tristan Hehnen, Lukas Arnold, and Saverio La Mendola. Numerical Fire Spread Simulation Based on Material Pyrolysis—An Application to the CHRISTIFIRE Phase I Horizontal Cable Tray Tests. *Fire*, 3(3):33, 2020.
- [10] Alexandra Viitanen, Simo Hostikka, and Jukka Vaari. CFD Simulations of Fire Propagation in Horizontal Cable Trays Using a Pyrolysis Model with Stochastically Determined Geometry. *Fire Technology*, July 2022.
- [11] Tristan Hehnen and Lukas Arnold. PMMA Pyrolysis Simulation – from Micro- to Real-Scale.
- [12] Morgan J. Hurley, Daniel Gottuk, John R. Hall, Kazunori Harada, Erica Kuligowski, Milosh Puchovsky, José Torero, John M. Watts, and Christopher Wiecek, editors. *SFPE Handbook of Fire Protection Engineering*. Springer New York, New York, NY, 5th ed edition, 2016.
- [13] Benjamin Batiot, Morgan Bruns, Simo Hostikka, Isaac Leventon, Yuji Nakamura, Pedro Reszka, Thomas Rogaume, and Stanislav Stoliarov. The MacCFP Condensed Phase Working Group - Experimental. April 2021.
- [14] W. R. Zeng, S. F. Li, and W. K. Chow. Review on Chemical Reactions of Burning Poly(methyl methacrylate) PMMA. *Journal of Fire Sciences*, 20(5):401–433, September 2002. Publisher: SAGE Publications Ltd STM.
- [15] SFPE. *SFPE Handbook of Fire Protection Engineering*. Springer, 5th edition, 2016.
- [16] Elementar. Vario el cube.
- [17] Sergey Vyazovkin, Konstantinos Chrissafis, Maria Laura Di Lorenzo, Nobuyoshi Koga, Michèle Pijolat, Bertrand Roduit, Nicolas Sbirrazzuoli, and Joan Josep Suñol. ICTAC Kinetics Committee recommendations for collecting experimental thermal analysis data for kinetic computations. *Thermochimica Acta*, 590:1–23, August 2014.
- [18] T. Hirata, Takashi Kashiwagi, and J. E. Brown. Thermal and oxidative degradation of poly(methyl methacrylate): weight loss. *Macromolecules*, 18(7):1410–1418, July 1985. Publisher: American Chemical Society.
- [19] Gregory J. Fiola, Dushyant M. Chaudhari, and Stanislav I. Stoliarov. Comparison of Pyrolysis Properties of Extruded and Cast Poly(methyl methacrylate). *Fire Safety Journal*, 120:103083, 2021.
- [20] T. Kashiwagi, A. Inaba, and J. E. Brown. Differences In PMMA Degradation Characteristics And Their Effects On Its Fire Properties. *Fire Safety Science*, 1:483–493, 1986.
- [21] Talal Fateh, Franck Richard, Thomas Rogaume, and Paul Joseph. Experimental and modelling studies on the kinetics and mechanisms of thermal degradation of polymethyl methacrylate in nitrogen and air. *Journal of Analytical and Applied Pyrolysis*, 120:423–433, July 2016.
- [22] Ho-Ming Tong and Augustus C. Ouano. Bubble formation mechanism during heat treatment of polymer films cast from solutions. *Polymer Engineering & Science*, 25(2):75–82, 1985.
- [23] S. M. Dakka. TG/MS of Poly (Methyl Methacrylate), The Effect of Heating Rate on the Rate of Production of Evolved Gases. *Journal of Thermal Analysis and Calorimetry*, 75(3):765–772, March 2004.
- [24] Röhm. Spektrale Transmissionsgrade  $\tau(\lambda)$  im nahen Infrarot-Bereich bis 2,8  $\mu\text{m}$  Wellenlänge.
- [25] P. Gabbott. *Principles and Applications of Thermal Analysis*. Wiley, 2008.
- [26] J.D. Menczel and R.B. Prime. *Thermal Analysis of Polymers: Fundamentals and Applications*. Wiley, 2014.
- [27] J. A. Brydson. *Plastics Materials*. Elsevier Science & Technology, Oxford, United Kingdom, 1999.
- [28] Philip J. Pritchard. *Fox and McDonald's introduction to fluid dynamics*. John Wiled & Sons, Inc., Hoboken, 8th edition, 2011.
- [29] B. A. Toms and D. J. Strawbridge. Elastic and viscous properties of dilute solutions of polymethyl methacry-

- late in organic liquids. *Transactions of the Faraday Society*, 49:1225, 1953.
- [30] Ketan Pancholi, Eleanor Stride, and Mohan Edirisinghe. Dynamics of Bubble Formation in Highly Viscous Liquids. *Langmuir*, 24(8):4388–4393, April 2008. Publisher: American Chemical Society.

Table 7: Comparison of the different effects studied in this paper. RMSE values of the normalized mass loss rate have to be multiplied with a factor  $10^{-6}$ . Difference in peak mass loss rate, indicated in  $10^{-3}/s$ , difference in onset temperature ( $^{\circ}C$ ), difference in peak temperature ( $^{\circ}C$ ).

Effect	2 K/min	5K/min	10 K/min	20 K/min	40 K/min	60 K/min	80 K/min
Colour (TGA L):							
• RMSE	-	2.36	4.45	7.69	15.7	-	-
• Max MLR	-	0.213 $\pm$ 0.048	0.486 $\pm$ 0.123	0.417 $\pm$ 0.071	0.416 $\pm$ 0.122	-	-
• Onset T	-	1.0 $\pm$ 1.1	5.6 $\pm$ 9.4	1.2 $\pm$ 4.9	3.7 $\pm$ 3.9	-	-
• Peak T	-	4.2 $\pm$ 2.3	6.3 $\pm$ 3.8	8.5 $\pm$ 7.0	10.3 $\pm$ 1.7	-	-
Flow rate (TGA S):							
• RMSE	-	0.608	-	-	-	-	-
• Max MLR	-	0.055 $\pm$ 0.050	-	-	-	-	-
• Onset T	-	5.0 $\pm$ 1.8	-	-	-	-	-
• Peak T	-	2.4 $\pm$ 2.4	-	-	-	-	-
Flow rate (TGA L):							
• RMSE	-	-	-	-	4.51	-	-
• Max MLR	-	-	-	-	0.431 $\pm$ 0.231	-	-
• Onset T	-	-	-	-	24.0 $\pm$ 3.4	-	-
• Peak T	-	-	-	-	0.4 $\pm$ 0.8	-	-
Device:							
TGA L vs TGA M:							
• RMSE	-	2.26	3.06	11.8	41.2	-	-
• Max MLR	-	0.113 $\pm$ 0.030	0.107 $\pm$ 0.172	0.403 $\pm$ 0.097	1.920 $\pm$ 0.101	-	-
• Onset T	-	4.0 $\pm$ 2.2	4.0 $\pm$ 5.7	24 $\pm$ 14.0	29 $\pm$ 3.0	-	-
• Peak T	-	0.2 $\pm$ 1.1	2.6 $\pm$ 0.9	7.6 $\pm$ 2.7	4.4 $\pm$ 11.0	-	-
TGA L vs TGA S:							
• RMSE	-	5.20	12.7	35.0	-	-	-
• Max MLR	-	0.431 $\pm$ 0.025	0.687 $\pm$ 0.140	1.350 $\pm$ 0.115	-	-	-
• Onset T	-	30.2 $\pm$ 0.5	29.2 $\pm$ 9.0	20.2 $\pm$ 4.7	-	-	-
• Peak T	-	14.7 $\pm$ 3.6	8.7 $\pm$ 4.7	6 $\pm$ 2.1	-	-	-
Mass (inert):							
8.5mg vs 17mg:							
• RMSE	-	1.37	-	-	-	-	-
• Max MLR	-	0.023 $\pm$ 0.009	-	-	-	-	-
• Onset T	-	16.5 $\pm$ 2.3	-	-	-	-	-
• Peak T	-	10.8 $\pm$ 3.6	-	-	-	-	-
8.5mg vs 15mg:							
• RMSE	-	-	5.92	-	-	75.2	-
• Max MLR	-	-	0.414 $\pm$ 0.169	-	-	0.898 $\pm$ 0.149	-
• Onset T	-	-	3.2 $\pm$ 3.3	-	-	4.5 $\pm$ 0.5	-
• Peak T	-	-	2.2 $\pm$ 0.8	-	-	21.5 $\pm$ 11.5	-
Mass (air):							
8.5mg vs 17mg:							
• RMSE	-	11.3	-	16.2	27.7	-	-
• Max MLR	-	0.201 $\pm$ 0.354	-	0.265 $\pm$ 0.077	0.816 $\pm$ 0.927	-	-
• Onset T	-	13.2 $\pm$ 20.7	-	29.0 $\pm$ 13.8	14.3 $\pm$ 8.0	-	-
• Peak T	-	18.4 $\pm$ 16.8	-	5.9 $\pm$ 2.1	1.8 $\pm$ 2.3	-	-
8.5mg vs 35mg:							
• RMSE	-	12.3	-	-	-	-	-
• Max MLR	-	0.321 $\pm$ 0.364	-	-	-	-	-
• Onset T	-	14.9 $\pm$ 20.7	-	-	-	-	-
• Peak T	-	19.4 $\pm$ 16.7	-	-	-	-	-
8.5mg vs 75mg:							
• RMSE	-	16.2	-	-	-	-	-
• Max MLR	-	0.361 $\pm$ 0.341	-	-	-	-	-
• Onset T	-	15.4 $\pm$ 20.7	-	-	-	-	-
• Peak T	-	32.6 $\pm$ 16.7	-	-	-	-	-
Atmosphere							
• RMSE	7.05	17.5	20.3	32.9	59.5	85.3	82.9
• Max MLR	0.632 $\pm$ 0.330	0.688 $\pm$ 0.341	0.262 $\pm$ 0.283	0.989 $\pm$ 0.393	2.492 $\pm$ 0.790	2.867 $\pm$ 1.1	4.420 $\pm$ 0.778
• Onset T	74.4 $\pm$ .6	48.3 $\pm$ 20.7	51.2 $\pm$ 5.6	42.1 $\pm$ 16.2	45.7 $\pm$ 7.4	29.5 $\pm$ 8.8	32.2 $\pm$ 14.3
• Peak T	30.4 $\pm$ 8.9	23.8 $\pm$ 16.7	1.2 $\pm$ 2.4	11.0 $\pm$ 3.8	1.2 $\pm$ 11.1	4.8 $\pm$ 11.5	3 $\pm$ 11.5





---

### The tube furnace with online mass loss measurement as a new bench scale experiment

---

**Note:** This article was submitted as K. De Lannoye, A. Belt, E.A. Reinecke and L. Arnold, "The tube furnace with online mass loss measurement as a new bench scale test", Fire Technology 60, 3689–3707 (2024). <https://doi.org/10.1007/s10694-024-01590-0>.

### Author Contributions

CONCEPTUALIZATION: KAREN DE LANNOYE, ALEXANDER BELT, ERNST-ARNDT REINECKE AND LUKAS ARNOLD

DATA CURATION: Karen De Lannoye

FORMAL ANALYSIS: Karen De Lannoye

FUNDING ACQUISITION: Ernst-Arndt Reinecke, Lukas Arnold

INVESTIGATION: Karen De Lannoye

METHODOLOGY: Karen De Lannoye, Alexander Belt and Lukas Arnold

PROJECT ADMINISTRATION: Lukas Arnold

SOFTWARE: Karen De Lannoye

SUPERVISION: Alexander Belt, Ernst-Arndt Reinecke and Lukas Arnold

VALIDATION: Karen De Lannoye, Alexander Belt and Ernst-Arndt Reinecke

VISUALIZATION: Karen De Lannoye

WRITING—ORIGINAL DRAFT PREPARATION: Karen De Lannoye

WRITING—REVIEW AND EDITING: Karen De Lannoye, Alexander Belt, Ernst-Arndt Reinecke and Lukas Arnold

---

# THE TUBE FURNACE WITH ONLINE MASS LOSS MEASUREMENT AS A NEW BENCH SCALE TEST FOR PYROLYSIS

---

**Karen De Lannoye<sup>a</sup>, Alexander Belt<sup>a</sup>, Ernst-Arndt Reinecke<sup>b</sup>, and Lukas Arnold<sup>a,c</sup>**

<sup>a</sup>Institute for Advanced Simulation, Forschungszentrum Jülich, Wilhelm-Johnen-Straße, 52428 Jülich, Germany

<sup>b</sup>Institute of Energy and Climate Research, Forschungszentrum Jülich, Wilhelm-Johnen-Straße, 52428 Jülich, Germany

<sup>c</sup>Chair of Computational Civil Engineering, University of Wuppertal, Pauluskirchstraße 7, 42285 Wuppertal, Germany

Karen De Lannoye: [k.de.lannoye@fz-juelich.de](mailto:k.de.lannoye@fz-juelich.de); ORCID: 0000-0003-2617-5557

Alexander Belt: [a.belt@fz-juelich.de](mailto:a.belt@fz-juelich.de); ORCID: 0000-0002-6091-9321

Ernst-Arndt Reinecke: [e.-a.reinecke@fz-juelich.de](mailto:e.-a.reinecke@fz-juelich.de); ORCID: 0000-0003-1414-9183

Lukas Arnold: [l.arnold@fz-juelich.de](mailto:l.arnold@fz-juelich.de); [arnold@uni-wuppertal.de](mailto:arnold@uni-wuppertal.de); ORCID: 0000-0002-5939-8995

## ABSTRACT

In this paper, a new gram scale experiment with well characterised boundary conditions is proposed for pyrolysis experiments. The set-up consists of a tube furnace, based on ISO19700, with a newly designed concept for a balance within the oven, allowing for online mass loss measurements. Samples with a length up to 50 cm can be investigated in this apparatus. The oven allows for experiments at fixed temperatures or at fixed heating rates, under controlled atmosphere, w.r.t. gas composition and flow rate. A thorough characterisation of the set-up is presented, including aspects like reproducibility of the heating rate or the precision of the balance. The functionality of the balance has been demonstrated with calcium carbonate ( $\text{CaCO}_3$ ) experiments. This material was chosen because it decomposes in a single reaction, which only releases  $\text{CO}_2$ . This allows for comparison between the mass loss rate of the balance and the  $\text{CO}_2$  production rate, measured by a gas analyser. Results for two different heating rates: 3 K/min and 5 K/min and for different masses (25 g and 8.5 g) are presented. The two measurement methods are in excellent agreement. Finally, the data obtained from the new experimental set-up is compared to results from thermogravimetric analyser (TGA) experiments.

**Keywords** tube furnace · pyrolysis · thermogravimetric analysis (TGA) · calcium carbonate ( $\text{CaCO}_3$ ) · balance · mass loss rate · ISO19700 · cable fires

## 1 Introduction

For several decades, extensive research has been done on cable fires [1, 2, 3]. Cables form a potential risk in many areas, e.g. in private homes, large industrial facilities, aircrafts, nuclear power plants. For example, France reported 73 fires in nuclear power plants throughout 2014 [4]. Of those fires, 53 % were caused by electrical malfunctioning. In some cases the malfunctioning started in a cable, in other cases cables were ignited as a secondary fuel. Despite the efforts being made, the fire dynamics of cables has not yet been fully understood. The conductive core surrounded by an often combustible polymer makes it a complex combined system in terms of fire safety. There is still a gap between the modelling of cable fires [5, 6, 7, 8] and experimental work. This work presents a newly proposed bench scale experiment, particularly for cable fires, that could help fill this gap [9].

In order to breach the gap between experiments and modelling, experiments with well-known boundary conditions are needed. One of the most often used bench scale experiments is the cone calorimeter [10, 11, 12]. In this set-up, a 10 cm by 10 cm sample is placed under a radiant heater, that delivers a defined heat flux to the sample surface. Due to the lay-out of the experiment, factors like flow rate around the sample or convective cooling on the side, are not well known. Especially for cables, there are additional degrees of freedom in arranging the cables to fill a 10 cm by 10 cm

square [13]. This makes the boundary conditions even more complex. Another often used small scale experiment is the thermogravimetric analyser (TGA). A TGA [14, 15] has well controlled boundary conditions, but is only meant to test very small samples (milligram range), since it is assumed that heat and mass transfer effects can be neglected. Due to the limitations on the sample size, it is very hard to take a representative sample of a cable to test in the TGA [16]. The new set-up presented in this paper aims to combine the advantages of the cone calorimeter and the TGA. It allows for larger, more representative samples, while experiments can be conducted under well-defined boundary conditions.

The tube furnace with online mass loss measurement is introduced as a new bench scale experiment. The design of the new set-up is based on the ISO 19700 [17]. The novelty of the oven lies in the enabling of an online mass loss measurement by installing a balance within the oven. This allows to obtain time resolved mass loss data under well controlled boundary conditions i.e. controlled atmosphere, temperature, flow rate. A thorough characterisation of the set-up is presented here. The functionality of the balance will be demonstrated with  $\text{CaCO}_3$  experiments. These experiments also serve to discuss the limitations of the oven. The aim of this paper is to carefully demonstrate the functionality of the new experiment set-up, therefore experiments with cables are out of the scope of this contribution. In the final part of this contribution, a comparison between the tube furnace and the TGA will be made. This comparison gives a first indication of heat and mass transfer effects which might have to be taken into account in the tube furnace set-up due to scaling effects.

## 2 Experimental Set-up

### 2.1 General Lay-out

A schematic view of the experimental set-up is outlined in figure 1. A quartz glass tube with an inner diameter of 90 mm and a wall thickness of 2.4 mm is surrounded by a tubular oven by Carbolite Gero Limited (type SR(A)). The oven consists of eleven circular heating elements, which are distributed equally over a length of 51 cm. A photograph of the bottom half of the oven is shown in figure 2a. The maximal temperature of the set-up is 1273 K. The maximal heating rate is 5 K/min, to avoid too high thermal tension in the quartz glass tube. In the upstream direction, here to the right of the oven, additional glass parts are installed. This allows to store the sample, while the oven is preheated, and move the sample in and out at specific oven temperatures. A step motor is used to move the sample in and out of the oven. The carrier gas is inserted at the upstream border of the set-up – about 1.50 m from the oven. Mass flow controllers allow composing an inflow mixture of air and nitrogen and adjusting the flow rate. On the downstream side of the oven, a gas mixer is installed, which will be described in more detail in the next section. Subsequently, a cone-shaped glass part reduces the diameter of the tube before it is connected to the gas analyser and the exhaust.

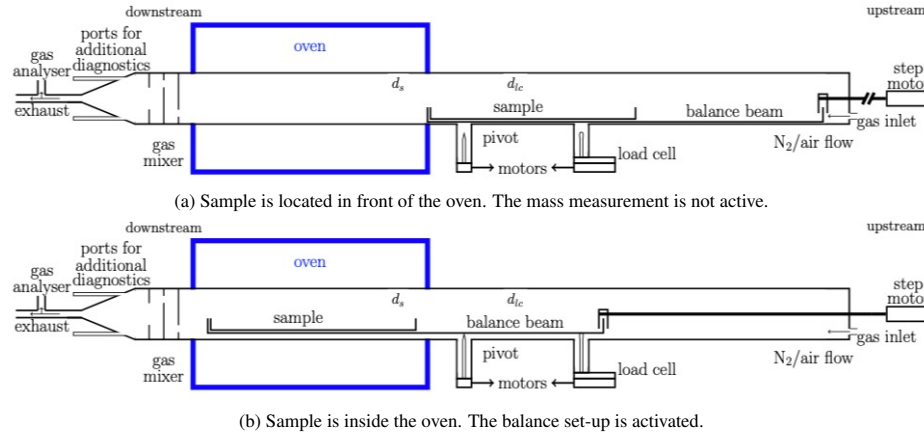
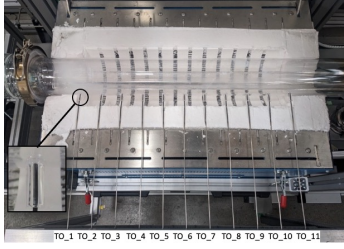
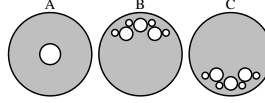


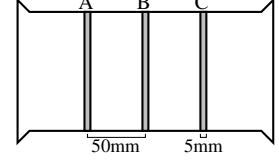
Figure 1: Schematic picture of the set-up.



(a) Part of the tube inside the oven, instrumented with eleven thermocouples at the outside of the tube: TO\_1 at the downstream end of the oven and TO\_11 at the upstream end.



(b) Cross-section of the gas mixer elements: upstream (right) to downstream (left).



(c) Side view of the gas mixer, showing the arrangement of the mixer elements.

Figure 2: Details of the thermocouple configuration in the oven and the configuration of the gas mixer.

## 2.2 Gas Analyser

The current apparatus is equipped with a gas analyser, (ports for) thermocouples and the newly designed balance. Additional access points are foreseen, to install extra diagnostics in the future. A more detailed description of the balance will be given in the next section. An X-stream gas analyser by Emerson, equipped with a paramagnetic sensor for  $O_2$  measurements and infrared sensors for CO and  $CO_2$  measurements, is connected to the tube at the downstream end. The analyser is calibrated before every experiment. The uncertainty on the data is specified by the manufacturer as 10 % of the gas concentration used to calibrate the analyser. The zero calibration is done with 100 % nitrogen. The concentrations for CO,  $CO_2$  and  $O_2$  are  $(9.90 \pm 0.01)$  vol%,  $(9.99 \pm 0.01)$  vol% and  $(20.8 \pm 0.1)$  vol% respectively. In order to ensure that the carrier gas and the volatiles released by the sample sufficiently mix, mixing tests have been performed. These tests have shown that it is necessary to install an additional gas mixer between the oven and the exhaust. A more detailed schematic of the gas mixer is shown in figure 2b and 2c. Table 1 displays the results of the mixing tests, i.e. expected vs. measured volume concentrations. For these tests, a tube was installed in the middle of the specimen region. This tube was connected with a  $CO_2$  bottle through a mass flow controller. The carrier gas was put to 10 l/min of nitrogen, while the amount of inserted  $CO_2$  gas was varied. Both for inserting gas in the sample region, as well as for inserting  $CO_2$  at the upstream end of the tube. Every measurement was averaged over three minutes, after a constant value was reached. As can be seen from the table, gas inserted at the  $N_2$  inlet is completely mixed. Due to the gas mixer, sufficient mixing is also achieved for gas mixed in the sample region.

Table 1: Results of the mixing tests: expected versus measured  $CO_2$  concentrations of the carrier gas for different  $CO_2$  flow rates and at two relevant injection locations.

$CO_2$ flow [l/h]	Expected concentration [vol%]	Measured concentration, injection at upstream inlet [vol%]	Measured concentration, injection at sample location [vol%]
3.7	0.612	$0.615 \pm 0.100$	$0.632 \pm 0.100$
7.4	1.217	$1.170 \pm 0.101$	$1.188 \pm 0.101$
11.1	1.814	$1.738 \pm 0.100$	$1.751 \pm 0.102$
14.8	2.405	$2.312 \pm 0.100$	$2.318 \pm 0.102$
18.5	2.988	$2.901 \pm 0.101$	$2.901 \pm 0.102$
22.2	3.564	$3.500 \pm 0.102$	$3.489 \pm 0.102$
44.4	6.883	$6.932 \pm 0.101$	$6.850 \pm 0.104$

## 2.3 Temperature measurements

Thermocouples are installed at the outside of the quartz glass tube. Small quartz glass tubes are connected perpendicularly to the main glass tube so that the thermocouples remain in position (see figure 2a). Eleven thermocouples are distributed over the heating part of the oven. These thermocouples will be used to refer to positions in the sample region and will be referred to as TO\_1 to TO\_11: e.g. TO\_6 is the thermocouple located at the middle of the sample region and is used for most temperature references in the following analyses. Additionally, thermocouples can be installed on

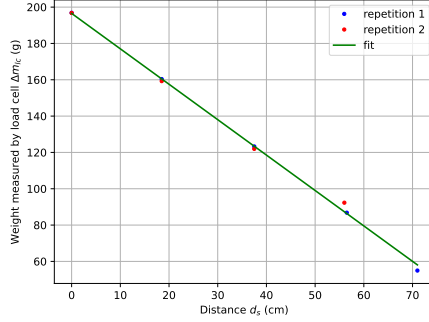


Figure 3: Apparent weight at load cell versus distance between a reference mass of 100 g and the pivot.

the inside of the glass tube for temperature measurements in the sample region. However, thermocouple measurements on the inside of the tube can not be done simultaneous with mass loss measurements.

## 2.4 Online mass loss measurement

The balance is based on a simple seesaw mechanism, see figure 1b. The specimen boat is connected with the load cell by the balance beam. The load cell is foreseen from a metal cylinder topped with a ball bearing to avoid any non-perpendicular forces to act on the load cell. Counterweights are installed on the load cell side to compensate for the weight of the sample and the specimen boat. The accuracy of the Sartorius WZA1203-N load cell is 1 mg.

The cantilever allows to measure the mass loss in the centre of mass. The mass loss of the sample can be determined from equating the torque on both sides of the pivot:

$$\Delta m_s g d_s = \Delta m_{lc} g d_{lc} \quad , \quad (1)$$

where  $d_s$  and  $d_{lc}$  are the distances between the middle of the sample and the pivot respectively the pivot and the load cell and  $\Delta m_s$  and  $\Delta m_{lc}$  are the mass lost by the sample, respectively the mass loss measured by the load cell and  $g$  is the gravitational constant. The  $\text{CaCO}_3$  experiments presented in this paper will serve as example to demonstrate how the load cell data is converted into mass loss data.

The balance beam and the sample boat are both made out of quartz glass. This material was chosen since it has a very small thermal expansion coefficient. Therefore, effects caused by thinning of the balance beam and sample boat on the apparent mass loss can be neglected.

In order to test the balance, a reference weight of 100 g was moved over a distance of 71 cm in the sample region. When plotting the mass value recorded by the load cell ( $\Delta m_{lc}$ ) versus the distance ( $d_s$ ) between the sample and the pivot, a linear relation is expected. Referring to equation 1, the slope of the linear function should be given by  $\Delta m_s / d_{lc}$ . The results of these tests are shown in figure 3. The first measurement point (0 cm) was at a distance of 20 cm from the pivot. The blue and the red dots are the results of two repetition experiments. The green line is a linear fit through the measurement points. The fitted value is  $(-1.95 \pm 0.03) \text{ g/cm}$ , compared to the expected value:  $-1.96 \text{ g/cm}$ .

Additionally, these tests allow to determine the conversion factor between the load cell measurement and the expected sample mass. For a mass middle point in the centre of the oven, the factor is 0.888. Deviating 3 cm (5 cm) in downstream direction results in a factor of 0.84 (0.82), respectively in the upstream direction of 0.94 (0.97).

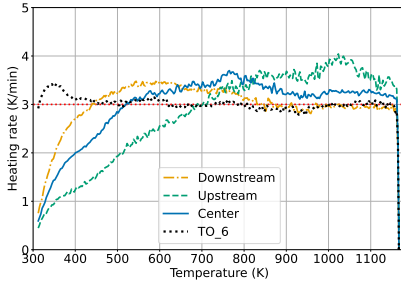
## 3 Characterisation of thermal boundary conditions

The temperature of the oven is regulated by the electrical power of the oven. Optimisations have to be run in order to find a power versus time curve that results in the desired heating rate. The temperature measurements by TO\_06 are used for the heating rate optimizations. The oven supplies the same power to all heating elements. Due to the flow through the tube and the isolation of the tube, a temperature distribution is present in the sample region. This is

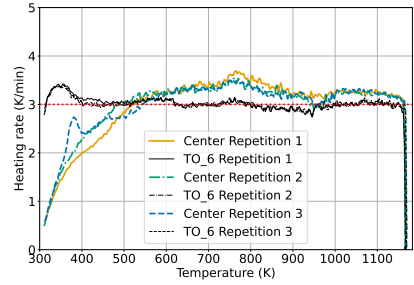
also the case for the oven used in ISO19700 [18]. For all experiments presented in this contribution, the same power versus time curve was used for the same heating rate. These curves are optimised to approximately reach a constant 3 K/min or 5 K/min heating rate. For some of the experiments, the oven is kept at a constant temperature at the end of the experiment. At a temperature of 1173 K, the temperature control of the oven was set to remain constant at this temperature.

To determine the heating rate and the temperature distribution within the oven, additional thermocouples were installed in the sample region inside the oven. One thermocouple was located in the middle of the sample region. The other two thermocouples were located in the middle between the first thermocouple and the sample end, respectively up and down stream. Small copper pieces were used to keep the thermocouples in position. The thermocouples were not in contact with the copper pieces, neither with the specimen boat. For 5 K/min four repetition experiments were conducted, for 3 K/min three repetitions were done.

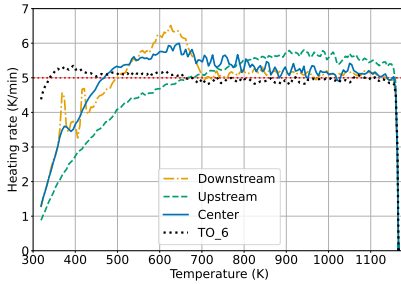
Figure 4 shows the heating rate of the sample region during the experiment as function of temperature, which is chosen here as the temperature value measured by TO\_6. A time derivative has been taken from the thermocouple data to present the heating rate. The temperature data was averaged over 60 s before calculating the derivative. Figures 4a and 4c show the evolution of the temperature at different locations through one measurement. Figures 4b and 4d show the heating rate in the middle for the repetition measurements.



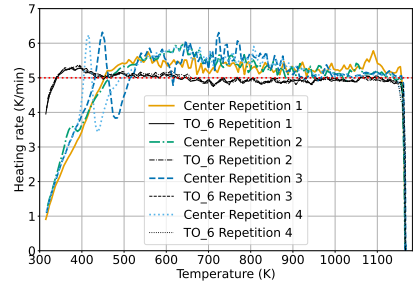
(a) Heating rate at 1/4, 1/2 and 3/4 of the sample length for 3 K/min.



(b) Repetitions of the heating rate, measured in the middle of the oven for 3 K/min.



(c) Heating rate at 1/4, 1/2 and 3/4 of the sample length for 5 K/min.



(d) Repetitions of the heating rate, measured in the middle of the oven for 5 K/min.

Figure 4: Heating rate in the tube furnace

During the first 200 K of heating, the oven needs time to ramp up the heating rate. For 5 K/min, the middle and downstream part of the oven have a more similar heating rate than the upstream side. While for 3 K/min, the upstream and middle part are more alike. The heating rate seems more reproducible for 3 K/min than for 5 K/min. For the 3 K/min experiments, the thermocouples were installed once and three repetition experiments were run, without removing the thermocouples. For the 5 K/min experiments, the thermocouples had to be re-installed several times.

Consequently, the poorer reproducibility for 5 K/min is expected, as the different measurements do not have the thermocouples at the exact same location. After reaching a temperature of 520 K, the heating rates are becoming similar for all repetitions, even for 5 K/min. The materials tested for this contribution does not react before a temperature of 520 K. Therefore, less time was invested in optimising the lower temperature part of the curve. It could be considered to further optimise the heating rate if necessary.

Figure 5 shows the temperature distribution in the oven at different points throughout the heating process at 3 K/min and 5 K/min. On the x-axes, the label numbers of the outside thermocouples are shown, while the individual figures are representing selected heating states, i.e. temperature values measured by TO\_6. The thermocouples are numbered from down- (TO\_1) to upstream (TO\_11) as seen in figure 2a. The thermocouples on the inside are shown at locations with respect to the outside thermocouples. The results are averaged over the repetition experiments. One standard deviation is displayed as uncertainty. Only for the thermocouples at the inside of the oven for 5 K/min, the uncertainty is large enough to be visible in the figure. The first eight frames display different parts of the heating process, with increments of 110 K. The temperature distribution, after the oven remained at 1173 K for 30 minutes, is shown in the last frame. During sample testing, a sample would be located between TO\_1 and TO\_11.

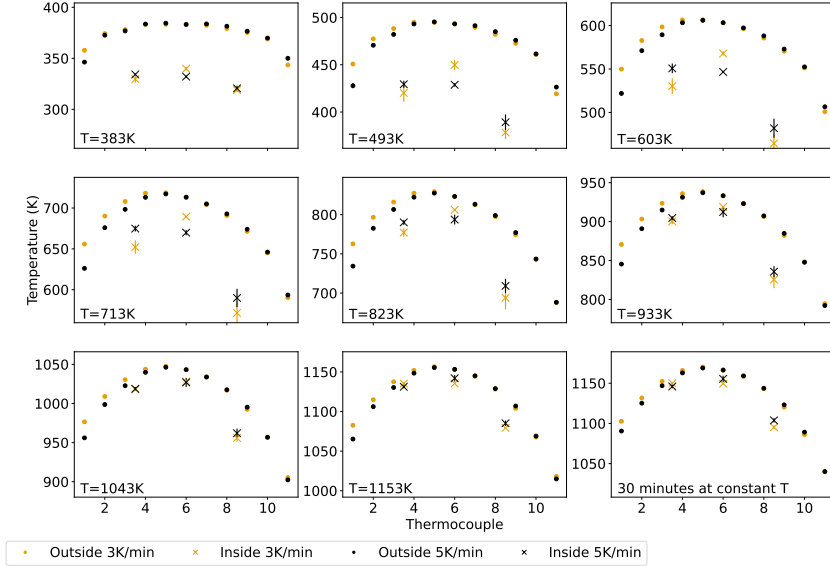


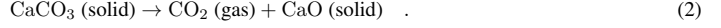
Figure 5: Temperature distribution at the in- and outside of the oven during heating. Temperature at the inside are indicated with crosses, temperatures measured at the outside are indicated in dots. The selected temperature points, indicated at the bottom left in each subfigure, are temperature values measured by TO\_6.

A temperature distribution throughout the sample region is present. Upon initial heating, the gradient between the different locations grows with increase in temperature, until the temperature reaches a value of around 823 K. For lower temperatures, the discrepancy between in- and outside temperature is larger. The outside temperatures show excellent reproducibility since they are always located at the exact same location due to small glass tubes (see figure 2a). The outside temperatures are exactly the same, independent of the heating rate. The maximal deviation in temperature in the sample region is 142 K. The most homogeneous region is between thermocouples TO\_4 and TO\_6.



## 4 Commissioning experiments with CaCO<sub>3</sub>

In order to demonstrate the functionality of the balance during heating, commissioning experiments were conducted. For these experiments, a material was selected that would release only CO<sub>2</sub> or CO upon heating. This allows to compare the data from the load cell with the data from the gas analyser. Calcium-carbonate (CaCO<sub>3</sub>) was chosen for these experiments. Upon heating, CaCO<sub>3</sub> releases solely CO<sub>2</sub> to the gas phase:



Experiments were conducted with two different amounts of CaCO<sub>3</sub>: 8.5 g and approx. 25 g, referred here to as small and large CaCO<sub>3</sub> experiments. Throughout the experiments, CaCO<sub>3</sub> powder with a purity of 99 % was used. For the small experiments, powder is distributed between TO\_4 and TO\_6. For the large ones, the full sample holder length is used, i.e. the 51 cm where the oven heats, thus between TO\_1 and TO\_11. The two different layouts were chosen to study the effect of the non-homogeneous temperature distribution on the mass loss rate. CaCO<sub>3</sub> powder was passed through a sieve, with grid size 400 µm, before placing it in the specimen boat. All experiments are conducted under nitrogen atmosphere with a flow rate of 10 l/min. The set-up is purged with nitrogen, experiments are not started before the O<sub>2</sub> concentration has reached 0.0 %.

### 4.1 Data processing

To verify the measurements from the balance, a gas analyser is utilised. As the gas analyser measures volume concentrations, here of CO<sub>2</sub>, this results need to be converted to a mass production rate. This is done using the total flow in the experiment. Since the concentration of CO<sub>2</sub> measured during the experiment is below 1.1 %, it is assumed that the total flow is the same as the nitrogen volume flow N<sub>2</sub> flow ( $\dot{V}_{\text{N}_2}$ ). This flow is controlled by a mass flow controller. Within the mass flow controller a volume flow is converted to a mass flow ( $\dot{m}_{\text{N}_2}$ ), using the normal density of N<sub>2</sub> ( $\rho_{\text{norm},\text{N}_2}$ ):

$$\dot{m}_{\text{N}_2} = \rho_{\text{norm},\text{N}_2} \cdot \dot{V}_{\text{N}_2} \quad . \quad (3)$$

The mass flow is converted to a molar flow ( $\dot{n}_{\text{N}_2}$ ) by dividing by the molecular mass of N<sub>2</sub> ( $M_{\text{N}_2}$ )

$$\dot{n}_{\text{N}_2} = \frac{\dot{m}_{\text{flow},\text{N}_2}}{M_{\text{N}_2}} \quad . \quad (4)$$

The CO<sub>2</sub> measurement cell of the gas analyser is heated. Therefore, a temperature factor needs to be added to determine the production rate of CO<sub>2</sub> ( $\dot{m}_{\text{CO}_2}$ ) at room temperature. The exact temperature of the cell is continuously measured by the gas analyser. During an experiment its value is 341 K and varies less than 0.2 K. Therefore, an average temperature of the measurement cell  $T_{\text{gas,cell}}$  can be used. Using the volume concentration of CO<sub>2</sub> ( $y_{\text{CO}_2}$ ) and the ideal gas law for the temperature correction, the production rate of CO<sub>2</sub> ( $\dot{m}_{\text{CO}_2}$ ) is given by:

$$\dot{m}_{\text{CO}_2} = y_{\text{CO}_2} \cdot \dot{n}_{\text{N}_2} \cdot M_{\text{CO}_2} \cdot \frac{T_{\text{gas,cell}}}{T_{\text{ambient}}} \quad , \quad (5)$$

where  $M_{\text{CO}_2}$  is the molar mass of CO<sub>2</sub> and  $T_{\text{ambient}}$  is the ambient temperature, which is assumed to be 293 K. The material and gas properties used for the calculation are given in table 2.

Table 2: Material and gas properties used to calculate production rate of CO<sub>2</sub>

Property	Value
$\rho_{\text{norm},\text{N}_2}$	1.234 kg/m <sup>3</sup> [19]
$M_{\text{N}_2}$	28.01 g/mol [20]
$M_{\text{CO}_2}$	44.01 g/mol [21]

The mass loss measured by the balance is corrected with a zero curve. This is a mass loss measurement, ran under the exact same conditions as the experiment but without sample. The empty run is subtracted from mass loss measurements to compensate for buoyancy effects. Several empty runs have been done to check the reproducibility. Figure 6 displays

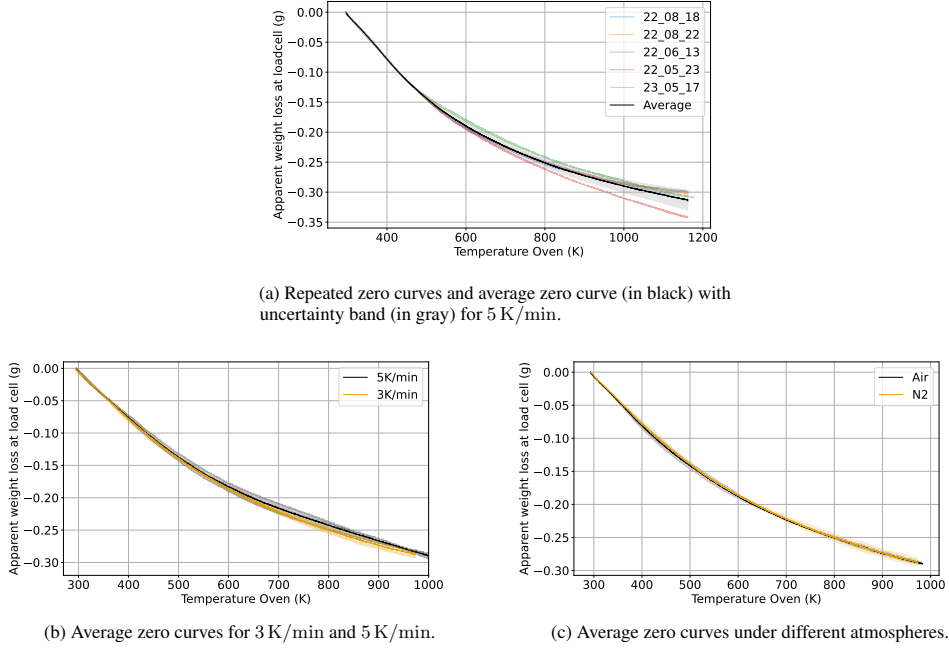


Figure 6: Analysis of zero curves

different zero curves for 3 K/min and 5 K/min, at a flow rate of 10 l/min. The apparent mass loss at the load cell is shown as function of temperature (TO\_6 values).

As can be seen in figure 6a, for 5 K/min buoyancy causes an apparent weight change up to  $(0.32 \pm 0.03)$  g in the load cell. This is an apparent increase in weight of  $(0.28 \pm 0.03)$  g in the middle of the sample region. For higher temperatures, the zero curves become less reproducible, with a maximal deviation of 0.05 g between the curves at 1173 K. After reaching a temperature of 1173 K, the oven was kept constant at this temperature. During this isotherm, the deviation in mass was less than 3 mg for all five zero curves, during 20 minutes. Therefore, experiments with an isotherm at 1173 K will be corrected with  $(0.32 \pm 0.03)$  g, here no time dependent compensation is needed for the isotherm part. In figure 6b, the zero curves for 3 K/min and 5 K/min are compared. As can be seen from the figure, buoyancy effects are similar for both heating rates. In figure 6c, 3 K/min zero curves run under nitrogen and under air atmosphere are compared, with the conclusion, that the atmosphere does not influence the zero curves. Thus, the correction procedure is to subtract the average of one to three zero curves from the measurement data by correlating over TO\_6. It is chosen to correlate over temperature rather than over time, since the starting temperature might differ due to different room temperatures for different experimental days. When results are averaged, this is done using TO\_6, unless explicitly stated otherwise.

After correcting with a zero curve, a conversion factor is calculated. This factor converts the mass measured by the balance to the actual mass loss of the sample. Despite all efforts to homogeneously distribute the powder over the specimen boat, the powder will not be spread perfectly homogeneous. Therefore, it would not be accurate to calculate the conversion factor based on the distance between the pivot and the centre of mass. Instead, the factor is determined from the global mass loss of the powder. Before and after an experiment, the sample boat with the powder is measured on an external balance ( $m_{\text{start}}$  and  $m_{\text{end}}$  respectively). A kern EW 4200-2NM balance with a resolution of 0.01 g is used. This allows to determine the conversion factor ( $c_{\text{cell}}$ ) between the mass loss measured by the load cell and the mass loss in the centre of mass of the sample by

$$c_{\text{cell}} = \frac{m_{\text{start}} - m_{\text{end}}}{m_{\text{cell, start}} - m_{\text{cell, end}}} \quad , \quad (6)$$

where  $m_{\text{cell,start}}$  and  $m_{\text{cell,end}}$  are the start and end mass, respectively, measured by the load cell after subtraction of the zero curve.

## 4.2 Results

Experiments are performed for two different heating rates and for two different initial masses. Figure 7 presents a comparison of these four variations with the focus on the comparison of the two independent mass loss measurement approaches. Repetition experiments have been performed in triplicate. The data of the experiments, including the repetition experiments, can be found in the following repository [22]. The mass loss data is smoothened using a Savitsky-Golay filter with a first order polynomial over 33 data points. The uncertainty on the  $\text{CO}_2$  production rate originates from the uncertainty of the gas analyses, specified by the manufacturer. The  $\text{CO}_2$  production rate was not smoothened. In all experiments, the oven was heated until 1173 K was reached and then kept constant at this temperature until no further mass loss was observed. For 8.5 g and 3 K/min the reaction was completely finished before 1173 K.

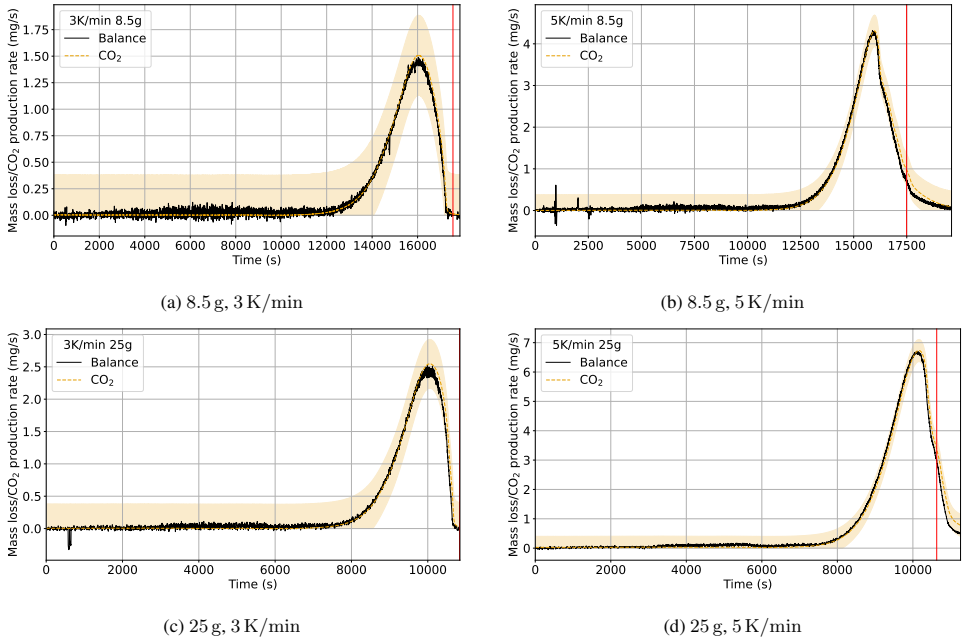


Figure 7: Comparison between the mass loss rate of  $\text{CaCO}_3$  measured by the balance and the  $\text{CO}_2$  production rate captured by the gas analyser. The red line indicates when 1173 K was reached.

From figure 7 it can be seen that the  $\text{CO}_2$  production rate and the mass loss rate are in excellent agreement for all four conditions, both under isothermal conditions as under dynamic conditions. It can be concluded that the balance mechanism works.

Figure 8 shows the impact of experiment variations, here now only with the balance measurements. Note that for different masses also the distribution of the powder throughout the oven is different. The mass loss rates have been normalised, using the total lost mass. For 8.5 g of  $\text{CaCO}_3$  around 3.5 g is gasified and for 25 g around 10.5 g. This results in a conversion rate of 0.42. Since the theoretical conversion rate of  $\text{CaCO}_3$  to  $\text{CO}_2$  is 0.44 it can be concluded that all  $\text{CaCO}_3$  has been converted to  $\text{CO}_2$  and  $\text{CaO}$ .

Figures 8a and 8b seem to indicate that the normalised mass loss rate in the centre of mass is the same for 8.5 g or 25 g of powder. It is important to note that the reactions are not finished at 1173 K, apart from 8.5 g heated at 3 K/min. Figure 8a indicates that differences might occur near the end of the reaction. This would be expected since the upstream

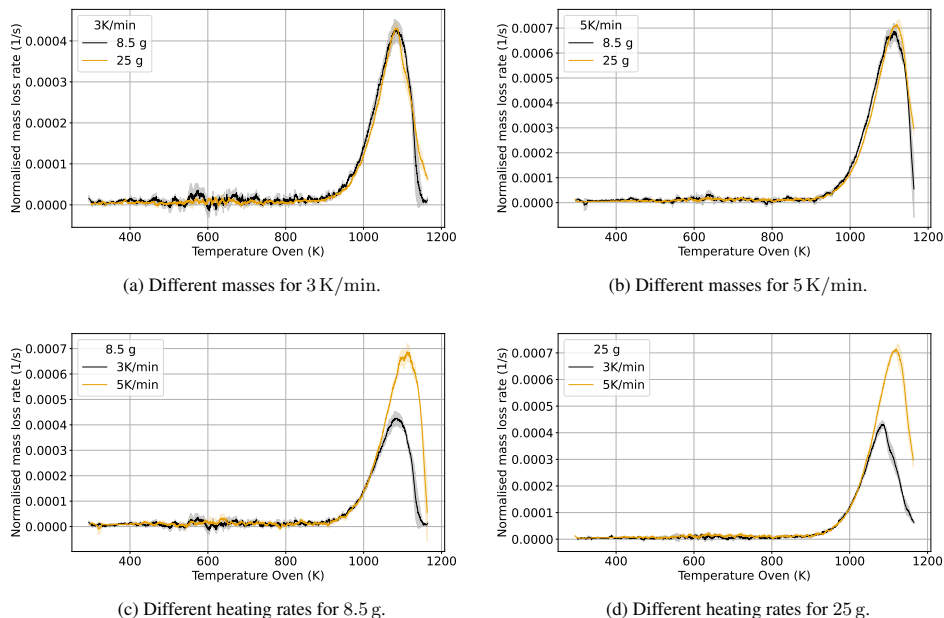


Figure 8: Comparison between the mass loss rate of  $\text{CaCO}_3$  under different conditions.

part of the oven is cooler than the downstream part of the oven, resulting in non-symmetrical mass loss near the end of the experiment. However, a material that reacts at lower temperature would have to be examined to confirm this hypothesis.

Different heating rates have the same onset temperature. For a higher heating rate, the maximum mass loss rate is larger and shifted to higher temperature. Considering the general pyrolysis equations of a single reaction and varying the heating rate, this is the expected behaviour. This implies that there is no significant difference in heat transfer effects between 3 K/min and 5 K/min.

Experiments have been performed to measure the temperature in the  $\text{CaCO}_3$  powder for the 5 K/min experiments. For this purpose three K-type thermocouples, with a 1 mm diameter, have been installed in the powder (at 1/4, 1/2 and 3/4 sample distance). Similar as to the thermocouple measurements, the thermocouples have been fixed to a small copper piece to remain in place. Afterwards, the powder was placed in the specimen boat. The tips of the thermocouples were not in contact with the copper pieces, neither with the specimen boat. The thermocouple tips were covered with the powder, it is difficult to know the exact location of the thermocouples within the solid material since the powder can not be distributed perfectly homogeneous. Three repetition experiments were conducted. In figure 9 the temperature measurements are presented. Both the temperatures of the thermocouples in the powder as the temperatures measured at the outside of the glass tube are shown. The temperature distribution without powder is also shown for reference. The temperature measured in the  $\text{CaCO}_3$  powder are higher than the temperatures measured in an empty specimen boat. This could be due to the cooling by the carrier gas flow of the thermocouples in the empty specimen boat.

## 5 Comparison with TGA measurements

In order to compare the tube furnace with TGA measurements, experiments have been run in both apparatuses with the same material. Several studies have been already done on TGA experiments with  $\text{CaCO}_3$  [23, 24, 25]. However, due to the large scatter in available literature data, new experiments with  $\text{CaCO}_3$  were conducted for this comparison. In these experiments, the exact same powder as for the tube furnace experiments was used. The TGA device used for these experiments was a Netsch STA449 F3 Jupiter.

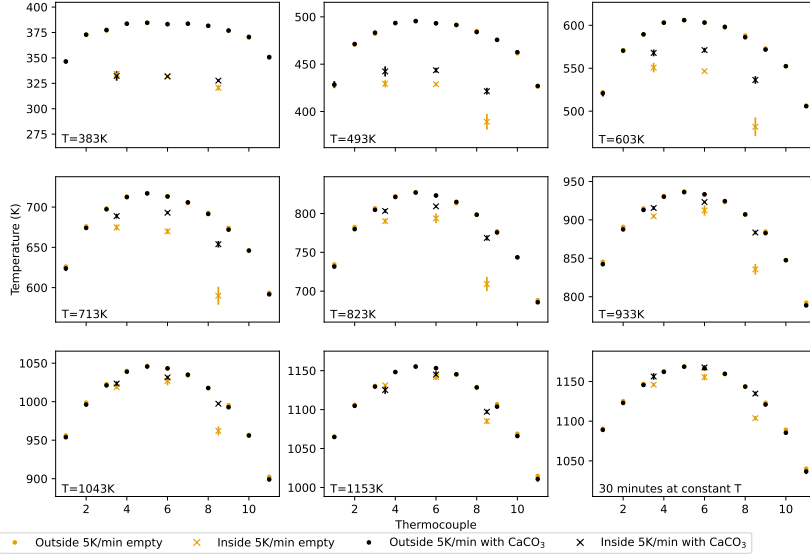


Figure 9: Temperature distribution in the sample and at the outside of the oven during  $\text{CaCO}_3$  experiments.

$\text{CaCO}_3$  powder was sieved with a  $400\ \mu\text{m}$  sieve before filling a  $85\ \mu\text{l}$  alumina crucible with  $8.5\ \text{mg}$  of the sample. Experiments were conducted for three different heating rates:  $3\ \text{K/min}$ ,  $5\ \text{K/min}$  and  $10\ \text{K/min}$ . Additionally, the impact of pressed and non-pressed powder into the crucible was investigated for  $5\ \text{K/min}$ . The effect of pressing was studied, since it is common practise for TGA purposes to press the powder in the crucible, while this was not done with the powder in the specimen boat of the tube furnace. The results of these measurements are shown in figure 10.

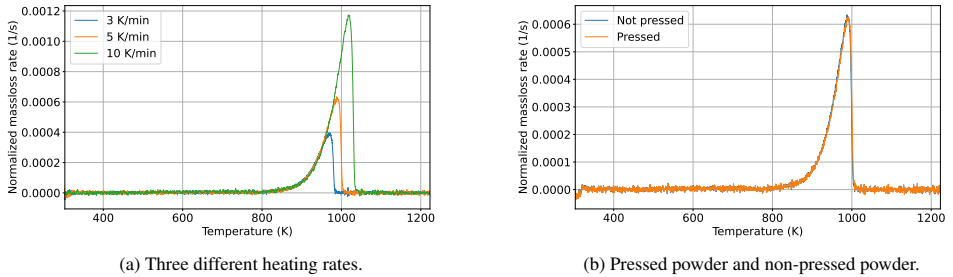
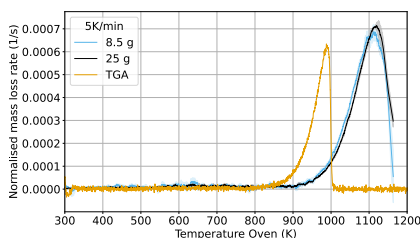


Figure 10: TGA results for  $\text{CaCO}_3$

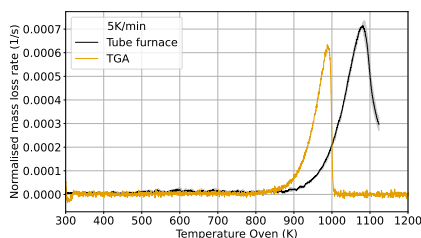
As can be seen from the figures, the mass loss rate of  $\text{CaCO}_3$  consists of one single reaction. As expected from literature, the onset temperature is the same for all heating rates and the peak mass loss rate is higher for higher heating rates. It does not make a difference whether the powder was pressed together or not in the crucible.

Figure 11 shows a comparison between the normalised mass loss rates obtained with the TGA and the tube furnace. For the tube furnace TO\_6 is used as reference temperature in figure 11a, while for figures 11b, 11c and 11d the

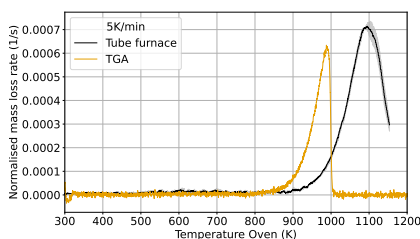
thermocouples installed in the samples were used. As can be seen in these figures, the shape of the mass loss rate is similar for the tube furnace and the TGA. The tube furnace has a wider peak in the mass loss rate. The temperature at which  $\text{CaCO}_3$  reacts is significantly higher in the tube furnace than in the TGA, as is expected due to the increased effect of thermal lag for a large solid sample. Nevertheless, similar temperatures at the onset of the reaction are expected. It should be noted that the sample temperature in the tube furnace is measured inside the powder. In order to determine the onset temperature, a thermocouple should be installed at the hottest point of the powder, which would be the sample surface around the location of TO\_6. This was not done for the  $\text{CaCO}_3$  experiments because of the unreliability of installing a thermocouple at the surface of the powder. It is recommended to conduct further experiments with a solid sample to compare the onset temperature in the TGA with the tube furnace. This would allow to install a thermocouple at the sample surface.



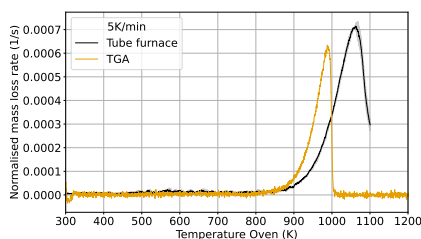
(a) Temperature at To\_6 .



(b) Temperature at 1/4 of sample – downstream from middle of the sample.



(c) Temperature in the middle of the sample.



(d) Temperature at 3/4 of sample – upstream from middle of the sample.

Figure 11: Normalised mass loss rate in the tube furnace versus TGA for  $\text{CaCO}_3$  using different measurement locations as reference values.

## 6 Conclusions and outlook

In this paper, the tube furnace with online mass loss measurement was introduced as a new bench scale experiment for the investigation of pyrolysis processes. In the sample region of the oven, a temperature difference of maximum 142 K is present for experiments with a heating rate of 3 K/min or 5 K/min and a flow rate of 10 l/min.

Commissioning experiments with  $\text{CaCO}_3$  were conducted to demonstrate the validity of the balance measurements of the mass loss rate. An excellent agreement was found between the  $\text{CO}_2$  production rate and the mass loss rate of the samples. These results were obtained both for 8.5 g as well as for 25 g of  $\text{CaCO}_3$  powder and for two different heating rates 3 K/min and 5 K/min, as well as for the isothermal parts at 1173 K at the end of the experiments. This demonstrates the functionality of the balance to perform online mass loss measurement during well-defined heating conditions.

The influence of sample size and heating rate was examined with the  $\text{CaCO}_3$  experiments. The onset temperature of the reaction remains the same for 3 K/min and 5 K/min, while the maximum mass loss rate and its temperature are larger

for the higher heating rate. The effect of different sample sizes needs to be further examined with a sample that finishes reacting before the end of the test.

Additionally, a comparison with TGA measurements was made. As expected, the temperature at the reaction peak is higher in the tube furnace than in the TGA. However, it is expected that the onset temperature of the reaction is the same. In order to accurately compare this, temperature data at the hottest point of the sample would be needed. This would be at the middle of the sample at the surface. Unfortunately, it is not feasible to accurately measure a surface temperature with powder. It should be considered to conduct experiments on solid samples to further compare mass loss measurements of the tube furnace and the TGA.

## Acknowledgements

The authors would like to thank Dr. Lucie Hasalová from the Technický ústav požární ochrany (Prague, Czech Republic) for the support with the TGA experiments. We would also like to thank the student workers at the Forschungszentrum Jülich, who have supported this work: Minh Tam Würzbürger, Leonie Labod and Tristan Lengeling.

## Authorship Contribution Statement, following [26]

**Karen De Lannoye:** conceptualisation, data curation, formal analysis, investigation, methodology, software, validation, visualisation, writing – original draft preparation, writing – review and editing

**Alexander Belt:** conceptualisation, methodology, validation, writing – review and editing

**Ernst-Arndt Reinecke:** conceptualisation, validation, writing – review and editing

**Lukas Arnold:** conceptualisation, methodology, project administration, resources, supervision, writing – review and editing, funding acquisition

## References

- [1] Kevin McGrattan, Andrew Lock, Nathan Marsh, Marc Nyden, Scott Bareham, Alexander B. Morgan, Mary Galaska, Kathy Schenck, and David Stroup. Cable Heat Release, Ignition, and Spread in Tray Installations During Fire (CHRISTIFIRE) Phase 1: Horizontal Trays. Technical report, National Institute of Standards and Technology Engineering Laboratory; Fire Research Division Gaithersburg, Maryland 20899, July 2012.
- [2] Kevin McGrattan, Scott Bareham, and David Stroup. Cable Heat Release, Ignition, and Spread in Tray Installations During Fire (CHRISTIFIRE) Phase 2: Vertical Shafts and Corridors. Technical report, National Institute of Standards and Technology Engineering Laboratory; Fire Research Division Gaithersburg, Maryland 20899, December 2013.
- [3] L. Audouin, L. Rigollet, H. Prétrel, W. Le Saux, and M. Röwekamp. OECD PRISME project: Fires in confined and ventilated nuclear-type multi-compartments - Overview and main experimental results. *Fire Safety Journal*, 62:80–101, November 2013. ISSN 0379-7112. doi:10.1016/j.firesaf.2013.07.008.
- [4] IRSN. Le risque incendie dans les centrales en 2014, 2014. URL <https://www.irsn.fr/savoir-comprendre/surete/risque-incendie-milieu-nucleaire#.Y1b72i07FhE>.
- [5] Alain Alonso, David Lázaro, Mariano Lázaro, and Daniel Alvear. Numerical Prediction of Cables Fire Behaviour Using Non-Metallic Components in Cone Calorimeter. *Combustion Science and Technology*, pages 1–17, February 2023. ISSN 0010-2202, 1563-521X. doi:10.1080/00102202.2023.2182198.
- [6] Tarek Beji and Bart Merci. Numerical simulations of a full-scale cable tray fire using small-scale test data. *Fire and Materials*, 43(5):486–496, 2019. ISSN 0308-0501. doi:10.1002/fam.2687.
- [7] Tristan Hehnen, Lukas Arnold, and Saverio La Mendola. Numerical Fire Spread Simulation Based on Material Pyrolysis—An Application to the CHRISTIFIRE Phase 1 Horizontal Cable Tray Tests. *Fire*, 3(3):33, 2020. doi:10.3390/fire3030033.
- [8] Alexandra Viitanen, Simo Hostikka, and Jukka Vaari. CFD Simulations of Fire Propagation in Horizontal Cable Trays Using a Pyrolysis Model with Stochastically Determined Geometry. *Fire Technology*, July 2022. ISSN 1572-8099. doi:10.1007/s10694-022-01291-6.
- [9] Xinyan Huang and Yujii Nakamura. A Review of Fundamental Combustion Phenomena in Wire Fires. *Fire Technology*, 56(1):315–360, January 2020. ISSN 1572-8099. doi:10.1007/s10694-019-00918-5.

- [10] ISO 5660-1:2015(E). Reaction-to-fire tests — Heat release, smoke production and mass loss rate — Part 1: Heat release rate (cone calorimeter method) and smoke production rate (dynamic measurement). Standard, International Organization for Standardization, Geneva, CH, March 2015.
- [11] B. Schartel and T. R. Hull. Development of fire-retarded materials—Interpretation of cone calorimeter data. *Fire and Materials*, 31(5):327–354, 2007. ISSN 1099-1018. doi:[10.1002/fam.949](https://doi.org/10.1002/fam.949).
- [12] Vytenis Babrauskas. Development of the Cone Calorimeter - A Bench-Scale Heat Release Rate Apparatus Based on Oxygen Consumption. Technical report, U.S. DEPARTMENT OF COMMERCE National Bureau of Standards Center for Fire Research, Washington, DC 20234, November 1982. URL <https://nvlpubs.nist.gov/nistpubs/Legacy/IR/nbsir82-2611.pdf>.
- [13] Jozef Martinka, Peter Rantuch, Janka Sulová, and Filip Martinka. Assessing the fire risk of electrical cables using a cone calorimeter. *Journal of Thermal Analysis and Calorimetry*, 135(6):3069–3083, March 2019. ISSN 1588-2926. doi:[10.1007/s10973-018-7556-5](https://doi.org/10.1007/s10973-018-7556-5).
- [14] A. W. Coats and J. P. Redfern. Thermogravimetric analysis. A review. *The Analyst*, 88(1053):906, 1963. ISSN 0003-2654, 1364-5528. doi:[10.1039/an9638800906](https://doi.org/10.1039/an9638800906).
- [15] Nooshin Saadatkhah, Adrián Carillo Garcia, Sarah Ackermann, Philippe Leclerc, Mohammad Latifi, Said Samih, Gregory S. Patience, and Jamal Chaouki. Experimental methods in chemical engineering: Thermogravimetric analysis—TGA. *The Canadian Journal of Chemical Engineering*, 98(1):34–43, 2020. ISSN 0008-4034. doi:[10.1002/cjce.23673](https://doi.org/10.1002/cjce.23673).
- [16] The influence of experimental conditions on the mass loss for TGA in fire safety science. *Fire Safety Journal*, 144: 104079, 2024. ISSN 0379-7112. doi:<https://doi.org/10.1016/j.firesaf.2023.104079>.
- [17] ISO/TS 19700:2016(E). Controlled equivalence ratio method for the determination of hazardous components of fire effluents — Steady-state tube furnace. Standard, International Organization for Standardization, Geneva, CH, 2016.
- [18] Anna A. Stec, T. Richard Hull, and Krzysztof Lebek. Characterisation of the steady state tube furnace (ISO TS 19700) for fire toxicity assessment. *Polymer Degradation and Stability*, 93(11):2058–2065, November 2008. ISSN 0141-3910. doi:[10.1016/j.polymdegradstab.2008.02.020](https://doi.org/10.1016/j.polymdegradstab.2008.02.020).
- [19] Bronkhorst. Property calculation n2., 2023. URL <https://www.fluidat.com/default.asp>. Last accessed 31 Mai 2023.
- [20] Bronkhorst. The intrinsic properties of N2 ("Nitrogen"), 2023. URL <https://www.fluidat.com/default.asp>. Last accessed 31 Mai 2023.
- [21] Bronkhorst. The intrinsic properties of CO2 ("Carbon dioxide"), 2023. URL <https://www.fluidat.com/default.asp>. Last accessed 31 Mai 2023.
- [22] Karen De Lannoye, Alexander Belt, Ernst-Arndt Reinecke, and Lukas Arnold. Zenodo: The tube furnace with online mass loss measurement as a new bench scale test for pyrolysis, 2023.
- [23] Haixiang Chen and Naian Liu. Application of Non-Arrhenius Equations in Interpreting Calcium Carbonate Decomposition Kinetics: Revisited. *Journal of the American Ceramic Society*, 93(2):548–553, 2010. ISSN 1551-2916. doi:[10.1111/j.1551-2916.2009.03421.x](https://doi.org/10.1111/j.1551-2916.2009.03421.x).
- [24] Isabel Galan, Fredrik P. Glasser, and Carmen Andrade. Calcium carbonate decomposition. *Journal of Thermal Analysis and Calorimetry*, 111(2):1197–1202, February 2013. ISSN 1572-8943. doi:[10.1007/s10973-012-2290-x](https://doi.org/10.1007/s10973-012-2290-x).
- [25] Rod Bottom. *Thermogravimetric Analysis*, chapter 3, pages 87–118. John Wiley & Sons, Ltd, 2008. ISBN 9780470697702. doi:<https://doi.org/10.1002/9780470697702.ch3>.
- [26] Liz Allen, Alison O'Connell, and Veronique Kiermer. How can we ensure visibility and diversity in research contributions? how the contributor role taxonomy (credit) is helping the shift from authorship to contributorship. *Learned Publishing*, 32(1):71–74, 2019. doi:<https://doi.org/10.1002/leap.1210>.





# APPENDIX I

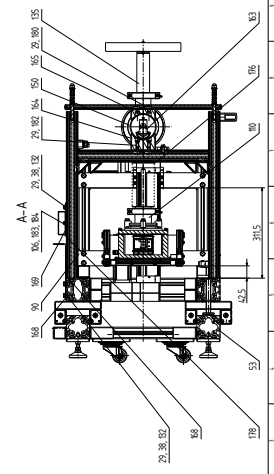
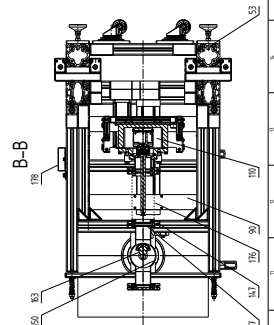
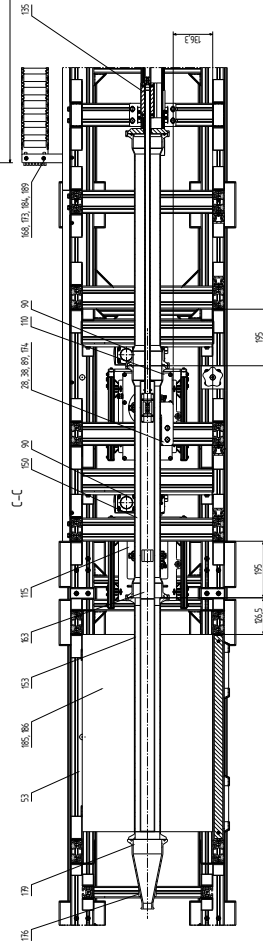
---

## Technical drawings tube furnace

---

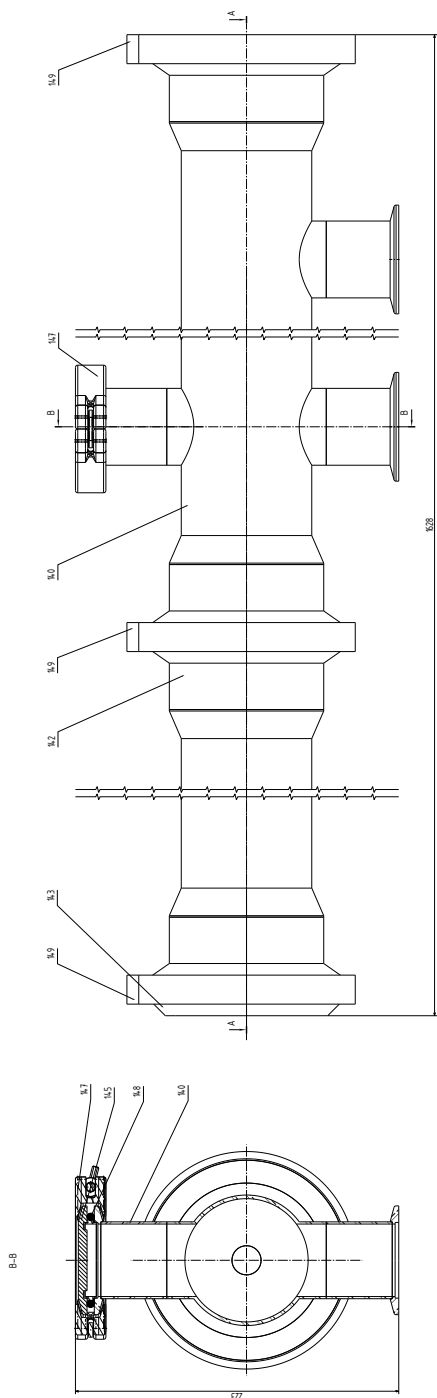
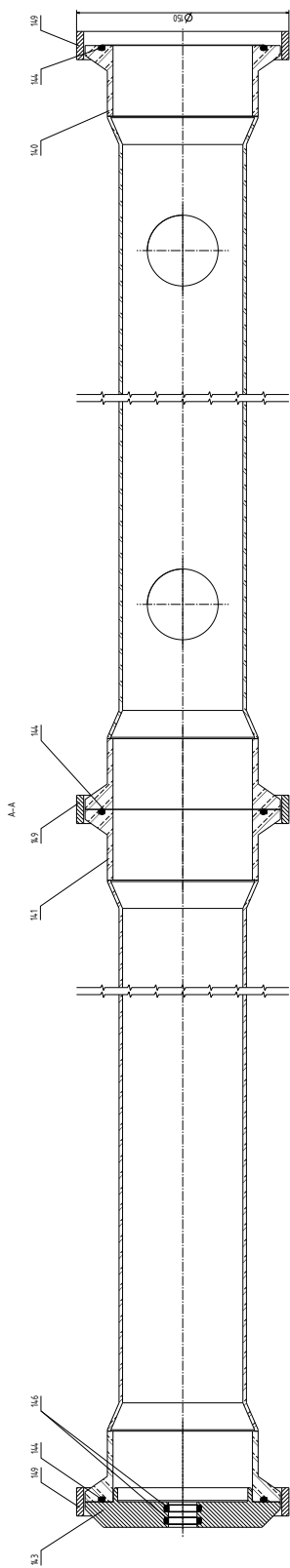
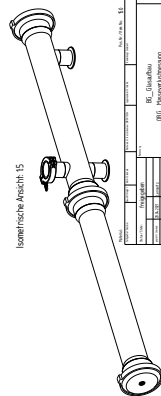
This appendix contains technical drawings of the tube furnace. These drawings were produced in cooperation with the institute of engineering and technology of Forschungszentrum Jülich. The drawings occur in the following order:

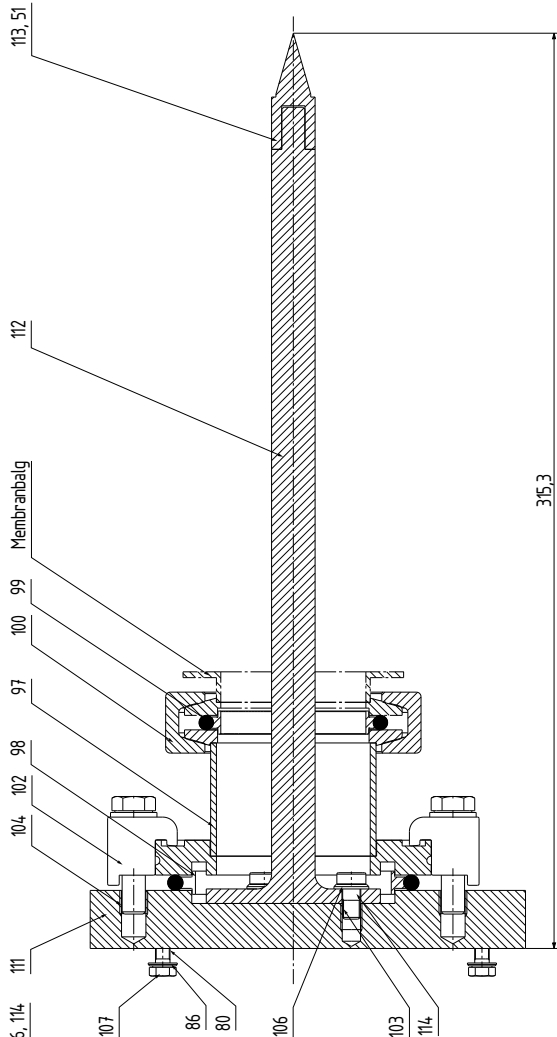
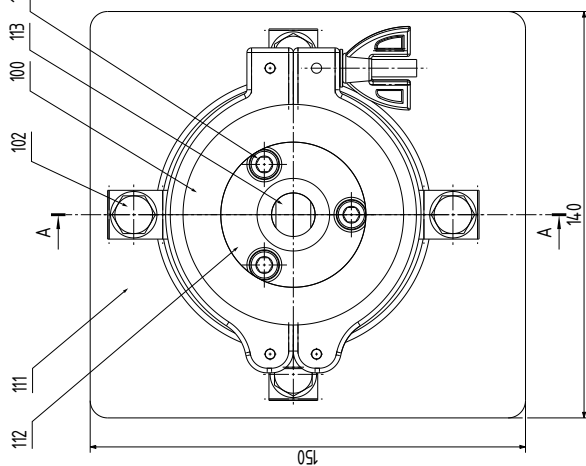
- overview of the whole setup;
- overview of the supporting structure of the setup;
- glaze tubes of the setup;
- pivot for the balance beam;
- support with step-motor to move pivot and load cell vertically;
- balance beam out of quartz glass.



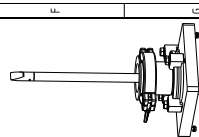
**Bemerkung:**  
 Offen Pos. 185, 186 wird auf Profil Pos. 17  
 mit Pos. 38, 43 montiert. Durchgangsbohrungen  
 in Pos. 17 bei Montage anpassen.

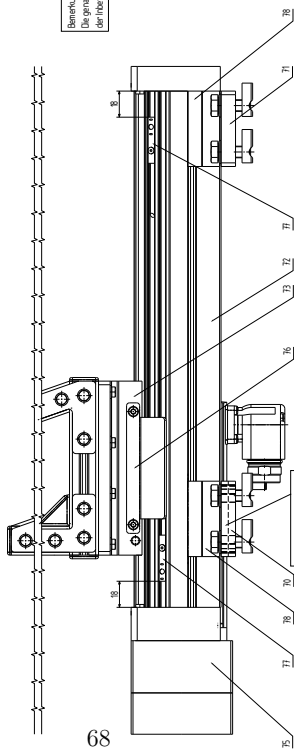






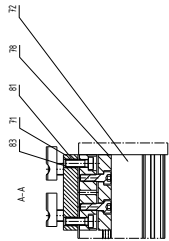
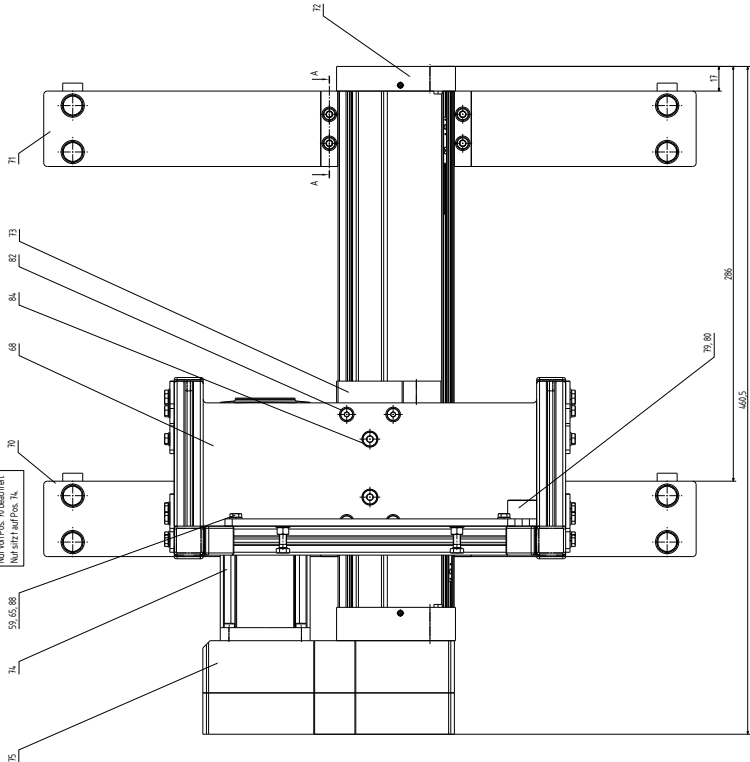
Isometrische Ansicht: 1:5

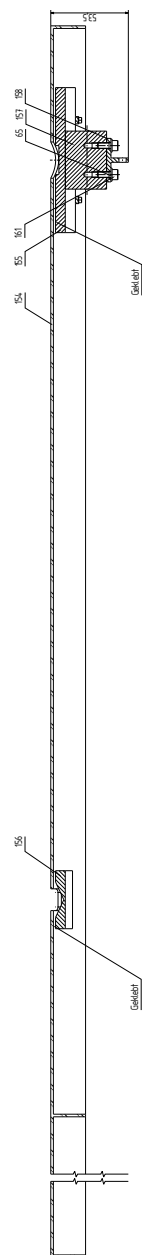
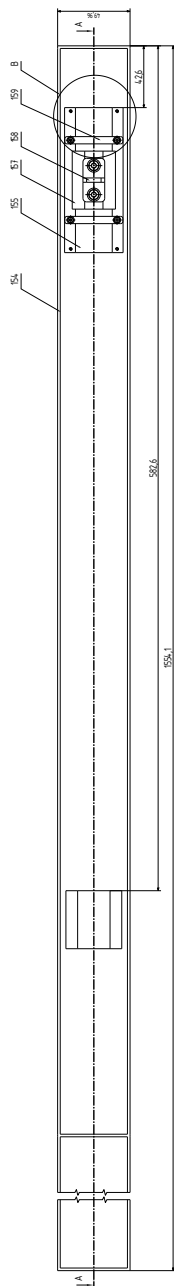
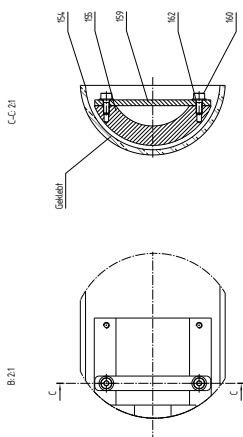
[illegible]



Bemerkung:  
Die genaue Position von Pos. 71 und 72  
ist nicht darstellbar, da sie liegen.

Bemerkung:  
Bei vorr. Position  
hat sich auf Pos. 71.





**Bemerkungen:**  
Die Positionen 155 und 156 mit DELO GUM 3699  
in 154 von Kunststoffwerkstatt eingeklebt.

[illegible]



# KAREN DE LANNOYE

## EDUCATION

---

<b>PhD</b>	PhD candidate at Bergische Universität Wuppertal	2019-present
<b>MS</b>	MSc Physics and astronomy (Minor research) with great distinction Vrije Universiteit Brussel (VUB), Belgium, International master Master thesis: Temperature dependence of the erosion performance of WCrY smart alloys	2017-2019
<b>BS</b>	BSc Physics and astronomy Vrije Universiteit Brussel(VUB), Belgium Bachelor thesis: The phenomenology of quarkphillic dark matter	2014-2017
	Secondary school (A-level, mathematics-sciences) School “Sint-Martinus Overijse” in Overijse (Belgium)	2008-2014

## PROFESSIONAL EXPERIENCE

---

### Doctoral Researcher

Forschungszentrum Jülich GmbH:

- IAS-7: Institute for Advanced Simulations
- IEK-6/IEK-14: Institute for Energy and Climate

### Internship

Internship at the Institute for Energy and Climate Research, Plasma Physics at the Forschungszentrum (Research Centre) Jülich (6 weeks)  
July-August 2018

### Teaching

Participating as a teacher-assistant in Fire simulations at the university of Wuppertal (summer semester 2020 and 2021)

Working as a teacher for mathematics preparatory course at the VUB, Brussels.  
September 2015, 2016, 2017, 2018. (2 weeks per year)

Working as teacher for a preparatory course in physics and chemistry at the VUB, Brussels  
September 2015, 2017. (1 week per year)

## PROJECTS & ACTIVITIES

---

### Forschungszentrum Jülich GmbH

Member of the JuDocs Committee for Counselling in Supervision Conflicts

Band / Volume 58

**Space Usage and Waiting Pedestrians at Train Station Platforms**

M. Küpper (2023), ix, 95 pp

ISBN: 978-3-95806-733-2

Band / Volume 59

**Quantum annealing and its variants: Application to quadratic unconstrained binary optimization**

V. Mehta (2024), iii, 152 pp

ISBN: 978-3-95806-755-4

Band / Volume 60

**Elements for modeling pedestrian movement from theory to application and back**

M. Chraïbi (2024), vi, 279 pp

ISBN: 978-3-95806-757-8

Band / Volume 61

**Artificial Intelligence Framework for Video Analytics:**

Detecting Pushing in Crowds

A. Alia (2024), xviii, 151 pp

ISBN: 978-3-95806-763-9

Band / Volume 62

**The Relationship between Pedestrian Density, Walking Speed and Psychological Stress:**

**Examining Physiological Arousal in Crowded Situations**

M. Beermann (2024), xi, 117 pp

ISBN: 978-3-95806-764-6

Band / Volume 63

**Eventify Meets Heterogeneity:**

**Enabling Fine-Grained Task-Parallelism on GPUs**

L. Morgenstern (2024), xv, 110 pp

ISBN: 978-3-95806-765-3

Band / Volume 64

**Dynamic Motivation in Crowds: Insights from Experiments and Pedestrian Models for Goal-Directed Motion**

E. Üsten (2024), ix, 121 pp

ISBN: 978-3-95806-773-8

Band / Volume 65

**Propagation of Stimuli in Crowds:**

**Empirical insights into mutual influence in human crowds**

H. Lügering (2024), xi, 123 pp

ISBN: 978-3-95806-775-2

Band / Volume 66

**Classification of Pedestrian Streams: From Empirics to Modelling**

J. Cordes (2024), vii, 176 pp

ISBN: 978-3-95806-780-6

Band / Volume 67

**Optimizing Automated Shading Systems in Office Buildings by  
Exploring Occupant Behaviour**

G. Derbas (2024), 9, x, 168, ccxxiii

ISBN: 978-3-95806-787-5

Band / Volume 68

**Speed-Density Analysis in Pedestrian Single-File Experiments**

S. Paetzke (2025), XIII, 107 pp

ISBN: 978-3-95806-818-6

Band / Volume 69

**Proceedings of the 35th Parallel Computational Fluid Dynamics International  
Conference 2024**

A. Lintermann, S. S. Herff, J. H. Göbbert (2025), xv, 321 pp

ISBN: 978-3-95806-819-3

Band / Volume 70

**Towards Improved Civil Safety: Experimental Insights into Impulse  
Propagation through Crowds**

S. Feldmann (2025), xi, 99 pp

ISBN: 978-3-95806-828-5

Band / Volume 71

**Development and Evaluation of Architecture Concepts for a System-on-Chip  
Based Neuromorphic Compute Node for Accelerated and Reproducible  
Simulations of Spiking Neural Networks in Neuroscience**

G. Trench (2025), 219, XXXV pp

ISBN: 978-3-95806-832-2

Band / Volume 72

**The tube furnace as a new bench scale experiment for pyrolysis**

K. De Lannoye (2025), ix, 70 pp

ISBN: 978-3-95806-839-1



IAS Series  
Band / Volume 72  
ISBN 978-3-95806-839-1